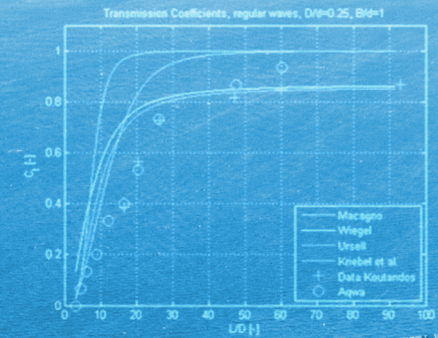
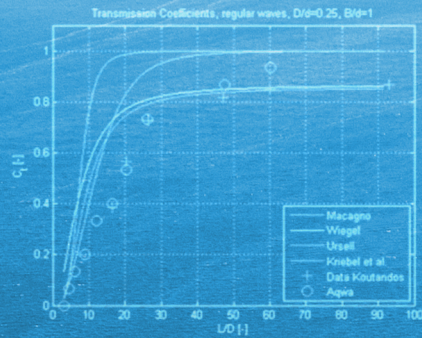
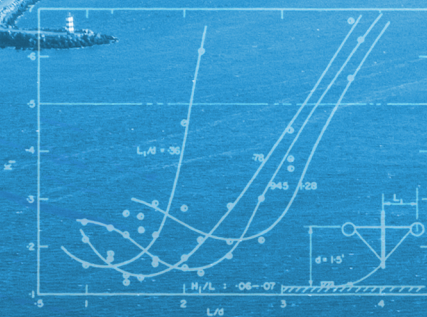


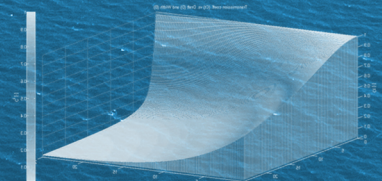
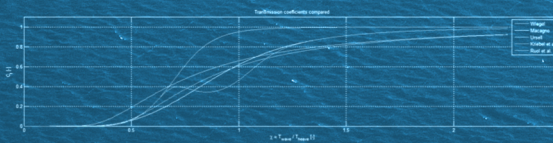
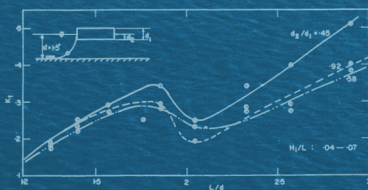
MASTER OF SCIENCE THESIS



EFFECTIVENESS OF FLOATING BREAKWATERS

Wave attenuating floating structures

A.C. Biesheuvel



Effectiveness of Floating Breakwaters

Wave attenuating floating structures

MASTER OF SCIENCE THESIS

For obtaining the degree of Master of Science in Civil Engineering at
Delft University of Technology

Arie Cornelis Biesheuvel

Photo cover image:

*Background picture: Breakwater at IJmuiden, The Netherlands. Online image.
Retrieved February 2013 from: <https://beeldbank.rws.nl>, Rijkswaterstaat / Rens Jacobs*

*Graph at bottom left and top left: Curves with experimental data of floating breakwaters
Retrieved February 2013 from: Brebner and Ofuya, 1968*

Note: This document has been designed for full colour double-sided printing

DELFT UNIVERSITY OF TECHNOLOGY
DEPARTMENT OF
Civil Engineering and Geosciences

In cooperation with

DELTARES
DEPARTMENT OF
Hydraulic Engineering

Dated: September 30, 2013

Committee Master Thesis:

| | |
|-----------------------|---|
| Prof. ir. T. Vellinga | Delft University of Technology Hydraulic Engineering, Section of Ports and Waterways |
| Ir. P. Quist | Delft University of Technology Hydraulic Engineering, Section of Ports and Waterways |
| Dr. ir. M. Zijlema | Delft University of Technology Hydraulic Engineering, Section of Environmental Fluid Mechanics |
| Ir. A.J. van der Hout | Deltares Hydraulic Engineering, Section of Harbour, Coastal and Offshore Engineering |
| Dr. ir. B. Hofland | Deltares Hydraulic Engineering, Section of Coastal Structures and Waves |

“You can’t stop the waves, but you can learn how to surf”

Jon Kabat-Zinn

Keywords: Floating breakwaters; Wave attenuation; Wave transmission; Numerical modelling.

Abstract

Breakwaters are structures located in the water and are used to protect an area against undesirable wave heights. Floating breakwaters are often applied where conventional breakwaters are less suitable to apply. In general it is attractive to apply floating breakwaters in deep waters where short waves occur. Situations like this are for example deep lakes where only wind waves (short waves) are present.

Because floating breakwaters are used to prevent undesirable wave heights, it is important to know the wave height which will be transmitted by the floating breakwater, given the incident wave height is known. The effectiveness of floating breakwaters is characterized by the transmission coefficient, which represents the fraction of the incident wave height which is transmitted by the floating breakwater. Depending on the boundary conditions of the area which needs to be protected by the floating breakwater, the maximum allowable transmitted wave height can be determined. From previous engineering projects it turned out that it is difficult to determine the transmitted wave height without performing physical model tests or making use of numerical models. The focus of this research is to identify the steps which can be taken during the design process, in order to determine the effectiveness of floating breakwaters more accurately.

In this thesis distinction is made between three pontoon (rectangular) types of structures, namely: fixed breakwaters (partially submerged structures), floating breakwaters anchored by piles (one degree of freedom) and floating breakwaters anchored by chains/cables (six degrees of freedom). A number of formulas which can be used to determine the transmitted wave height are compared with each other. From this comparison it is concluded that there are large deviations, especially for short waves. These formulas are also compared with physical model data obtained from different researchers. Based on this comparison conclusions are drawn regarding to the applicability of the most appropriate formula which can be used to determine the wave transmission. These conclusions are graphically shown in the form of a flowchart which can be used as a design tool for engineering purposes.

Areas of interest for engineering purposes where physical model data is missing are modelled numerically with the linear three dimensional radiation diffraction model AQWA (Ansys). First it is investigated how well AQWA can model fixed breakwaters and floating breakwaters, by comparing the calculation results of the numerical models with the results of the physical models. From this comparison a good agreement is found. Secondly, the calculation results of the areas of interest are compared with the formulas to determine the transmission coefficient. Based on this comparison the flowchart solely based on physical model data is extended with numerical model data. The final result of this thesis is a flowchart which indicates the applicability of the most appropriate formula which can be used to determine the wave transmission. This flowchart is suitable to apply during preliminary design stages and gives a good impression of the effectiveness of the floating breakwater.

Preface

This thesis is submitted in order to obtain the degree of Master of Science in Civil Engineering at the Delft University of Technology. The work was carried out in close cooperation with the Hydraulic Engineering department of Deltares.

In this thesis it is investigated which steps should be taken during the design process in order to predict the effectiveness of floating breakwaters more accurately. The final product is a flowchart which can be used as a guideline during the preliminary design stage in order to predict the wave transmission of floating breakwaters.

Acknowledgements

I would like to thank all the members of my graduation committee for their great support and comments during this research. Their experience and knowledge has been very helpful to me and increased my enthusiasm for the subject. I would like to thank Prof. ir. Tiedo Vellinga for his guidance and feedback during this research, ir. Peter Quist for his clever and useful comments on my work and dr. ir. Marcel Zijlema for helping me to overcome several challenges which I encountered with the numerical model and for the interesting conversations about wave modelling.

In addition to this I would like to thank Deltares for giving me the opportunity to perform my M.Sc. thesis within their company and to cooperate with highly skilled researchers. Most of the supervision at Deltares was done by ir. Arne van der Hout who spent a lot of time in reading and commenting my work. Arne greatly supported me during the whole process. His knowledge and enthusiasm for floating structures and waves was extremely helpful and encouraging. The supervision of Dr. ir. Bas Hoffland (Deltares) was very valuable and often resulted in new ideas. All the conversations with Bas were very inspiring and his knowledge of waves and coastal structures is amazing.

Furthermore, I would like to thank all my friends at the Delft University of Technology for all the interesting discussions and relaxing moments we often had on Thursday afternoons at Psor. Special thanks goes to Hans Peter van den Heuvel for the great years we had in Delft and for sharing our common interests in Hydraulic Engineering. Also a special thanks to Alexander Mauchle for being an incredible motivator and friend, who often told me during my thesis work: 'you have to shoot for the moon'.

Finally, I want to thank my family, friends and house mates for their interest and support during my studies in Delft.

Cees Biesheuvel
Delft, September 2013

Table of Contents

| | |
|---|-------------|
| Abstract | i |
| Preface | iii |
| List of Symbols | xvii |
| 1 Introduction | 1 |
| 1.1 Background | 1 |
| 1.2 Motivation for research | 1 |
| 1.3 Scope and research objectives | 2 |
| 1.3.1 Problem definition | 2 |
| 1.3.2 Research objective | 2 |
| 1.3.3 Research questions | 2 |
| 1.4 Approach | 3 |
| 2 Breakwaters in general | 5 |
| 2.1 Wave protection | 5 |
| 2.2 Wave-structure interaction | 5 |
| 2.2.1 Wave reflection | 5 |
| 2.2.2 Wave run-up | 6 |
| 2.2.3 Wave transmission | 6 |
| 2.2.4 Overtopping | 6 |
| 2.2.5 Diffraction | 6 |
| 2.2.6 Wave-floating breakwater interaction | 7 |
| 2.3 Types of breakwaters | 7 |
| 2.3.1 Conventional breakwaters | 7 |
| 2.3.2 Unconventional Breakwaters | 9 |
| 2.4 Breakwater applicability based on economic considerations | 9 |
| 3 Floating Breakwaters | 11 |
| 3.1 History of floating breakwaters | 11 |
| 3.2 Advantages and disadvantages of floating breakwaters | 12 |
| 3.2.1 Advantages | 12 |
| 3.2.2 Disadvantages | 12 |

| | | |
|----------|--|-----------|
| 3.3 | Classification of floating breakwaters | 12 |
| 3.3.1 | Reflective structures | 12 |
| 3.3.2 | Dissipative structures | 14 |
| 3.4 | Applicability in special cases | 16 |
| 3.5 | Conclusion | 17 |
| 4 | Physics of waves and floating structures | 19 |
| 4.1 | Linear wave theory | 19 |
| 4.1.1 | Regular waves | 21 |
| 4.1.2 | Irregular waves | 22 |
| 4.2 | Wave energy transport | 23 |
| 4.3 | Dynamics of floating breakwaters | 24 |
| 4.3.1 | Dynamics of floating structures in regular waves | 25 |
| 4.3.2 | Dynamics of floating structures in irregular waves | 27 |
| 5 | Performance of floating breakwaters | 29 |
| 5.1 | Wave transmission theories | 29 |
| 5.1.1 | Wave transmission theories for fixed rigid reflective structures | 30 |
| 5.1.2 | Wave transmission theories for non-fixed rigid structures | 34 |
| 5.1.3 | Comparison of wave transmission theories | 37 |
| 5.2 | Wave transmission theories compared with experimental data | 40 |
| 5.2.1 | Fixed breakwaters | 42 |
| 5.2.2 | Floating breakwaters anchored by piles | 43 |
| 5.2.3 | Floating breakwaters anchored by chains | 46 |
| 5.2.4 | Oblique incident waves | 49 |
| 5.3 | Conclusion | 50 |
| 6 | Modelling of Floating Breakwaters | 53 |
| 6.1 | Approach | 53 |
| 6.1.1 | Theory used in AQWA | 54 |
| 6.1.2 | Model set up | 58 |
| 6.1.3 | Model calibration and validation | 64 |
| 6.2 | New simulations for areas of interest | 70 |
| 6.2.1 | Fixed breakwaters | 70 |
| 6.2.2 | Floating breakwaters anchored by piles | 72 |
| 6.2.3 | Floating breakwaters anchored by chains | 74 |
| 6.2.4 | Oblique incident waves | 74 |
| 6.3 | Conclusion | 76 |
| 7 | Conclusions and Recommendations | 79 |
| 7.1 | Conclusions | 79 |
| 7.2 | Recommendations | 82 |

| | | |
|----------|---|-----------|
| A | Performance of floating breakwaters | A1 |
| A.1 | Definition of Performance | A1 |
| A.1.1 | Wave transmission theories for reflective structures | A1 |
| A.1.2 | Wave transmission theories for dissipative structures | A4 |
| B | Linear wave theory | B1 |
| B.1 | Linear wave theory | B1 |
| B.1.1 | Regular waves | B3 |
| B.1.2 | Irregular waves | B4 |
| C | Experimental data | C1 |
| C.1 | Experimental datasets | C1 |
| C.1.1 | Fixed breakwaters | C1 |
| C.1.2 | Breakwaters anchored by piles | C5 |
| C.1.3 | Breakwaters anchored by chains | C13 |
| D | Modelling of floating breakwaters | D1 |
| D.1 | Theory used in AQWA | D1 |
| D.1.1 | Waves | D1 |
| D.2 | Potential flow | D2 |
| D.2.1 | Potential flow around floating structures | D5 |
| D.2.2 | Potential flow elements | D6 |
| D.2.3 | Hydrodynamic loads | D9 |
| D.3 | Validation of AQWA | D11 |
| D.3.1 | Fixed breakwaters | D11 |
| D.3.2 | Floating breakwaters anchored by piles | D12 |
| D.4 | New simulations for areas of interest | D12 |
| D.4.1 | Fixed breakwater | D12 |
| D.4.2 | Floating breakwater anchored by piles | D14 |

List of Figures

| | | |
|-----|---|----|
| 1.1 | Pontoon type of breakwater | 4 |
| 2.1 | Diffraction of waves around a headland | 6 |
| 2.2 | Interaction between wave and floating breakwater | 7 |
| 2.3 | Mound breakwater types | 8 |
| 2.4 | Monolithic breakwater type | 8 |
| 2.5 | Composite breakwater types | 8 |
| 2.6 | Special breakwater types and oscillations floating structures | 9 |
| 2.7 | Comparison of breakwater costs per running meter | 10 |
| 3.1 | Rotational equilibrium | 13 |
| 3.2 | Pontoon type of breakwater | 13 |
| 3.3 | A-frame type of breakwater | 14 |
| 3.4 | Hinged type of breakwater | 14 |
| 3.5 | Scrap tire type of breakwater | 15 |
| 3.6 | Tethered float type of breakwater | 15 |
| 3.7 | Porous wall type of breakwater | 16 |
| 3.8 | Wave trap type of breakwater (membrane type) | 16 |
| 4.1 | Linearised basic equations and boundary conditions for linear wave theory | 21 |
| 4.2 | Propagating harmonic sine wave | 22 |
| 4.3 | Wave record analysis | 23 |
| 4.4 | Two-dimensional variance density spectrum | 23 |
| 4.5 | Interaction between wave and floating breakwater | 23 |
| 4.6 | Integral from bottom to surface as a function of $f(z)$ beneath the wave | 24 |
| 4.7 | Degrees of freedom for a floating body in a three-dimensional space | 25 |
| 4.8 | Superposition of Hydromechanical and Wave loads | 26 |
| 5.1 | Interaction between wave and floating breakwater | 29 |
| 5.2 | Transmission coefficient in deep water for Ursell and Wiegel | 31 |
| 5.3 | Definitions of Macagno's formula and theoretical results | 32 |
| 5.4 | Theory of Wiegel | 32 |

| | | |
|------|--|----|
| 5.5 | C_t values for the theory of Wiegel | 33 |
| 5.6 | Comparison of three wave transmission theories with experimental data | 34 |
| 5.7 | Added mass for Pi-type- and pontoon type floating breakwater | 35 |
| 5.8 | Results of the formula of Ruol et al.,(2012) | 36 |
| 5.9 | Wave transmission theories compared for T_{wave}/T_{heave} and $L_{wave}/waterdepth$ | 38 |
| 5.10 | Wave transmission theories compared for draft vs. water depth, D/d | 38 |
| 5.11 | Wave transmission theory of Macagno and Ruol et al. as function of (L_{wave}/B) | 38 |
| 5.12 | Wave transmission theory of Macagno as function of width (B) and draft (D) | 39 |
| 5.13 | Contour plot formula Macagno as function of B and D | 39 |
| 5.14 | Different types of anchorage for floating breakwaters | 40 |
| 5.15 | Experimental data of Pena et al. | 41 |
| 5.16 | Differences between theories and experimental data of Figure 5.15 | 41 |
| 5.17 | Data of Brebner and Ofuya, regular waves | 48 |
| 5.18 | Data of Gesraha, irregular waves | 48 |
| 5.19 | Transmission coefficient for oblique incident waves | 50 |
| 5.20 | Flow chart of application for wave transmission theories | 52 |
| 6.1 | Stokes waves | 55 |
| 6.2 | Summary of fluid forces | 57 |
| 6.3 | Result AQWA presented in pressures on floating structure | 58 |
| 6.4 | Mesh of floating breakwater | 58 |
| 6.5 | Sketch of wave flume | 59 |
| 6.6 | Sommerfeld solution for diffraction of waves | 60 |
| 6.7 | Numerical solution of diffraction | 60 |
| 6.8 | Snapshot of surface elevation of diffracted wave in AQWA | 61 |
| 6.9 | Diffraction coefficients behind breakwater | 62 |
| 6.10 | Maximum wave amplitudes solely due to diffraction | 63 |
| 6.11 | Experimental data of Koutandos et al. for fixed breakwater | 65 |
| 6.12 | Exp. data compared with numerical data for fixed breakwater | 65 |
| 6.13 | Measured heave motion of experiments obtained from Koutandos | 67 |
| 6.14 | Response Amplitude Operator (RAO) for heave by AQWA | 67 |
| 6.15 | Experimental data heave floating breakwater compared with numerical model data | 68 |
| 6.16 | Comparison AQWA with experimental data, FB anchored by chains, undamped | 69 |
| 6.17 | Comparison AQWA with experimental data, FB anchored by chains, damped | 69 |
| 6.18 | RAO's for translations of floating breakwater anchored by chains | 70 |
| 6.19 | RAO's for rotations of floating breakwater anchored by chains | 70 |
| 6.20 | Data AQWA compared with theories for fixed breakwaters | 71 |
| 6.21 | Influence of the variation of width on C_t | 72 |
| 6.22 | Influence of the variation of draft on C_t | 72 |
| 6.23 | Flow chart of application for wave transmission theories | 73 |
| 6.24 | Influence of the variation of width on C_t | 73 |
| 6.25 | Influence of the variation of draft on C_t | 73 |

| | | |
|------|--|----|
| 6.26 | Transmission coefficient for oblique incident waves | 74 |
| 6.27 | Effective width for oblique incident waves | 74 |
| 6.28 | Location where the transmitted waves are calculated due to oblique incident waves | 75 |
| 6.29 | Oblique waves in AQWA | 75 |
| 6.30 | Effect of oblique incident waves on C_t for fixed breakwaters | 76 |
| 6.31 | Effect of oblique incident waves on C_t for FB anchored by piles | 76 |
| 6.32 | Flowchart with applicable transmission theories based on exp. and num. data | 78 |
| | | |
| A.1 | Transmission coefficient for single and double pontoon type breakwater | A2 |
| A.2 | Transmission coefficient for A-frame type of breakwater | A2 |
| A.3 | Principle sketch of hinged floating breakwater | A3 |
| A.4 | Theoretical and experimental Transmission coefficients hinged type breakwater | A4 |
| A.5 | Performance for Goodyear and Pipe-tire type breakwaters | A5 |
| A.6 | Theoretical performance of tethered float type of breakwater | A6 |
| A.7 | Porous walled breakwater | A6 |
| A.8 | Performance of perforated walled type breakwater | A7 |
| A.9 | Performance of the wave trap type breakwater | A8 |
| | | |
| B.1 | Linearised basic equations and boundary conditions for linear wave theory | B3 |
| B.2 | Propagating harmonic sine wave | B4 |
| B.3 | Wave record analysis | B5 |
| B.4 | One-dimensional variance density spectrum | B5 |
| B.5 | Two-dimensional variance density spectrum | B6 |
| | | |
| C.1 | Experimental data for fixed FB compared with wave transmission theories, regular waves | C2 |
| C.2 | Differences of C_t between theories and experimental data, fixed FB, regular waves | C2 |
| C.3 | Experimental data for fixed FB compared with wave transmission theories, irregular waves | C3 |
| C.4 | Differences of C_t between theories and experimental data, fixed FB, irregular waves | C4 |
| C.5 | Experimental data for fixed FB compared with wave transmission theories, irregular waves | C4 |
| C.6 | Differences of C_t between theories and experimental data, fixed FB, irregular waves | C4 |
| C.7 | Data from Deltares, regular waves | C6 |
| C.8 | Differences between theories and experimental data Figure C.7 | C6 |
| C.9 | Data from Deltares, regular waves | C6 |
| C.10 | Differences between theories and experimental data Figure C.9 | C6 |
| C.11 | Data from Deltares, regular waves | C6 |
| C.12 | Differences between theories and experimental data Figure C.11 | C6 |
| C.13 | Data from Deltares, regular waves | C7 |
| C.14 | Differences between theories and experimental data Figure C.13 | C7 |
| C.15 | Data from Deltares, irregular waves | C7 |
| C.16 | Differences between theories and experimental data Figure C.15 | C7 |
| C.17 | Data from Deltares, irregular waves | C8 |
| C.18 | Differences between theories and experimental data Figure C.17 | C8 |
| C.19 | Data from Deltares, irregular waves | C8 |

| | |
|---|-----|
| C.20 Differences between theories and experimental data Figure C.19 | C8 |
| C.21 Data from Deltares, irregular waves | C8 |
| C.22 Differences between theories and experimental data Figure C.21 | C8 |
| C.23 Experimental data Cox et al. compared with transmission theories, regular waves . . . | C10 |
| C.24 Experimental data Cox et al. compared with transmission theories, irregular waves . . | C10 |
| C.25 Differences between theories and experimental data Figure C.23 for $H_s=0.4m$ | C10 |
| C.26 Differences between theories and experimental data Figure C.23 for $H_s=0.8m$ | C10 |
| C.27 Differences between theories and experimental data Figure C.24 for $H_s=0.4m$ | C10 |
| C.28 Differences between theories and experimental data Figure C.24 for $H_s=0.8m$ | C10 |
| C.29 Data Koutandos et al. compared with transmission theories, regular waves, fixed FB . | C11 |
| C.30 Data Koutandos et al. compared with transmission theories, irregular waves, fixed FB . | C11 |
| C.31 Data Koutandos et al. compared with transmission theories, irregular waves, heave FB | C11 |
| C.32 Differences between theories and experimental data Figure C.31 | C11 |
| C.33 Data Martinelli et al. compared with transmission theories, irregular waves, heave FB . | C12 |
| C.34 Differences between theories and experimental data Figure C.33 | C12 |
| C.35 Data Pena et al. compared with transmission theories, regular waves, free FB | C14 |
| C.36 Differences between theories and experimental data of Figure C.35 | C14 |
| C.39 Data Pena et al. compared with transmission theories, regular waves, free FB | C14 |
| C.40 Differences between theories and experimental data of Figure C.39 | C14 |
| C.37 Data Pena et al. compared with transmission theories, regular waves, free FB | C14 |
| C.38 Differences between theories and experimental data of Figure C.37 | C14 |
| C.41 Data Brebner and Ofuya compared with transmission theories, regular waves, free FB . | C15 |
| C.42 Differences between theories and experimental data of Figure C.41 | C15 |
| C.43 Data Brebner and Ofuya compared with transmission theories, regular waves, free FB . | C16 |
| C.44 Differences between theories and experimental data of Figure C.43. | C16 |
| C.45 Data Brebner and Ofuya compared with transmission theories, regular waves, free FB . | C16 |
| C.46 Differences between theories and experimental data of Figure C.45. | C16 |
| C.47 Data Martinelli et al compared with transmission theories, regular waves, free FB . . . | C17 |
| C.48 [Differences between experimental data and theories, 3D tests, regular waves | C17 |
| C.49 Differences between experimental data and theories, 2D tests, regular waves | C17 |
| C.50 Experimental data from Gesraha [2006], $(d) = 0.425m$ and $(Th) = 5.89s$, irregular waves | C18 |
| C.51 Differences between theories and experimental data Figure C.50 | C18 |
| | |
| D.1 Stokes waves | D2 |
| D.2 Applicability for different wave theories | D2 |
| D.3 Definition of velocity potential | D3 |
| D.4 Streamlines | D4 |
| D.5 Streamlines and potential lines | D5 |
| D.6 Potential flow element, source and sink | D7 |
| D.7 Potential flow element, uniform flow | D7 |
| D.8 Potential flow of line source and sink | D8 |
| D.9 Doublet or Dipole flow | D8 |

| | |
|---|-----|
| D.10 Rankine oval | D8 |
| D.11 Summary of fluid forces | D10 |
| D.12 Effect of draft on Ct modeled with AQWA | D12 |
| D.13 Effect of width on Ct modelled with AQWA | D13 |
| D.14 Effect of draft on Ct modelled with AQWA, heave FB | D14 |
| D.15 Effect of width on Ct modelled with AQWA, heave FB | D15 |

List of Tables

| | | |
|------|---|----|
| 5.1 | Experimental data floating breakwaters used in Figure 5.8 | 37 |
| 5.2 | RMSE Pena et al, regular waves, floating breakwater anchored by chains | 42 |
| 5.3 | Experimental data fixed floating breakwaters | 42 |
| 5.4 | Ratios of wavelength to water depth | 42 |
| 5.5 | RMSE for Kriebel and Bollmann | 43 |
| 5.6 | RMSE for Macagno | 43 |
| 5.7 | Experimental data floating breakwaters anchored by piles | 44 |
| 5.8 | RMSE for the theory of Wiegel for the dataset of Deltares | 44 |
| 5.9 | RMSE Cox et al. heave floating breakwater | 45 |
| 5.10 | RMSE of Koutandos et al. heave floating breakwater | 45 |
| 5.11 | RMSE for the theory of Kriebel and Bollmann for the dataset of Martinelli | 46 |
| 5.12 | Experimental data floating breakwaters anchored by chains | 47 |
| 5.13 | Lowest RMSE for different theories for the dataset of Martinelli et al. | 47 |
| 5.14 | Ratios of wavelength to breakwater width | 47 |
| 5.15 | Lowest RMSE for different theories for the dataset of Brebner and Ofuya | 48 |
| 5.16 | RMSE for different theories of for the dataset of Martinelli et al. | 49 |
| 5.17 | RMSE for different theories for the dataset of Gesraha | 49 |
| | | |
| 6.1 | Diffraction results of AQWA for a bottom mounted breakwater | 61 |
| 6.2 | Number of panels used for the calculations to investigate the effect of the mesh size | 64 |
| 6.3 | Input (T) and the computed output (Ct) used for the model to investigate mesh sizes | 64 |
| 6.4 | Results AQWA compared with data obtained for fixed breakwater | 65 |
| 6.5 | Peak wave period as input for wave periods in AQWA | 66 |
| 6.6 | Results AQWA compared with data for heave floating breakwater | 67 |
| | | |
| C.1 | Experimental data fixed floating breakwaters | C1 |
| C.2 | RMSE Koutandos et al. regular waves | C3 |
| C.3 | RMSE Koutandos et al. irregular waves | C3 |
| C.4 | RMSE Gesraha irregular waves | C5 |
| C.5 | Experimental data floating breakwaters anchored by piles | C5 |
| C.6 | RMSE Deltares regular waves | C7 |
| C.7 | RMSE Deltares irregular waves | C9 |

| | | |
|------|--|-----|
| C.8 | RMSE Cox et al. regular waves | C9 |
| C.9 | RMSE Cox et al. irregular waves | C9 |
| C.10 | RMSE Koutandos et al. irregular waves, heave | C12 |
| C.11 | RMSE Koutandos et al. regular waves, heave | C12 |
| C.12 | RMSE Marinelli et al. irregular waves, heave | C13 |
| C.13 | Experimental data floating breakwaters anchored by chains | C13 |
| C.14 | RMSE Pena et al. regular wave, free floating breakwater | C15 |
| C.15 | RMSE Brebner and Ofuya, regular waves, free floating breakwater | C16 |
| C.16 | RMSE Martinelli et al. irregular waves, free floating breakwater | C17 |
| C.17 | RMSE Gesraha, irregular waves, free floating breakwater | C18 |
| | | |
| D.1 | Results AQWA compared with data for fixed breakwater $D=0.4$ | D11 |
| D.2 | Results AQWA compared with fixed breakwaters $D=0.5m$ | D11 |
| D.3 | Results AQWA compared with fixed breakwater $D=0.67m$ | D11 |
| D.4 | Results AQWA compared with data heave floating breakwater | D12 |

List of Symbols

Roman symbols

| Symbol | Meaning | Unit |
|--------|-------------------------------|-----------------------|
| a | Wave amplitude | [m] |
| A | Added mass | [kg] |
| B | Width of floating structure | [m] |
| c | Phase speed of a wave | [m/s] |
| C | Hydrodynamic damping constant | [N s/m] |
| C_r | Reflection coefficient | [-] |
| C_t | Transmission coefficient | [-] |
| C_d | Diffraction coefficient | [-] |
| D | Draft of floating structure | [m] |
| d | Water depth | [m] |
| E | Expected value | [-] |
| E_d | Dissipated wave energy | [J/m ²] |
| E_i | Incident wave energy | [J/m ²] |
| E_r | Reflected wave energy | [J/m ²] |
| E_t | Transmitted wave energy | [J/m ²] |
| F | Force | [N] |
| f | Frequency | [Hz] |
| g | Gravitational acceleration | [m/s ²] |
| H | Wave height | [m] |
| H_i | Incident wave height | [m] |
| H_r | Reflected wave height | [m] |
| H_R | Radiated wave height | [m] |
| H_t | Transmitted wave height | [m] |
| k | Wave number | [rad/m] |
| K | Hydrodynamic spring constant | [N/m] or [Nm/rad] |
| L | Wavelength | [m] |
| m | Mass | [kg] |
| M | External moment | [Nm] |
| p | Pressure | [N/m ²] |
| Q | Amount of overtopping water | [m ³ /m/s] |
| Q | Discharge | [m ³ /s] |
| t | Time | [s] |
| T | Wave period | [s] |
| T_p | Peak wave period | [s] |
| u_x | Velocity in x-direction | [m/s] |
| u_y | Velocity in y-direction | [m/s] |

| Symbol | Meaning | Unit |
|--------|-------------------------|-------|
| u_z | Velocity in z-direction | [m/s] |
| x_a | Amplitude surge motion | [m] |
| y_a | Amplitude sway motion | [m] |
| z_a | Amplitude heave motion | [m] |

Greek symbols

| Symbol | Meaning | Unit |
|-----------------------------|---------------------------------------|---------|
| α | Phase angle | [rad] |
| η | Surface elevation | [m] |
| ω | Radian frequency | [rad/s] |
| ϕ | Velocity potential function | [-] |
| ϕ_a | Amplitude roll motion | [rad] |
| ψ_a | Amplitude yaw motion | [rad] |
| θ | Angle relative to the positive x-axis | [rad] |
| θ_a | Amplitude pitch motion | [rad] |
| $\varepsilon_{\phi\zeta}$ | Phase angle roll motion | [rad] |
| $\varepsilon_{\psi\zeta}$ | Phase angle yaw motion | [rad] |
| $\varepsilon_{\theta\zeta}$ | Phase angle pitch motion | [rad] |
| $\varepsilon_{x\zeta}$ | Phase angle surge motion | [rad] |
| $\varepsilon_{y\zeta}$ | Phase angle sway motion | [rad] |
| $\varepsilon_{z\zeta}$ | Phase angle heave motion | [rad] |
| ζ_{ϕ} | Roll motion | [rad] |
| ζ_{ψ} | Yaw motion | [rad] |
| ζ_{θ} | Pitch motion | [rad] |
| ζ_x | Surge motion | [m] |
| ζ_y | Sway motion | [m] |
| ζ_z | Heave motion | [m] |

Chapter 1

Introduction

This chapter introduces the thesis topic: '*Effectiveness of Floating Breakwaters*' and discusses the motive for conducting research on this topic together with the scope of work, objectives and research questions.

1.1 Background

Breakwaters are structures located in water and are used to protect an area against waves, a port for instance. Floating breakwaters are classified as a special type of breakwater and are applied at locations where conventional breakwaters are not suitable to apply [Verhagen et al., 2009]. In general it is attractive to apply a floating breakwater in deep waters where short waves occur. Situations like this are for example deep lakes where only wind waves are present. One of the main advantages of applying a floating breakwater in a marina is that the layout of the marina can easily be changed and the floating structure can also be used as walkway. From an economical point of view it is often cheaper to apply a floating breakwater in deep waters instead of a conventional breakwater [Elchahal et al., 2008].

The application of floating breakwaters for ports is less common. This is because ports are often located near seas or oceans where higher and longer waves occur than in (deep) lakes. Floating breakwaters have historically been ineffective in these harsher ocean environments [Briggs et al., 2002]. The main reason for this is that the wave length relative to the width of the floating breakwater is large, causing the floating breakwater to move up- and downwards on the wave without attenuating wave energy. In order to achieve better wave attenuation, the floating breakwater needs to have a large width relative to the wave length, resulting in very large and uneconomical designs.

1.2 Motivation for research

The main objective of a floating breakwater is to protect an area against undesirable wave heights. One of the most important boundary conditions of a marina design is the allowable downtime. This is the time period in which the marina cannot fulfill its function, which is preventing unwanted ship movements. Downtime occurs when a certain wave height is exceeded that causes unwanted ship movements. This implies that waves transmitted by the floating breakwater into the marina determine the downtime. Therefore, the wave transmission coefficient of the floating breakwater is

the most important parameter determining its effectiveness. The wave transmission coefficient, C_t , is defined as the ratio of the transmitted wave height (H_t) to the incident wave height (H_i). A low wave transmission coefficient implies effective wave attenuation. Because the wave transmission coefficient is an important parameter for the determination of the effectiveness, it is necessary to determine this parameter as accurate as possible during the design stage.

Over the past two decades, floating breakwaters are applied more often in marinas, particularly in areas with large water depths [Elchahal et al., 2008]. The effectiveness of a floating breakwater strongly depends on the incident wave period and the dimensions of the structure, which makes it a complex problem. From previous engineering- and research projects on floating breakwaters, it turned out that the effectiveness of floating breakwaters is often overestimated during the design stage. One of the main reasons for the overestimation of the effectiveness of floating breakwaters are the simplified design formulas used to calculate the wave transmission. These design formulas do not take all the processes of wave attenuation into account, e.g. energy dissipation, overtopping and motions of the floating structure (a more detailed description is given in section 2.2.6). This overestimation of the effectiveness of floating breakwaters created the need for a method to predict the effectiveness of floating breakwaters more accurately during the design stage.

1.3 Scope and research objectives

The research motive is divided into a problem definition and into a research objective. From this a research question and a number of sub-research questions are formulated, which are shown below.

1.3.1 Problem definition

The problem is defined as follows:

'The effectiveness of floating breakwaters is often overestimated during the design process'

1.3.2 Research objective

The objective is defined as follows:

'Identifying the steps which can be taken during the design process, in order to predict the effectiveness of floating breakwaters more accurately'

1.3.3 Research questions

The research question is defined as follows:

'Which steps should be executed during the design process in order to predict the effectiveness of a floating breakwater more accurately?'

The sub-research questions are:

1. Which simplified design formula for wave transmission is the most appropriate to apply for the design of floating breakwaters?
2. Which processes are missing in the present design methods that cause the overestimation of the effectiveness of floating breakwaters?

3. How can these processes be included in the design process?
4. Does the wave transmission coefficient change for more realistic wave conditions than generally included in design formulas, like a 2D-wave spectrum with oblique incident waves?
5. What are the differences related to wave transmission when a floating breakwater is designed according to the simplified design formulas and a more complete model?

1.4 Approach

This thesis is divided into two phases. Each phase consists out of a number of steps which will be elaborated in order to obtain answers for the research questions.

Phase I

This phase is a study of literature on floating breakwaters. In this study several types of floating breakwaters are examined together with their transmission coefficients. Besides this, the most commonly used formulas for wave transmission are compared with each other and are compared with experimental data. The following steps are part of this phase:

- Step 0: Thesis approach and brief introduction to breakwaters in general.
- Step 1: Gain information about the types of floating breakwaters and their wave attenuating characteristics.
- Step 2: Describe the processes which are involved regarding wave attenuation with a floating breakwater.
- Step 3: Describe and compare the most commonly used design formulas determining wave transmission for pontoon type floating breakwaters.
- Step 4: Comparing the formulas for wave transmission (step 3) with data of physical models for pontoon type floating breakwaters and conclude which theory is the most suitable to apply in practice. The result will be presented in the form of a flow-chart.

Phase II

In this phase the areas of interest for engineering purposes where physical model data is missing or where a poor data agreement is found will be identified. Based on these results a numerical model will be used in order to obtain additional data in these areas of interests. The steps which are part of this phase are:

- Step 5: Identifying the areas of interest for engineering purposes where physical model data is missing and where a poor data agreement is found between the wave transmission theories and physical model data.
- Step 6: Validating the numerical model with existing data.
- Step 7: Use the numerical model to obtain new data in the areas identified in step 5 and investigate the effects of more realistic wave conditions, e.g. oblique incident waves. Finally, the flowchart of step 4 will be modified with the new data and can be used as a guideline during the design process to predict the wave transmission coefficient of floating breakwaters more accurately.
- Step 8: General conclusions are drawn and the research questions are answered.

These above introduced steps will be included in a number of chapters. The outline of chapters and steps is graphically shown in Figure 1.1.

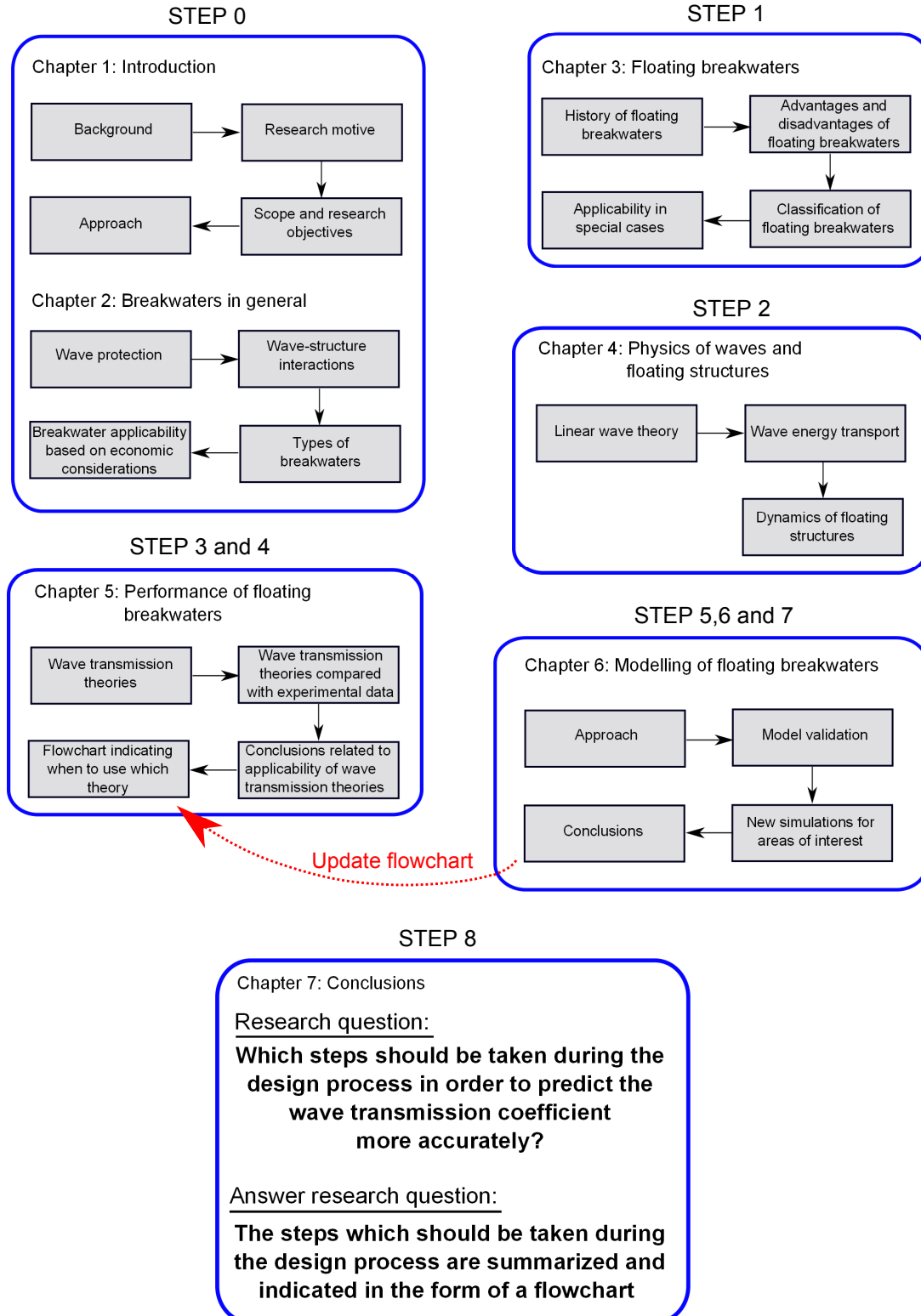


Figure 1.1: Thesis outline

Chapter 2

Breakwaters in general

This chapter introduces the general purpose of a breakwater and the processes involved between the breakwater and waves. Besides this, the most common types of breakwaters are briefly discussed and based on water depth and construction costs a conclusion is drawn related to the applicability of the types of breakwaters.

2.1 Wave protection

Ports are used for decades to receive ships which are transporting all kind of goods around the world. Large ports are playing an important role in the economic development of a country. The first ports were located in sheltered areas, but these areas became soon too small to accommodate larger ships. This resulted in the establishment of ports along the coastline, where higher waves are present. In order to create a suitable area for moored ships, breakwaters were developed to protect ports against waves. Breakwaters are also used to protect coasts against erosion caused by waves.

2.2 Wave-structure interaction

Depending on the type of breakwater, the following phenomena might occur when a wave hits the breakwater:

- Wave reflection;
- Wave run-up;
- Wave transmission;
- Overtopping;
- Diffraction.

2.2.1 Wave reflection

Wave reflection occurs in front of the structure. The reflected wave height (H_r) depends on the porosity and the slope of the structure. The reflected wave height is the product of the reflection coefficient (C_r) and the incoming wave height (H_i), where the reflection coefficient is defined as the ratio of the reflected wave height and the incident wave height, $C_r = H_r/H_i$. For vertical non-porous high walls, where no overtopping occurs, the reflection coefficient can be assumed as 1.0 when energy losses are neglected. In this case all the incoming wave energy will be reflected.

2.2.2 Wave run-up

Wave run-up occurs on the slope of the structure and is defined as the phenomenon in which an incoming wave crest runs up along the slope up to a level that may be higher than the original wave crest [Verhagen et al., 2009]. Run-up plays an important role in the determination of the required crest level for dikes and breakwaters. The wave run-up can be limited by applying a berm or by increasing the roughness of the slope.

2.2.3 Wave transmission

Wave transmission is the phenomenon in which wave energy is passing over, under or through a breakwater, creating a reduced wave (transmitted wave) at the lee side of the structure [Verhagen et al., 2009]. The amount of wave transmission is often expressed with a transmission coefficient, which is defined as the ratio of the transmitted wave height (H_t) and the incident wave height (H_i), $C_t = H_t/H_i$. Wave transmission through a breakwater is possible for relatively long waves and permeable structures. Wave transmission under a breakwater occurs in the case of a floating breakwater. Wave transmission over a breakwater occurs at low crested breakwaters, where a lot of overtopping may occur.

2.2.4 Overtopping

Overtopping is the amount of water passing the crest of a structure per unit of time, it can be seen as the discharge (Q) of water passing the crest of the structure. The dimension is often expressed as the amount of discharge per running meter of the structure [$m^3/s/m$]. At low crested structures considerable amounts of water can overtop the structure causing waves (transmission) at the lee side of the structure.

2.2.5 Diffraction

Diffraction is the turning of waves around objects towards areas which are more sheltered against waves. The wave amplitudes will be lower in these areas due to the lateral spreading of energy. This is illustrated by Figure 2.1. In this figure normal incident waves are approaching the headland. If diffraction were ignored there would be no waves present behind the headland. Due to diffraction there are waves behind the headland. These waves have a lower amplitude compared to the incident waves.

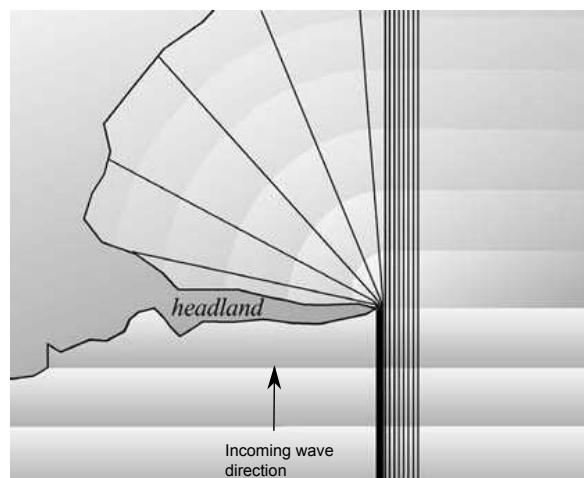


Figure 2.1: Diffraction of waves around a headland with wave rays, [Holthuijsen, 2007]

2.2.6 Wave-floating breakwater interaction

A number of processes occur when a wave hits a breakwater. Figure 2.2 shows the processes which occur when an wave hits a floating breakwater. The incident wave with a wave height H_i contains a certain amount of energy (E_i). When the wave hits the floating breakwater, a part of the incoming wave energy is reflected (E_r), causing a reflected wave (H_r). Another part of the incoming wave energy is transmitted (E_t). The transmitted wave height (H_t) is caused by the transmitted wave energy under the breakwater, the overtopped amount of water and by the radiated waves (H_r) caused by the motions of the floating structure. The flow under the floating structure encounters friction of the structure and loses energy. At the edges of the structure energy is dissipated and converted into turbulence (E_d).

Due to the motions of the floating breakwater waves are induced which are radiating away from the floating breakwater. Depending on the type of anchoring system the breakwater is free to move with a number degrees of freedom. For each motion in each degree of freedom a wave is generated, called the radiated wave. This will be discussed in more detail in Section 4.3.

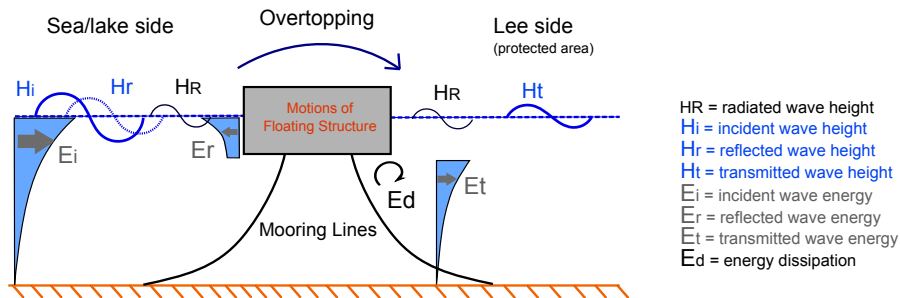


Figure 2.2: Interaction between wave and floating breakwater

2.3 Types of breakwaters

There are many types of breakwaters and they are classified according to their structural features. In literature often distinction is made between conventional and unconventional types of breakwaters. Below these types of breakwaters will be discussed briefly.

2.3.1 Conventional breakwaters

Conventional types of breakwaters are used all around the world and a lot of research has been performed on this topic. This type of breakwater works by reflecting the incoming wave and is mounted on the bottom. Three different types of conventional breakwaters are discussed below, which are the Mound types, Monolithic types and Composite types.

Mound types

Mound types of breakwaters are large heaps of loose elements. These elements may consists out of rock or concrete blocks. This type of breakwater is attractive to apply if the loose elements are available in the vicinity of the breakwater location and in shallow waters (depth < 10m) [Fousert, 2006]. In deeper waters the costs will raise up rapidly because the structure becomes large which requires an enormous amount of materials.

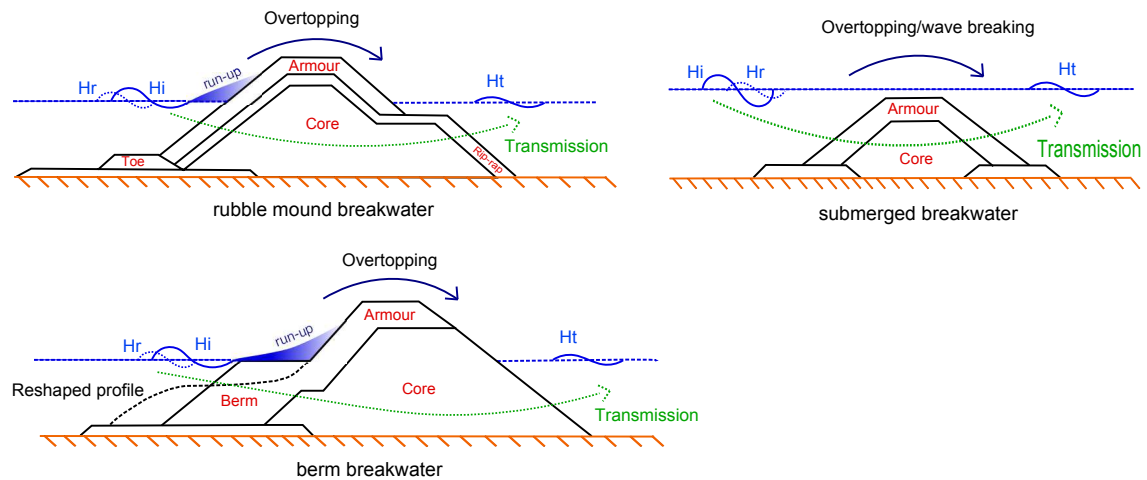


Figure 2.3: Mound breakwater types

Monolithic types

Monolithic breakwaters have a cross-section which acts as one large solid block. Structures of this type are including: a block wall, masonry wall and caissons. This type of breakwater is suitable to apply in medium water depths ($10\text{m} < \text{depth} < 24\text{m}$) [Fousert, 2006], where it becomes cheaper to apply this type of breakwater instead of a mound type of breakwater. It should be noted that the soil conditions must be appropriate to enable a stable foundation of these relatively heavy block elements.

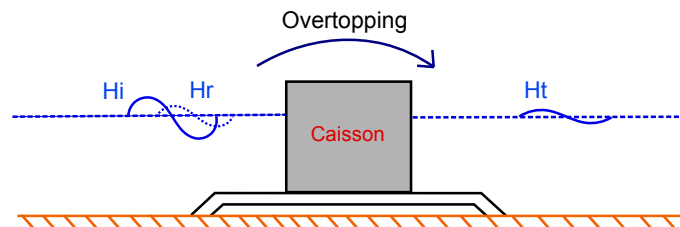


Figure 2.4: Monolithic breakwater type

Composite types

A composite type of breakwater is a monolithic breakwater in combination with a low-crested berm. This type of breakwater is good applicable in deeper waters ($24\text{m} < \text{depth} < 32\text{m}$) [Fousert, 2006] and in areas which have appropriate soil conditions for a stable foundation.

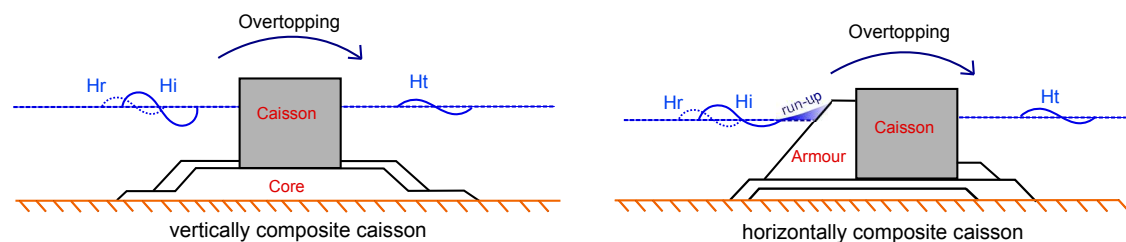


Figure 2.5: Composite breakwater types

2.3.2 Unconventional Breakwaters

Besides the conventional breakwaters, there are many other possibilities to attenuate waves. All these possibilities are included in the group of unconventional- or special type of breakwaters and are often only suitable in special cases. In most standard cases this type of breakwater appears to be uneconomical because of the required high structural strength of the breakwater elements. In deep waters (depths > 20m) floating breakwaters start to become attractive. The following breakwaters are considered to be unconventional [Verhagen et al., 2009]:

- Floating breakwaters;
- Pneumatic breakwaters/hydraulic breakwaters;
- Pile breakwaters;

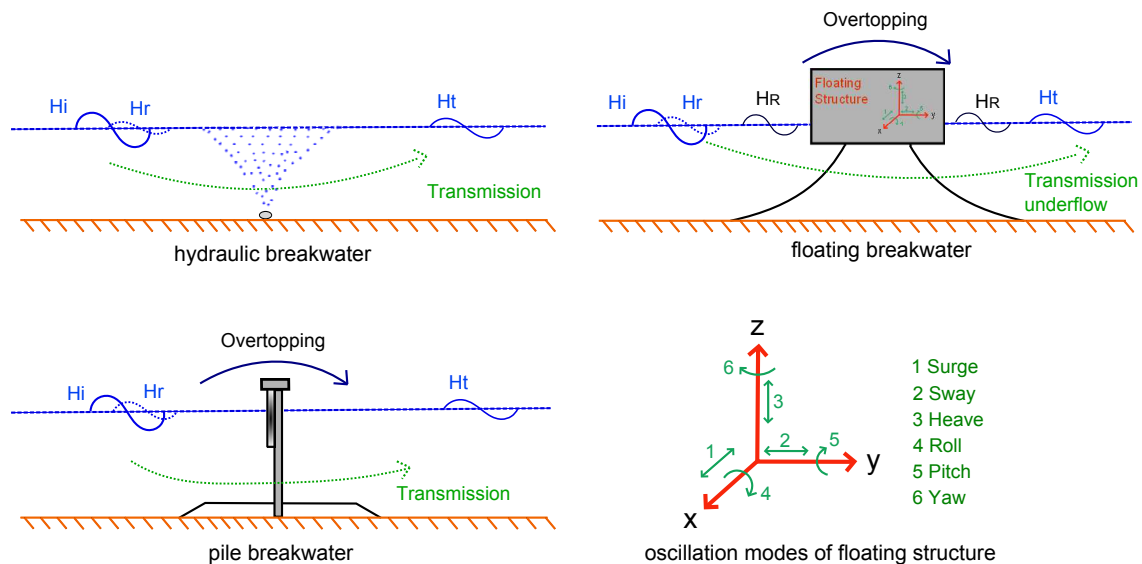


Figure 2.6: Special breakwater types and oscillations floating structures

2.4 Breakwater applicability based on economic considerations

From the above it becomes clear that the applicability of each type of breakwater strongly depends on the water depth, availability of stones in the vicinity of the breakwater location and the local soil conditions. Several publications discuss the construction costs of conventional breakwaters. Fousert [2006] compared these results and added the construction costs of a floating breakwater, his result is shown in Figure 2.7. From this figure it can be seen that the costs of a floating breakwater do not vary a lot with water depth compared to the costs of a conventional breakwater versus water depth. From this it can be concluded that floating breakwaters are an attractive alternative for water depths larger than approximately 30m. This figure shows only the construction costs of four types of breakwaters. Other aspects like maintenance costs and specific site conditions are not taken into account. If these aspects are taken into account the results may vary.

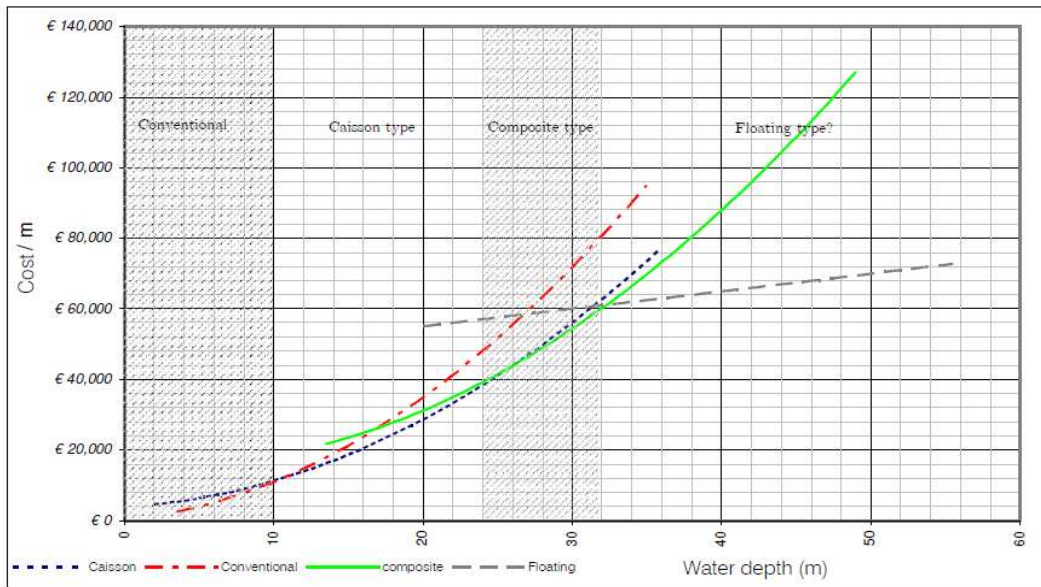


Figure 2.7: Comparison of breakwater costs per running meter depending on the water depth [Fousert, 2006]

Chapter 3

Floating Breakwaters

In the previous chapter different types of breakwaters are discussed. In this chapter the focus will solely be on floating breakwaters. This chapter discusses the history of floating breakwaters and the most commonly used floating breakwaters.

3.1 History of floating breakwaters

One of the first applications of a floating breakwater was in the year 1811, in Great Britain. The aim of this floating breakwater was to provide shelter for the fleet at Plymouth [Morey, 1998]. Since then some small research projects on floating breakwaters were executed mainly in Ireland and in Great Britain, but unfortunately they did not result in building a floating breakwater.

Research continued on floating breakwaters during World War II when a floating breakwater was required during the Normandy invasion. Great Britain developed a floating breakwater to protect men and materials against waves during offloading activities in front of the Normandy coast. This floating breakwater was called the 'Bombardon' and consisted out of several iron elements. The Bombardon breakwater failed during a severe storm which occurred 9 days after the invasion. During this storm stresses occurred which were eight times higher than the elements were designed for. Since this event the interest in floating breakwaters declined until 1957, when the U.S. Navy Civil Engineering Laboratory (NCEL) started to investigate transportable floating units [Hales, 1981]. The objective of these floating units was to protect small working platforms used in cargo transfer operations.

During the 1970s the demand for floating breakwaters for the protection of marinas increased. At that time there was a large demand for marinas while appropriate locations for marinas were scarce. The result was that marinas had to be constructed in deeper waters which were less protected against waves. Floating breakwaters were used to create an appropriate area for these marinas. Due to the increasing demand of floating breakwaters many new types of floating breakwaters were developed. This increased the stimulation for engineers and scientists to develop theoretical models which were able to describe the behaviour of floating structures exposed to waves [Hales, 1981]. Numerical computer models were developed in order to design and to predict the behaviour of floating breakwaters.

3.2 Advantages and disadvantages of floating breakwaters

Whether a floating breakwater is attractive to apply depends strongly on the site specific conditions and on the requirements the floating breakwater has to fulfil. Therefore, determining if a floating breakwater is suitable to apply the advantages and disadvantages have to be taken into consideration. The advantages and disadvantages of a floating breakwater in comparison with a conventional breakwater are briefly summarized below.

3.2.1 Advantages

- At larger water depths they are attractive to apply from economical point;
- Transportability, which enables to change the lay-out of a port easily;
- Applicable at poor soil conditions;
- Hardly any interference with sediment transport processes and water circulation;
- Multiple functions, such as: mooring facilitation, walkway or parking facility (Monaco).

3.2.2 Disadvantages

- Provides less protection against waves;
- Sensitive for wave frequencies close to its natural frequency (resonance);
- Less effective for longer waves;
- Dynamic response to the incoming waves can result into fatigue problems and heavy mooring forces;
- Maintenance costs are higher due to the dynamic response.

3.3 Classification of floating breakwaters

There are many types of floating breakwaters developed throughout the years. In this study only the most common types of floating breakwaters are discussed. Information regarding to the transmission coefficients for these types of floating breakwaters is enclosed as Appendix A.1. Based on the principle on how floating breakwaters attenuate waves, they can be classified into two classes [PIANC, 1994]:

- Reflective structures, these types of structures reflect the incoming wave and are often rigid structures. The term rigid implies here that the structure does not deform under the wave load. In Appendix A.1.1 information of the wave transmission coefficients is shown for these types of floating breakwaters.
- Dissipative structures, these types of structures dissipate wave energy by turbulence, friction and non-elastic deformation. Often these structures are flexible. In Appendix A.1.2 information of the wave transmission coefficients is shown for these types of floating breakwaters.

3.3.1 Reflective structures

Single pontoon and double pontoon

This type of floating breakwater is one of the simplest forms of floating breakwaters and is extensively researched with numerical models and physical models in wave flumes. Its prismatic shape offers good possibilities for multiple use such as mooring facility for ships, storage areas and walkways.

The effectiveness of floating breakwaters anchored by chains or cables is determined by the metacenter and the radius of gyration. The metacenter is the intersection point of the lines through the vertical buoyant forces at a zero angle of heel and at an angle of heel, ϕ . The position of the metacenter depends on the shape of the structure at and near its water plane [Journee and Massie, 2001]. When a floating object is making an angle ϕ , the position of the metacenter changes. Due to the angle ϕ , the shape of the under water part of the structure will also change and the center of buoyancy will shift. This is graphically shown in Figure 3.1, where B represents the center of buoyancy, G represents the center of gravity and N_ϕ represents the metacenter due to the angle ϕ . In order to obtain equilibrium with the external heeling moment, M_H , there must be a righting stability moment M_S which equals M_H :

$$M_H = M_S = \rho g \nabla \overline{GZ} = \rho g \nabla \overline{GN}_\phi \sin(\phi) \tag{3.1}$$

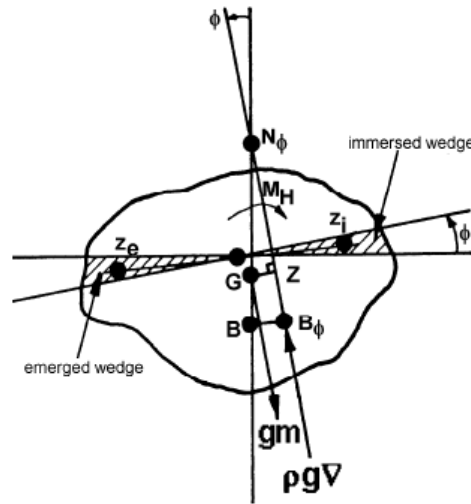


Figure 3.1: Rotational equilibrium at an angle of heel ϕ , [Journee and Massie, 2001]

In Eq.(3.1) ∇ is the displaced volume of water, \overline{GZ} is the righting stability lever arm and \overline{GN}_ϕ is the distance between the center of gravity and the metacenter. From Eq.(3.1) it becomes clear that the distance between the metacenter and the center of gravity (\overline{GN}_ϕ) has a large influence on the stability of the pontoon. From this equation it also follows that for a wide pontoon the righting stability lever arm will be large, hence a more stable pontoon. For double pontoons this is the case and therefore these types can serve as a floating pier where cargo can be offloaded. Appropriate materials to construct these pontoons are concrete and steel.

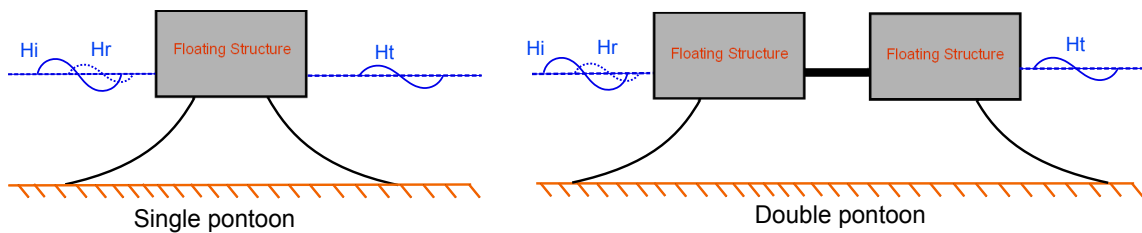


Figure 3.2: Floating breakwater, Pontoon type

A-frame

This type of floating breakwater is applied in many parts of the United States and in Canada. In these countries there is a large availability of timber by which these breakwaters can be constructed [Hales, 1981]. Its effectiveness can be increased significantly by increasing the metacentric height, which is discussed previously. This type of floating breakwater may also be classified as a double pontoon breakwater, because it consists out of two pontoons in which between a vertical wall is located.

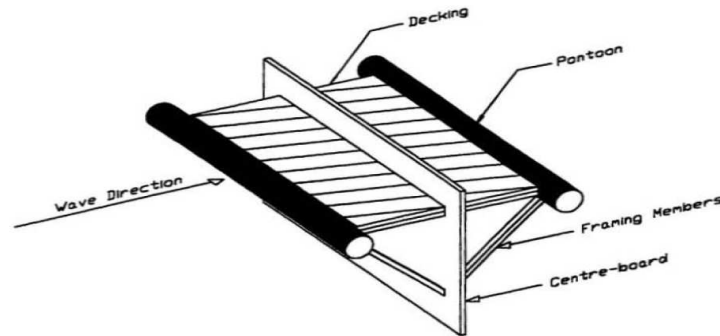


Figure 3.3: Floating breakwater, A-frame type [Morey, 1998]

Hinged floating breakwater

The hinged floating breakwater [Leach et al., 1985] is a vertical wall extending through the water level and is connected by a hinge at the bottom. Cables which are running under an angle of 45 degrees relative to the bottom connect the top of the wall with the bottom. The restoring forces are coming from the buoyancy of the wall and from the cables.

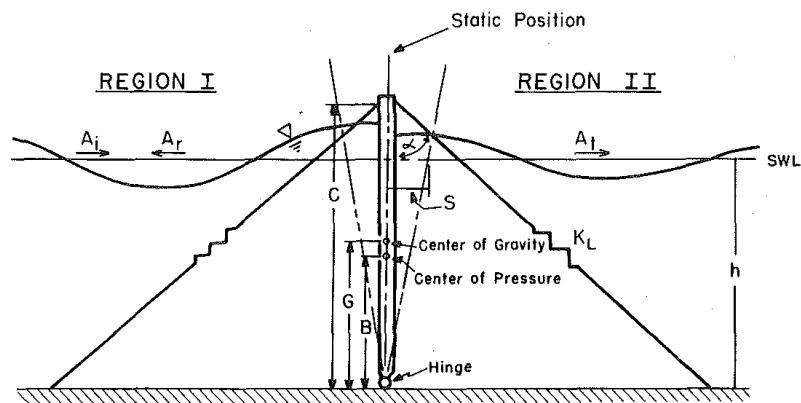


Figure 3.4: Floating breakwater, Hinged type [Leach et al., 1985]

3.3.2 Dissipative structures

Scrap-tire floating breakwater

Different floating breakwater designs are made which consists out of old tires of trucks and cars. Several investigators like rubber companies and coastal engineers investigated the possibilities to absorb wave energy with rubber [Hales, 1981]. Some floating breakwaters are consisting completely

out of rubber, like the design developed by Goodyear. The wave is influenced by this type of breakwater in at least three ways [PIANC, 1994]:

- Their mass, inertia and damping characteristics induce the first attenuation;
- They form a semi-flexible sheet which tends to follow the fluctuations of the water surface. This sheet will limit the vertical displacements;
- Their large porosity generates drag forces which contributes to energy losses.

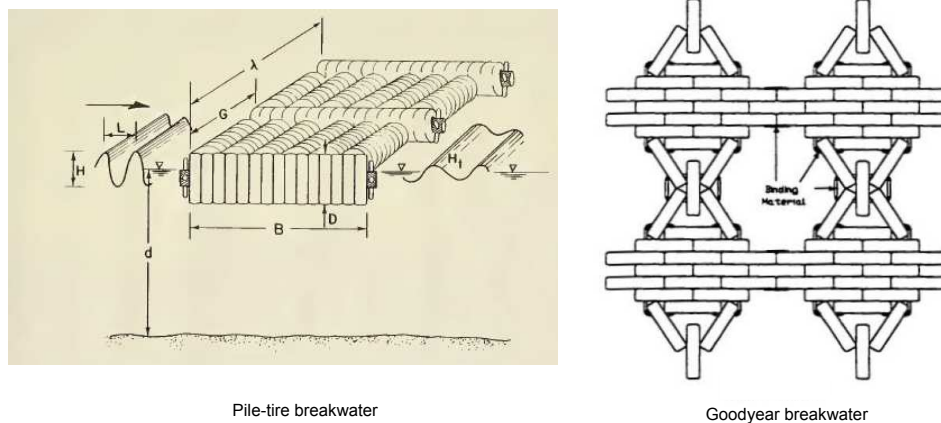


Figure 3.5: Floating breakwater, scrap tire types [Harms et al., 1982]

Tethered-float breakwater

The tethered-float breakwater consists of a submerged pontoon which is anchored with cables to the seabed. Due to the buoyancy of the pontoon the cables are always under tension. On the pontoon a large number of floats are attached with cables. The floats are at or just below the water level surface. The wave attenuating effect can be achieved as follows:

- Due to the fluctuating pressure gradient the floats will move and cause drag which results in energy losses [Hales, 1981];
- When the floats are excited by a wave which period is near to the natural period of the floats, the floats tends to oscillate out of phase with the incident wave and cause high relative flow velocities which results in large friction, hence large energy dissipation [PIANC, 1994].

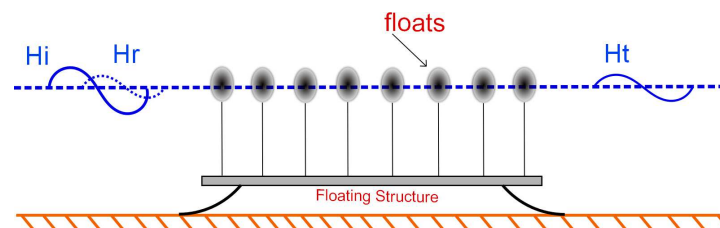


Figure 3.6: Floating breakwater, Tethered float

Porous-Walled

These types of structures float at or just below the water surface and are the most effective in short period wave conditions. The wave attenuating effect is obtained by creating drag and turbulence.

Major eddy formation occurs as well as the fluid moves between the breakwater members, which increases the loss of energy.

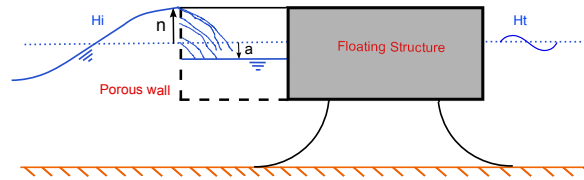


Figure 3.7: Floating breakwater, porous wall

Flexible membrane

For short waves in deep water most wave energy is presented in the upper part of the water column, therefore it is not necessary to have a floating structure with a deep draft. A flexible floating breakwater may attractive to apply in short wave and deep water situations.

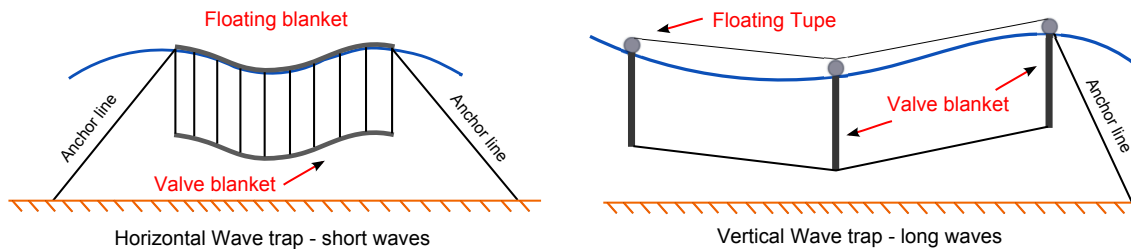


Figure 3.8: Floating breakwater, Wave trap (membrane)

The most successful membrane-type for shorter waves consists of a floating blanket on which a second blanket, below the floating blanket is attached by lines. The submerged blanket has valves creating a maximum resistance when rising and minimum resistance when falling. The wave amplitude will be reduced by the large water mass between the blankets, this is because the incoming wave tends to accelerate the water mass. This type of wave attenuator is developed by the U.S. rubber company.

For longer waves the valved blankets are placed vertically and are attached to floating tubes. The orbital motions of the water particles will be reduced by the blankets and hence energy dissipation. Figure 3.8 shows the wave trap principle for relatively short and long waves.

3.4 Applicability in special cases

Besides the application of a floating breakwater in deep waters in combination with short waves, there are some other applications where floating breakwaters maybe suitable to apply.

Floating Ports

Due to the rapidly increasing growth of ships, ports needs to have larger water depths in order to accommodate these large ships. Ports with large water depths are often very expensive to construct because of the high quay walls and the large amount of dredging works required. Therefore it might be attractive to build floating ports which can be located in deep waters. From studies which are covering this topic (see also Ali [2006] and De Rooij [2006]) it can be concluded that the efficiency of floating ports is strongly determined by the wave climate. To enable save (off)loading of cargo,

it is necessary to prevent high waves in the port which causes unwanted ship movements. In order to make a floating port feasible a floating breakwater will be necessary to attenuate the wide wave spectrum of oceans and large seas [Ali, 2006]. A major disadvantage of a floating breakwater in an oceanic environment, are storms with waves heights up to 6 meter and associated periods up to 18 seconds [Briggs et al., 2002]. In order to attenuate these waves, a very large floating breakwater is required which is in most cases an uneconomic solution.

Offshore Engineering

Another field in which floating breakwaters may be attractive to apply is in offshore engineering. Offshore windmill parks are booming business these days and the development of these parks is growing rapidly. In order to execute maintenance on these windmills it is not desirable to have large waves, resulting in a large downtime of maintenance works. A floating breakwater is relatively easy to transport and may be suitable to reduce large wave heights to acceptable wave heights, which do not hinder maintenance activities. In this case maintenance can be continued for a longer period of time. The same holds for maintenance activities to other offshore located structures. Because the floating breakwater is not a permanent structure in this case and maintenance will not be executed during storms, the major drawback related to the difficulty of attenuating long waves might be rejected here. However, further research related to the feasibility of this applicability has to be performed.

Local Regulations

Sometimes floating breakwaters are applied at locations where conventional breakwaters seems to be more attractive to apply. Reasons for this are often local regulations. An example of this are the local regulations in Bulgaria. When a conventional breakwater is applied in Bulgaria, it is necessary to apply for a construction permit, which is a time and money consuming job in Bulgaria. When a floating breakwater is applied in Bulgaria, only a mooring permit is necessary, which is much easier to obtain [Drieman, 2011].

3.5 Conclusion

There are different ways to attenuate waves and during the years many different types of floating breakwaters are developed. Each type of floating breakwater has its own theory to determine the wave transmission coefficient. These different theories are discussed in Appendix A.

In the following sections of this report the focus will be on pontoon type floating breakwaters. The reasons to focus on this type of floating breakwater are as follows:

- There is a lot of experimental data available for pontoon type floating breakwaters which makes it possible to compare theories with experimental data;
- Pontoon type floating breakwaters can fulfill several functions, e.g. floating jetty or storage platforms and are therefore attractive to apply;
- There are a number of theories to predict the wave transmission coefficient of pontoon type floating breakwaters.

Chapter 4

Physics of waves and floating structures

This chapter discusses the motions of floating breakwaters (pontoon types) caused by the incoming waves. The effectiveness of floating breakwaters largely depends on the incoming waves, therefore a short description of waves will be given first. Secondly, a simple model will be given which describes the motions of the floating breakwater due to the incoming waves.

4.1 Linear wave theory

Ocean waves can be described by linear wave theory. The most interesting result of this theory is a long-crested propagating harmonic wave. Based on this theory, many wave characteristics can be derived. Besides this, most theories on wave transmission (see also Chapter 5) are based on linear wave theory. In order to understand the behaviour of waves and its characteristics, an explanation of linear wave theory is given. For more detailed information and the derivations of the formulas given below, reference is made to Holthuijsen [2007] and Appendix B.

Linear wave theory is based on two equations: a mass balance equation and a momentum balance equation. These two equations are describing the kinematic and dynamic aspects of waves. Waves can be described by linear wave theory when the amplitude of the wave is small compared to the water depth and wave length. In this case non-linear effects of waves are negligible. Furthermore it is assumed that water is an ideal fluid, which implies: incompressible, constant density, no viscosity and no rotation of water particles around their own axis. From the mass balance equation the continuity equation can be derived:

$$\frac{\partial u_x}{\partial x} + \frac{\partial u_y}{\partial y} + \frac{\partial u_z}{\partial z} = 0 \quad (4.1)$$

In which:

- u = velocity
- x, y, z = indicating direction of a 3-dimensional reference frame

The position of the reference frame is located on the mean water level surface, with the positive x-axis towards the right and the positive z-axis upwards, see also Figure 4.1.

To solve this equation use is made of the velocity potential function $\phi = \phi(x, y, z, t)$, shown below as Eq.(4.2). This function is defined as a function of which the spatial derivatives are equal to the velocities of the water particles [Holthuijsen, 2007]. Substituting this in Eq.(4.1) the Laplace equation is obtained (Eq.(4.3)).

$$\text{Velocity potential function : } u_x = \frac{\partial \phi}{\partial x}, \quad u_y = \frac{\partial \phi}{\partial y}, \quad u_z = \frac{\partial \phi}{\partial z} \quad (4.2)$$

$$\text{Laplace equation : } \frac{\partial^2 \phi}{\partial x^2} + \frac{\partial^2 \phi}{\partial y^2} + \frac{\partial^2 \phi}{\partial z^2} = 0 \quad (4.3)$$

Boundary conditions can be defined at the water surface (η) and at the bottom in terms of the velocity potential function. The kinematic boundary conditions are:

$$\text{Kinematic boundary conditions } \begin{cases} \frac{\partial \phi}{\partial z} = \frac{\partial \eta}{\partial t} & \text{at } z=0 \\ \frac{\partial \phi}{\partial z} = 0 & \text{at } z=-d \end{cases} \quad (4.4)$$

With the kinematic boundary conditions and the velocity potential function the Laplace equation can be solved. The kinematic boundary condition at the water surface ($z = 0$) represents the vertical velocity of the surface elevation. The kinematic boundary condition at the sea bed ($z = -d$) implies a zero vertical velocity at the seabed. One of the analytical solutions of the Laplace equation with the kinematic boundary conditions is a long-crested harmonic wave, propagating in the positive x-direction. In fact, this wave represents the surface elevation and can be defined as:

$$\eta(x, t) = a \sin(\omega t - kx) \quad (4.5)$$

In which:

- a = wave amplitude [m]
- ω = radian frequency [rad/s], defined as $\frac{2\pi}{T}$, where T is the wave period [s]
- t = time [s]
- k = wave number [rad/m], defined as $\frac{2\pi}{L}$, where L is the wave length [m]

The above solution of the Laplace equation is based on a mass balance (continuity equation) and the kinematic boundary conditions only. This implies that all the kinematic aspects (velocities and accelerations) can be derived from Eq.(4.5). Since wave energy implies the movement of water particles, the equations above are essential for describing the distribution of wave energy in the water column.

When waves are propagating they are transporting energy in the direction of propagation. This horizontal transport of energy is due to the work done by the wave induced pressure [Holthuijsen, 2007]. This wave induced pressure can be described by the dynamic aspects of waves, which are derived from the momentum balance.

Momentum is by definition the mass density of water times the velocity of the water particles. The second law of Newton states that the rate of change of momentum equals force. For momentum in the x-direction the following momentum balance equation is obtained:

$$\frac{\partial(\rho u_x)}{\partial t} + \frac{\partial u_x(\rho u_x)}{\partial x} + \frac{\partial u_y(\rho u_x)}{\partial u_y} + \frac{\partial u_z(\rho u_x)}{\partial z} = F_x \quad (4.6)$$

$$\text{The dynamic boundary condition is defined as pressure } (p): p = 0 \text{ at } z = 0 \quad (4.7)$$

The pressure (p) at the water surface is assumed as zero and functions as a reference pressure since the interest is in the pressures below the water surface. In Eq.(4.6) F_x is the body force in x-direction per unit volume. The second, third and fourth terms are the advective terms and contain non-linear terms. In order to make the theory linear, these terms should be removed from the momentum equation. After applying some mathematics and ignoring the non-linear terms in Eq.(4.6) the linearised Bernoulli equation for unsteady flow is obtained, shown as Eq.(4.8).

$$\frac{\partial \phi}{\partial t} + \frac{p}{\rho} + gz = 0 \quad (4.8)$$

Just as the kinematic boundary condition, it is possible to express the dynamic boundary condition in terms of the velocity potential. This implies $z = \eta$ with $p = 0$ and results in:

$$\frac{\partial \phi}{\partial t} + g\eta = 0 \quad \text{at } z=0 \quad (4.9)$$

The equations above together with the boundary conditions are summarized in Figure 4.1. In this figure the Laplace equation together with the kinematic boundary conditions and the linearised Bernoulli equation with the dynamic boundary conditions are shown.

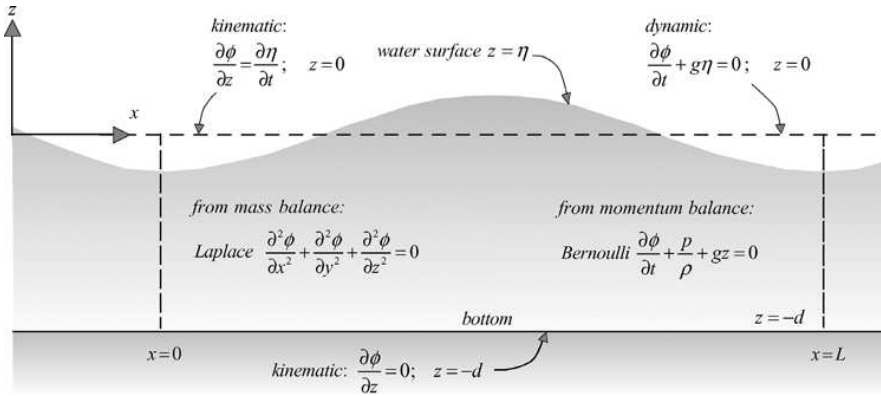


Figure 4.1: Linearised basic equations and boundary conditions for the linear wave theory, in terms of velocity potential [Holthuijsen, 2007]

4.1.1 Regular waves

The most interesting result of linear wave theory is a long-crested propagating harmonic wave. This harmonic wave (regular wave) can be defined as a propagating sinusoidal wave with an amplitude (a), radian frequency (ω) and wave number (k). The equation of the sinusoidal harmonic wave is shown below.

$$\eta(x, t) = \frac{H}{2} \sin \left(\frac{2\pi}{T} t - \frac{2\pi}{L} x \right) = a \sin(\omega t - kx) \quad (4.10)$$

The phase speed is the forward speed (c) by which the wave propagates while the phase ($\omega t - kx$) remains constant. Mathematically this implies that the time derivative of the phase is zero. From this the phase speed is obtained (Eq.4.11). The parameters used in the equations are shown in Figure 4.2.

$$c = \frac{\omega}{k} = \frac{L}{T} \quad (4.11)$$

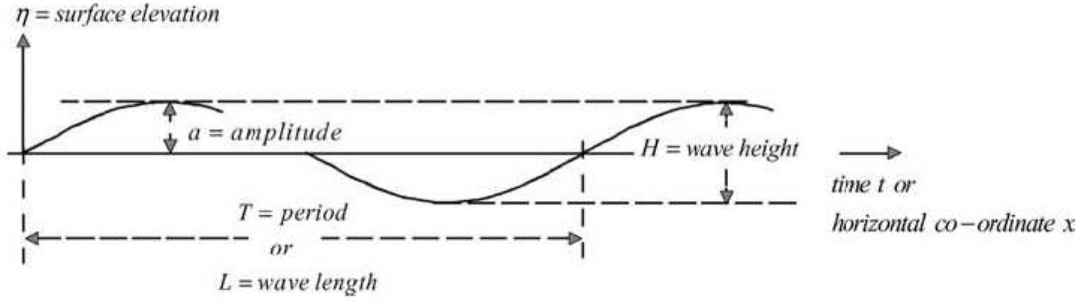


Figure 4.2: Propagating harmonic sine wave, [Holthuijsen, 2007]

4.1.2 Irregular waves

If one observes the water surface, it can be seen that it continuously changes without repeating itself. When the water surface elevation is measured, the resulting signal will be like an irregular wave signal, which can be modelled by the sum of a large number of harmonic wave components:

$$\eta(t) = \sum_{i=1}^N a_i \cos(2\pi f_i t + \alpha_i) \quad (4.12)$$

In which:

- N = large number of frequencies
- α_i = phase
- a_i = amplitude
- f_i = wave frequency

Each wave component is a propagating regular wave which has a sinusoidal shape. From this it follows that the irregular wave signal, which describes the surface elevation, can be decomposed by a Fourier series into a number of harmonic waves, see Figure 4.3. The result is a set of values for the amplitude (a_i) and phase (α_i). Each set of values of a_i and α_i belongs to the frequency f_i . The benefit of this model is that it is possible to describe the waves as a spectrum.

Waves are propagating in a certain direction. The direction can be taken into account by considering the propagation of the harmonic wave in the x, y -plane. If θ is the angle relative to the positive x -axis and using the principles for the one-dimensional variance density spectrum (See Section B.1.2), the two-dimensional variance density spectrum (Figure 4.4) is obtained:

$$E(f, \theta) = \lim_{\Delta f \rightarrow 0} \lim_{\Delta \theta \rightarrow 0} \frac{1}{\Delta f \Delta \theta} E\left\{\frac{1}{2}a^2\right\} \quad (4.13)$$

In which:

- $E(f, \theta)$ = variance density as function of frequency (f) and direction (θ) [$m^2/\text{Hz}/\text{radian}$]
- a = amplitude as a random variable [m]

From the variance density spectrum it is relatively easy to obtain a wave energy density spectrum. This can be obtained by multiplying the variance density spectrum with the density of the water and with the gravitational acceleration. Besides obtaining an energy density spectrum from a variance density spectrum, it is also possible to obtain the response spectrum of motion of a floating breakwater from the variance density spectrum, which is discussed in more detail in Section 4.3.2.

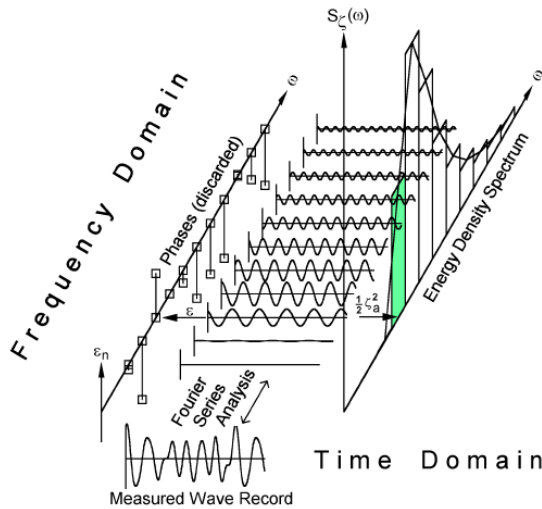


Figure 4.3: Wave record analyses, ζ_a represent wave amplitude, [Journee and Massie, 2001]

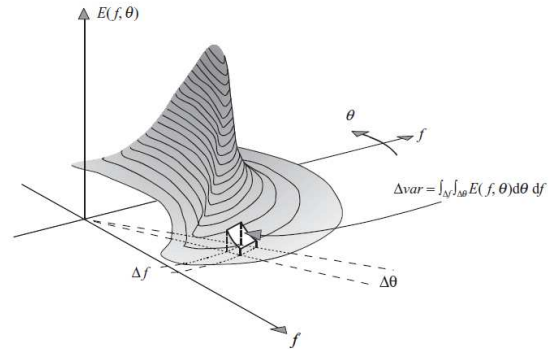


Figure 4.4: Two-dimensional variance density spectrum as the distribution of the total variance of the sea-surface elevation over frequency and direction (polar coordinates), [Holthuijsen, 2007]

4.2 Wave energy transport

In section 2.2.6 a short overview is given of the processes which occur when a wave hits a floating breakwater. These processes are shown in Figure 4.5. Because the transmitted wave depends largely on the amount of wave energy transmission below the structure, the concept of wave energy transport is briefly discussed below.

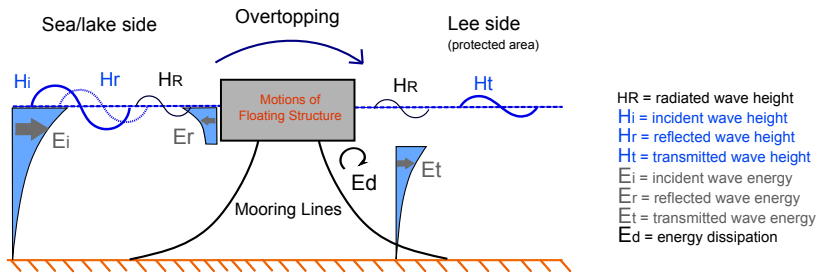


Figure 4.5: Interaction between wave and floating breakwater

A wave at the water surface implies movement of water particles, which represents potential and kinetic energy. The wave induced potential energy (per unit horizontal surface area) can be obtained by considering potential energy as a function of water depth (z) and integrating this function from the mean water level surface ($z = 0$) to the actual water level (η), the result is shown as Eq.(4.14). In this equation the overbar represents time-averaging (one wave period) and a represents the amplitude of a harmonic wave. Figure 4.6 shows the upper and lower boundaries of the integrals.

$$E_{potential} = \overline{\int_0^\eta \rho g z dz} = \frac{1}{2} \overline{\rho g \eta^2} = \frac{1}{4} \rho g a^2 \quad (4.14)$$

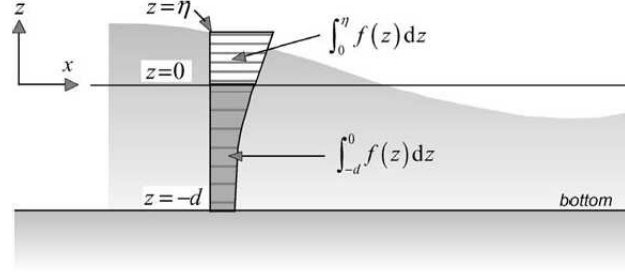


Figure 4.6: Integral from bottom to surface as a function of $f(z)$ beneath the wave, divided into two integrals: one below the mean surface ($z = 0$) and one above. [Holthuijsen, 2007]

Kinetic energy is defined as $\frac{1}{2} \times \text{mass} \times \text{velocity squared}$. The kinetic energy in the entire water column, time-averaged and per unit surfaced area is then:

$$E_{kinetic} = \overline{\int_{-d}^{\eta} \frac{1}{2} \rho u^2 dz} = \frac{1}{4} \rho g a^2 \quad (4.15)$$

With $u = \sqrt{u_x^2 + u_z^2}$ and a represents the amplitude of a harmonic wave. The total wave induced energy density can be described as a function of amplitude (a) or as a function of wave height (H), under the assumption of $a = \frac{1}{2}H$.

$$E = E_{potential} + E_{kinetic} = \frac{1}{2} \rho g a^2 = \frac{1}{8} \rho g H^2 \quad (4.16)$$

The transport of wave energy consists of three contributions, namely: transport of potential energy, kinetic energy and work done by pressure. These contributions are shown in Eq.(4.17). Per unit crest length and time-averaged the energy transport in the positive x-direction is:

$$P_{energy} = \underbrace{\int_{-d}^{\eta} (\rho g z) u_x dz}_{\text{potential energy transport}} + \underbrace{\int_{-d}^{\eta} (\frac{1}{2} \rho u^2) u_x dz}_{\text{kinetic energy transport}} + \underbrace{\int_{-d}^{\eta} (-\rho g z + P_{wave}) u_x dz}_{\text{work done by pressure}} \quad (4.17)$$

The term $\rho g z$ of the first and third expression on the right-hand side of Eq.(4.17) will cancel each other out. The second expression on the right-hand side is third order in amplitude and may be ignored in a second-order approximation. The third expression on the right-hand side is second-order in amplitude and is therefore the only integral to be evaluated. For details of the evaluation of Eq.(4.17) and integration to a certain order accuracy reference is made to Holthuijsen [2007]. If the phase speed is represented by c then the solution of Eq.(4.17) is:

$$P_{energy} = Enc \quad \text{with} \quad E = \frac{1}{2} \rho g a^2 \quad \text{and} \quad n = \frac{1}{2} \left(1 + \frac{2kd}{\sinh(2kd)} \right) \quad (4.18)$$

4.3 Dynamics of floating breakwaters

Water waves cause periodic loads on floating breakwaters. In response to these periodic loads the floating structure accelerates and displaces, causing internal forces in the structure and in the mooring system. In this section the equations which describes the motion of the floating breakwater are discussed.

A floating body in a three-dimensional reference frame has six degrees of freedom. Three translations of the structures center of gravity in the direction of the x -, y - and z -axes and three rotations around these axes. Figure 4.7 shows these translations and rotations for a pontoon type floating breakwater.

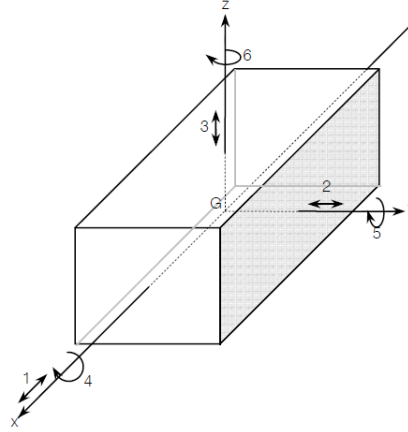


Figure 4.7: Degrees of freedom for a floating body in a three-dimensional space, [Fousert, 2006]

The incoming wave is a harmonic wave and therefore the equations describing the motions of the structure will be harmonic as well. When the motions of the centre of gravity are known, the motions in any point on the structure can be calculated by the use of superposition. The motions of the floating body's center of gravity can be described by the following equations [Journee and Massie, 2001]:

$$\begin{aligned}
 1. \text{ Surge: } & x = x_a \cos(\omega_e t + \varepsilon_{x\zeta}) \\
 2. \text{ Sway: } & y = y_a \cos(\omega_e t + \varepsilon_{y\zeta}) \\
 3. \text{ Heave: } & z = z_a \cos(\omega_e t + \varepsilon_{z\zeta}) \\
 4. \text{ Roll: } & \phi = \phi_a \cos(\omega_e t + \varepsilon_{\phi\zeta}) \\
 5. \text{ Pitch: } & \theta = \theta_a \cos(\omega_e t + \varepsilon_{\theta\zeta}) \\
 6. \text{ Yaw: } & \psi = \psi_a \cos(\omega_e t + \varepsilon_{\psi\zeta})
 \end{aligned} \tag{4.19}$$

In which:

$$\begin{aligned}
 n_a &= \text{Motion amplitude [m], [rad]} \\
 \varepsilon_{n\zeta} &= \text{Phase angle [rad]} \\
 \omega &= \text{Circular wave frequency [rad/s]}
 \end{aligned}$$

4.3.1 Dynamics of floating structures in regular waves

The equations which are describing the motion of a floating rigid structure are derived from the second law of Newton. From this two vector equations are obtained [Journee and Massie, 2001], one for describing translations (Eq.4.20a) and one for describing rotations (Eq.4.20b).

$$\vec{F} = \frac{d}{dt} (m\vec{U}) \tag{4.20a}$$

$$\vec{M} = \frac{d}{dt} (\vec{H}) \tag{4.20b}$$

In which:

- \vec{F} = resulting external force acting in the center of gravity [N]
- m = mass of rigid body [kg]
- \vec{U} = instantaneous velocity of the center of gravity [m/s]
- \vec{M} = resulting external moment acting about the center of gravity [Nm]
- \vec{H} = instantaneous angular moment about the center of gravity [Nms]
- t = time [s]

In many cases the motions of floating structures have a linear behaviour. This implies that when the amplitude of the excitation force is doubled, the amplitude of response will be doubled as well, while the phase shifts between the response and excitation does not change.

Because a floating structure is a linear system, superposition of the oscillations of the structure in still water and the forces acting on the restrained structure in waves can be applied in order to derive the resulting motion of the structure. This is illustrated by Figure 4.8 below.

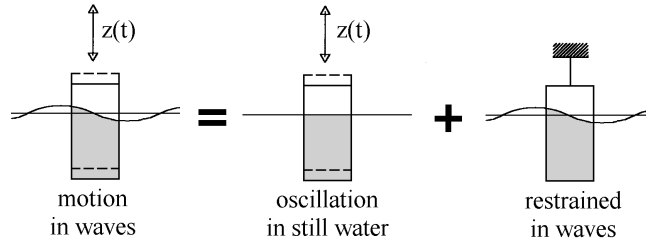


Figure 4.8: Superposition of Hydromechanical and Wave loads, [Journée and Massie, 2001]

From this superposition, two important assumptions are made for the terms on the right hand side of Figure 4.8.

1. The so-called hydromechanical forces and moments are induced by the harmonic oscillations of the rigid body, moving in the undisturbed surface of the fluid.
2. The so-called wave exciting forces and moments are produced by waves coming in on the restrained body.

The hydromechanical forces and moments acting on an oscillating structure in still water are the linear hydrodynamic reaction forces and moments, e.g., damping- and spring forces. The coupled equations of motion in six degrees of freedom in waves can be written as:

$$\sum_{j=1}^6 m_{i,j} \ddot{x}_j = F_i \quad \text{for: } i = 1, \dots, 6 \quad (4.21)$$

In which:

- $m_{i,j}$ = 6×6 matrix of solid mass and inertia of the structure
- \ddot{x}_j = acceleration of the structure in direction j (6×1 vector)
- F_i = sum of forces or moments acting in direction i (6×1 vector)

Eq.(4.21) states that the resulting force (F_i) equals mass \times acceleration (second law of Newton), in which the acceleration is defined as the second derivative of location (x) as a function of time, $x(t)$. From this equation, the six equations of motions are derived.

The resulting force (F_i) consists out of three components:

1. Harmonic (regular) wave exciting forces and moments (\vec{f})
2. Linear hydrodynamic damping force ($c\vec{\dot{x}}$)
3. Linear hydrostatic spring force ($k\vec{x}$)

Eq.(4.21) can be expressed as a damped-mass-spring-system. This results in a coupled second order differential equation, governing six degrees of freedom:

$$(\mathbf{M} + \mathbf{A})\vec{\ddot{x}} + \mathbf{C}\vec{\dot{x}} + \mathbf{K}\vec{x} = \vec{f} \quad (4.22)$$

In which:

- \mathbf{M} = 6×6 matrix of solid mass and inertia of the structure
- \mathbf{A} = 6×6 matrix of the added mass
- $\vec{\ddot{x}}$ = acceleration of the structure (6×1 vector)
- $\vec{\dot{x}}$ = velocity of the structure (6×1 vector)
- \vec{x} = location of the structure with respect to reference frame (6×1 vector)
- \mathbf{C} = 6×6 matrix of hydrodynamic damping coefficient
- \mathbf{K} = 6×6 matrix of hydrodynamic spring constant
- \vec{f} = excitation force acting on the structure (6×1 vector)

When Eq.(4.22) is solved for vector $\vec{\ddot{x}}$, the solution is \vec{x} , which is an expression of the deflection and rotation of the structure for each degree of freedom for a specific wave forcing (f).

4.3.2 Dynamics of floating structures in irregular waves

The variance density spectrum (Fig.4.4) describes the surface elevation of water waves generated by wind in a statistical sense. From the variance density spectrum the response spectrum of the motion can be obtained by using a transfer function of the motion. For a system which is linear and constant in time, the two-dimensional amplitude response function is shown as Eq.(4.23).

$$\hat{R}(f, \theta) = \frac{\hat{X}(f, \theta)}{\hat{x}(f, \theta)} \quad (4.23)$$

In which:

- $\hat{X}(f, \theta)$ = indicates the amplitude of the response wave
- $\hat{x}(f, \theta)$ = indicates the amplitude of the excitation (harmonic wave)

The response spectrum $E_X(f, \theta)$ is defined as the excitation spectrum $E_x(f, \theta)$ times the square of the amplitude response function $\hat{R}(f, \theta)$:

$$E_X(f, \theta) = E_x(f, \theta) \left[\hat{R}(f, \theta) \right]^2 \quad (4.24)$$

The exciting harmonic wave has a direction of propagation. The response of the structure is not a wave propagating with a certain direction. Depending on the anchor system the motion of the structure is fixed into one or several directions. The amplitude of the non-directional response spectrum can be determined from the two-dimensional response spectrum. This can be achieved by integrating the two-dimensional response spectrum (Eq.4.24) over all directions, resulting in the one-dimensional response spectrum shown as Eq.(4.25).

$$E_X(f) = \int_0^{2\pi} E_X(f, \theta) d\theta \quad (4.25)$$

Performance of floating breakwaters

This chapter discusses the different theories which are available to predict the wave transmission of pontoon-type floating breakwaters. These theories will be compared with each other and with experimental data obtained from different researches. Based on this conclusions are drawn regarding to the applicability of these theories. Formulas to determine the wave transmission coefficients for non-pontoon floating breakwaters discussed in Section 3 can be found in Appendix A.

5.1 Wave transmission theories

The performance of floating breakwaters is defined by the amount of wave attenuation, which strongly depends on the amount of energy reflection (E_r), energy transmission (E_t) and energy dissipation (E_d). This is graphically shown in Figure 5.1. Many wave transmission theories are related to wave energy transport (Section 4.2) and are derived from linear wave theory, which is discussed in Section 4.1.

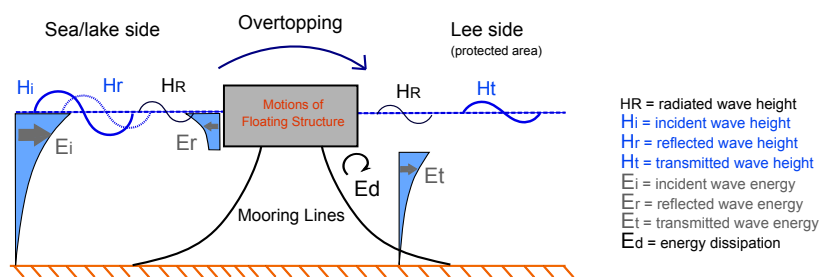


Figure 5.1: Interaction between wave and floating breakwater

For effective attenuation of short waves only blockage of the upper part of the water column is necessary, because there is the most amount of wave energy present. For longer waves the structure should have a larger draft in order to block a larger part of the water column where the wave energy is present. A large draft also implies large mooring forces on the structure. This requires an optimization between draft and wave attenuation in order to obtain an economical design.

In general, for all common types of floating breakwaters the effectiveness is defined by the transmission coefficient. This coefficient is defined as the transmitted wave height over the incident wave height:

$$C_t = \frac{H_t}{H_i} \quad (5.1)$$

This equation only holds for regular waves. A wave climate consists of short-crested irregular waves and in this case it might be better to use the transmitted wave energy instead of the transmitted wave height according to Hales [1981], the result is shown below:

$$C_t = \frac{H_t^2}{H_i^2} = \frac{E_t}{E_i} \quad (5.2)$$

In this thesis most of the time regular waves are considered and Eq.(5.1) will be used in order to determine the wave transmission coefficient. In the case of irregular waves, the significant wave height of the incident wave record $H_{s;i}$ and transmitted wave record $H_{s;t}$ will be used in Eq.(5.1), instead of the wave height H . The significant wave height is the mean of the highest one-third of waves in the wave record [Holthuijsen, 2007].

5.1.1 Wave transmission theories for fixed rigid reflective structures

Fixed rigid structures are structures which movements relative to the bottom are negligible small and no deformations of the structure itself occur. The term fixed may be unrealistic in conditions where the frequency of the excitation is close to the natural frequency of the structure, in this case large motions of the structure may occur.

One of the first researchers who studied wave transmission for partially submerged structures was Ursell [1947] and Macagno [1954]. Several years later Wiegel (1960) developed a linear theory, named as: "Power transmission theory". This is the time rate of energy propagation and is one of the most well known theories. All the theories discussed below are assuming a fixed structure which only blocks wave energy in the upper part of the water column. Processes such as, turbulence (energy dissipation), radiated waves due to the motions of the floating structure and overtopping are not taken into account by these theories.

Ursell (1947)

Ursell [1947] developed a theory for partial transmission and partial reflection of waves in deep water. The theory of Ursell is based on the following assumptions:

- Rigid structures;
- Fixed structures;
- Infinitely small width;
- Deep water (linear wave theory);
- Full reflection of the upper part of the water column where the structure is present;
- No overtopping.

With the aid of the modified Bessel function, Ursell obtained the following expression for the transmission coefficient:

$$C_t = \frac{K_1 \frac{2\pi D}{L_i}}{\sqrt{\pi^2 I_1^2 \frac{2\pi D}{L_i} + K_1^2 \frac{2\pi D}{L_i}}} \quad (5.3)$$

In which:

- $I_1\left(\frac{2\pi D}{L_i}\right)$ = first order modified Bessel function of the first kind
 $K_1\left(\frac{2\pi D}{L_i}\right)$ = first order modified Bessel function of the second kind
 D = draft of the structure [m]
 L_i = incident wave length [m]

The modified Bessel functions are the solutions to the Bessel equation, which is a second order ordinary differential equation.

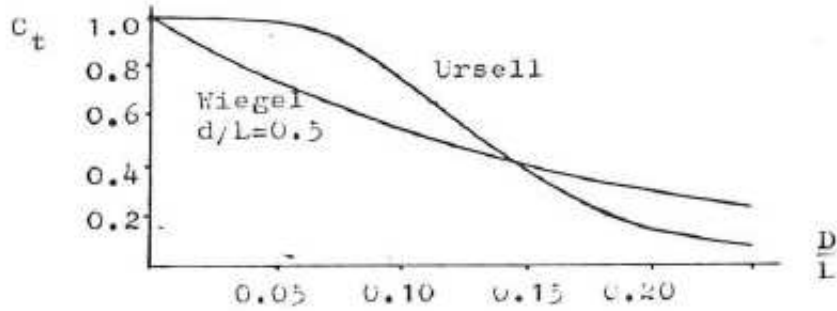


Figure 5.2: Transmission coefficient in deep water for Ursell and Wiegel, [Bouwmeester and Van der Breggen, 1984]

From Figure 5.2 it becomes clear that the influence of draft relative to wavelength (D/L) plays an important role in wave transmission. The larger the draft of the structure the lower the wave transmission coefficient will be.

Macagno (1954)

Macagno made the following assumptions:

- Rigid structures;
- Fixed structure;
- Finite width;
- Deep water (linear wave theory);
- Not known if reflection is taken into account;
- No overtopping.

Based on the above, assumptions Macagno developed the following equation [Bouwmeester and Van der Breggen, 1984]:

$$C_t = \frac{1}{\sqrt{1 + \left[\frac{k_i B \sinh(k_i d)}{2 \cosh(k_i d - k_i D)} \right]^2}} \quad (5.4)$$

In which:

k_i = incident wave number [rad/m]

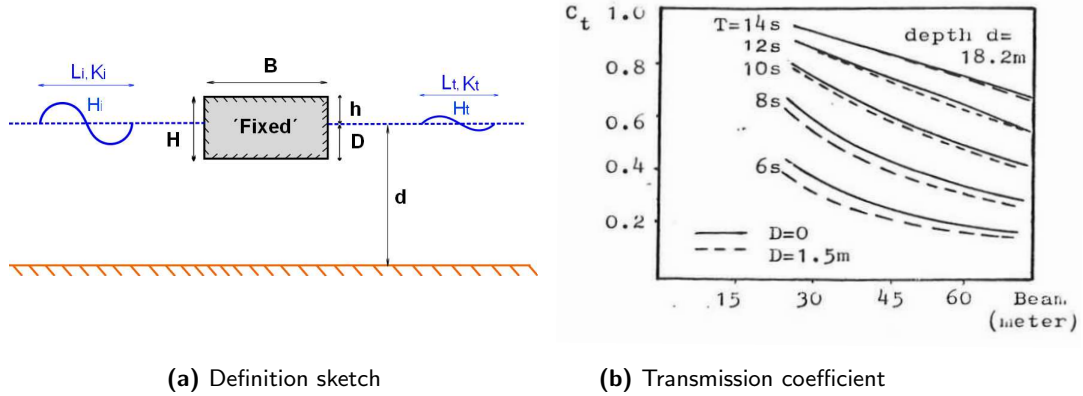


Figure 5.3: Definitions of Macagno's formula and theoretical results

Wiegel (1960)

Wiegel investigated the concept of wave power transmission and developed a theory which considers wave power. His assumptions are as follows:

- Rigid structures;
- Fixed structure;
- Deep water (linear wave theory);
- No reflection;
- No overtopping.

Wave power is the product of the wave induced pressure (P_{wave}) and wave-induced horizontal fluid velocities (u), time-averaged over one wave period. Wiegel assumed in his model that the transmitted wave power over the full water depth occurs between the bottom of the structure and the bottom of the sea/lake, which is in fact a fraction of the incident wave power. When use is made of the distribution of the wave power in the water column, Eq.(5.5) is derived. In this equation the left hand side represents the transmitted wave power over the full water depth and the right hand side represents a fraction of the incident wave power (wave power below structure). The overbar represents time-averaging over one wave period. The theory of Wiegel is graphically shown in Figure 5.4.

$$\overline{\int_{-d}^0 P_{wave;t} u_t dz} = \overline{\int_{-d}^{-D} P_{wave;i} u_i dz} \tag{5.5}$$

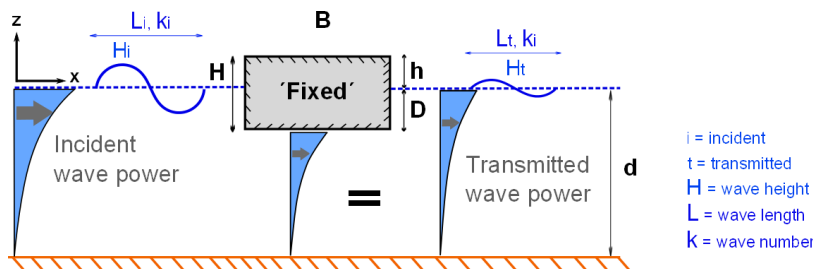


Figure 5.4: Theory of Wiegel

The transmission coefficient is obtained by substituting the expressions of P_{wave} and u in Eq.(5.5) and evaluating this integral, which results in:

$$C_t = \sqrt{\frac{2k_i(d-D) + \sinh(2k_i(d-D))}{\sinh(2k_id) + 2k_id}} \quad (5.6)$$

Figure 5.5 shows the influence of the draft of the structure over wavelength (D/L) and the influence of water depth over wavelength (d/L) on the transmission coefficient. From this figure it can be seen that for deep water conditions ($d/L \geq 0.5$) the amount of wave attenuation becomes larger than for intermediate water depth conditions ($0.05 < d/L < 0.5$).

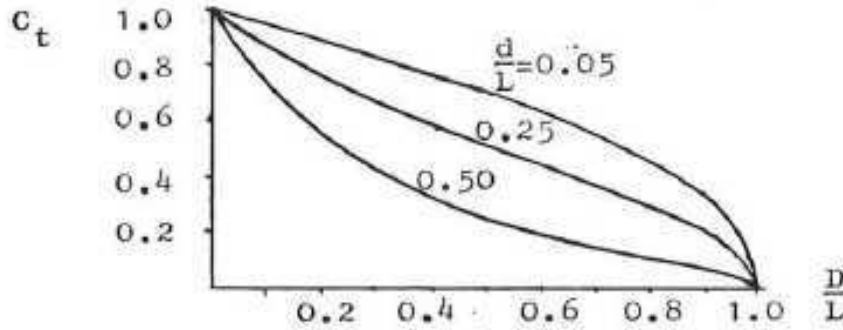


Figure 5.5: C_t values for the theory of Wiegel, shallow water $d/L = 0.05$, intermediate water depth $d/L = 0.25$ and deep water $d/L = 0.50$, [Bouwmeester and Van der Breggen, 1984]

Modified Power Transmission Theory (1996)

Several researchers investigated the theory of Wiegel and compared this theory with physical model tests. From this it turns out that in general Wiegel's theory over-predicts wave transmission in deep water conditions and under-predicts wave transmission in shallow water conditions. The theory of Wiegel does not take partial wave reflection and energy dissipation into account. Kriebel and Bollmann [1996] developed the Modified Power Transmission Theory based on the theory of Wiegel, but they included partial wave reflection.

In this theory it is assumed that the wave induced pressure under the structure equals the sum of the incident wave induced pressure ($P_{wave;i}$) and the reflected wave induced pressure ($P_{wave;r}$). The result is that the net pressure under the structure is larger than assumed by Wiegel. The horizontal fluid velocity is modified by subtracting the reflective horizontal fluid velocity (u_r) from the incident horizontal fluid velocity (u_i), resulting in a lower fluid velocity than assumed by Wiegel. From this a similar equation like Eq.(5.5) can be obtained. The equation proposed by Kriebel and Bollmann [1996] is:

$$\int_{-d}^0 (P_{wave;i} + P_{wave;r})(u_i - u_r) dz = \int_{-d}^{-D} P_{wave;t} u_t dz \quad (5.7)$$

Due to the implementation of the reflective wave, the solution of the equation above contains two unknowns. To solve this problem use is made of continuity of fluid velocities below the floating structure which is defined as, $u_t = u_i - u_r$. Ignoring phase shifts and assuming linear wave theory, Kriebel and Bollmann found the following relationship:

$$C_t = 1 - C_r \quad \text{with} \quad C_r = \frac{H_r}{H_i} \quad (5.8)$$

With this relationship and the solution of Eq.(5.7), the following expression is obtained for the wave transmission coefficient:

$$C_t = \frac{2C_{t,Wiegel}}{1 + C_{t,Wiegel}} \quad (5.9)$$

Kriebel and Bollman compared the theory of Wiegel, with their own developed Modified Power Transmission Theory and with the Eigenfunction Solution theory. This latter theory is the exact mathematical solution for a linear wave interaction with a thin vertical structure. From Figure 5.6 it can be seen that the Modified Power Transmission Theory shows a better agreement with the experimental data than the theory of Wiegel.

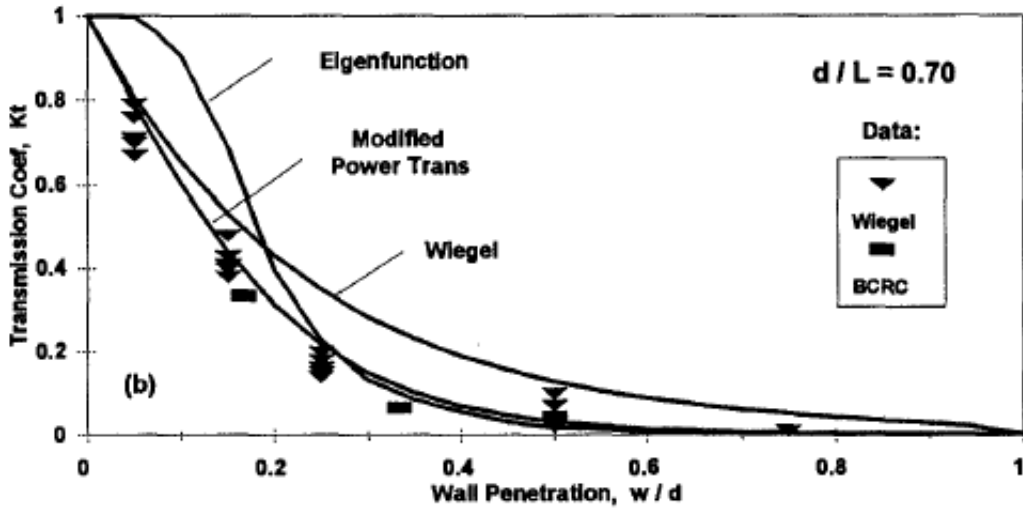


Figure 5.6: Comparison of three wave transmission theories in deep water with experimental data, $w = \text{draft}$, $d = \text{water depth}$ and $L = \text{wavelength}$, [Kriebel and Bollmann, 1996]

5.1.2 Wave transmission theories for non-fixed rigid structures

The previous formulas are valid for structures which are fixed relative to the bottom. Since floating breakwaters are non-fixed and are able to move, it would be better to implement the motions of the structure into the formula for the wave transmission coefficient. Recently, Ruol et al. [2013a] developed a modification factor for the formula of Macagno in order to approximate the wave transmission coefficients of floating breakwaters which are anchored by chains or cables. The other formula's presented in most literature are computer models based on numerical codes.

Ruol (2012)

The formula of Ruol et al. [2013a] is a function of the relative period χ , which is defined as the wave peak period over the natural heave period (T_p/T_h). Initially this formula was developed for pi-type floating breakwaters anchored by chains, shown on the left-hand side in Figure 5.7. The vertical plates on both sides of the pontoon resembles the Greek letter π , which explains the name of this type of floating breakwater. The pi-type floating breakwater is an effective solution for increasing the draft without increasing the mass too much. The vertical attached plates will increase the

vortices on the edges of the plates resulting in energy dissipation. Due to these vertical plates the effectiveness of the floating breakwater increases, which is also shown by experimental models performed by Koutandos et al. [2005]. The applicability of this formula is examined by Ruol et al. [2013b]. Based on this, it is concluded that this formula is also valid for ordinary pontoon type floating breakwaters anchored by chains. Furthermore, the formula is valid for a relative draft (D/d) range between 0.20 and 0.60 and for relative period range ($T_p/T_h = \chi$) between 0.50 and 1.50.

The formula developed by Ruol is in fact a modification factor for the existing formula of Macagno (Eq.5.4). This modification factor is based on a dataset of experimental data and is a function of the relative period. The natural period for heave motion of a floating structure is difficult to obtain without performing experiments. This is because of the added mass which has to be taken into account. The added mass can be seen as additional mass which represents the mass of the fluid which has to be accelerated when the structure accelerates. Therefore, this additional mass has to be taken into account when the mass of the structure is considered. The natural frequency of heave motion when neglecting damping can be described as:

$$\omega_h = \sqrt{\frac{K}{M_{total}}} = \sqrt{\frac{K}{M + M_a}} = \sqrt{\frac{\rho_w g B}{M + M_a}} \quad (5.10)$$

In which:

- K = linear spring constant [N/m]
- M, M_a = mass of structure and added mass respectively [kg]
- ρ_w = density of the water [kg/m³]
- g = gravitational acceleration [m/s²]
- B = width of structure [m]
- ω_h = natural heave radian frequency [rad/s]

For heave motion the added mass can be assumed as the volume of water under the floating structure, where the boundary of the volume is described by a semicircle with a radius equal to half the width of the structure. This is graphically shown in Figure 5.7. Because the additional mass can be approximated, it follows that the natural frequency of heave can be described by Eq.(5.11).

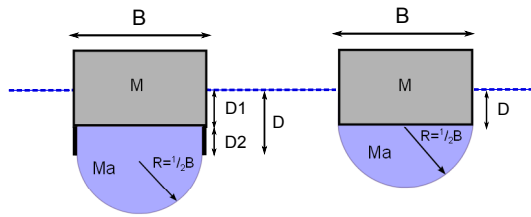


Figure 5.7: Added mass for pi-type- (left) and pontoon type (right) floating breakwater

$$\omega_h = \sqrt{\frac{\rho_w g B}{\rho_w B D + \rho_w \frac{\pi}{8} B^2}} = \sqrt{\frac{g}{D + \frac{\pi}{8} B}} \quad (5.11)$$

Ruol et al. [2013a] investigated the natural heave period for pi-type floating breakwaters and compared analytical calculations with experimental measurements. Based on this Ruol et al. concluded that the value $\frac{\pi}{8} \approx 0.39$ should be 0.35. From Eq.(5.11) the natural heave period can be determined:

$$\omega_h = \frac{2\pi}{T_h} \quad \rightarrow \quad T_h = \frac{2\pi}{\sqrt{\frac{g}{D + 0.35B}}} \quad (5.12)$$

Deltares performed experiments for a pontoon type floating breakwater anchored by piles. Based on a free decay test a natural heave period of 3.95 s was found for the pontoon. When Eq.(5.12) is used to determine the natural heave period, a natural heave period of 4.06 s is found. The difference of the natural heave period between the experiment and calculation is very small (0.11 seconds). Therefore, it is concluded that Eq.(5.12) is suitable to apply to determine the natural heave period.

The dimensionless parameter χ , which has been mentioned earlier, is defined as follows by Ruol et al. [2013a]:

$$\frac{T_p}{T_h} \approx \chi = \frac{T_p}{2\pi} \sqrt{\frac{g}{D + 0.35B}} \quad (5.13)$$

Eq.(5.13) considers the peak period T_p , which implies irregular waves. Macagno assumes in his theory only regular waves, hence the mean period T . In general the peak period is 10% larger than the mean period T . In order to apply Macagno in combination with χ , the wave period T for the calculation of χ should be multiplied with a factor of 1.1, i.e. χ should be increased with 10%. Another remark related to this formula is that it contains several parameters describing the system, such as: width of the structure B , draft of the structure D and the wave period T or T_p .

Based on a number of experimental datasets and curve fitting, Ruol et al. developed a modification factor $\beta(\chi)$ for the formula of Macagno. With the developed modification factor β the "new" formula for wave transmission becomes as follows:

$$C_t = \beta(\chi)C_{t;Macagno} \quad \text{with} \quad \beta(\chi) = \frac{1}{1 + \left(\frac{\chi - \chi_0}{\chi_0}\right) \exp - \left(\frac{\chi - \chi_0}{\sigma}\right)} \quad (5.14)$$

In which:

- β = modification factor based on curve fitting
- χ_0 = 0.7919, with 95% confidence interval 0.7801, 0.8037
- σ = 0.1922, with 95% confidence interval 0.1741, 0.2103

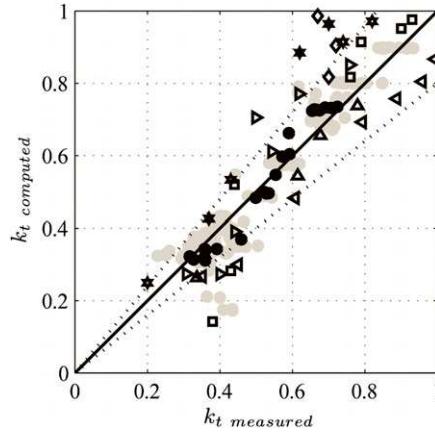


Figure 5.8: Results of the formula of Ruol et al. [2013a], applied on floating breakwaters anchored by chains and piles, the legend of this figure is presented in Table 5.1

Figure 5.8 shows the results of the formula obtained by Ruol et al. [2013a], presented as Eq.(5.14). In this figure experimental results for floating breakwaters anchored by piles and chains are shown. These data points are obtained from the authors themselves and from several other researchers in order to validate their proposed formula. The dotted lines represents $\pm 20\%$ confidence limits. Based on this figure Ruol et al. concluded that an excellent agreements is found for pi-type floating breakwaters anchored by chains for the datasets of Gesraha [2006] and Martinelli et al. [2008]. A good agreement is found for the three models anchored by cables for Peña et al. [2011]. Floating breakwaters anchored by piles are generally overestimated. The table below shows the datasets used in Figure 5.8. All these datasets excluding Ruol et al., 2013a (first line of this table) are used to validate this formula.

| Symbol | Dataset | Type of anchorage | Pontoon type | Waves |
|-----------------|-----------------------------|-------------------|--------------|-----------|
| shaded circle | Ruol et al., 2013a | cables | pi-type | irregular |
| solid circle | Martinelli et al., 2008 | cables | pi-type | irregular |
| square | Gesraha, 2006 | cables | pi-type | regular |
| diamond | Koutandos et al., 2005 | piles | pontoon | regular |
| open asterisk | Cox et al., 2007 | piles | pontoon | regular |
| solid asterisk | Cox et al., 2007 | piles | pontoon | irregular |
| left triangle | Peña et al., 2011 (Model A) | chains | pi-type | regular |
| upward triangle | Peña et al., 2011 (Model B) | cables | pi-type | regular |
| right triangle | Peña et al., 2011 (Model C) | cables | pi-type | regular |

Table 5.1: Experimental data floating breakwaters used in Figure 5.8

5.1.3 Comparison of wave transmission theories

In the foregoing sections a number of theories are discussed related to wave transmission. All these theories are valid for fixed structures in deep water, except for the theory of Ruol et al. In order to gain insight in the differences between these theories, the discussed theories are plotted in Figure 5.9. In this figure the transmission coefficient is shown as a function of the dimensionless values χ (used for non-fixed structures) and L/d (can be used for all structures). Although nearly all the theories are valid for fixed structures, comparisons will also be made for non-fixed structures in order to investigate how well these theories approximate floating structures. The values used to perform this calculation are typical conditions for a floating breakwater used to protect a marina located in a lake.

From the graphs below it becomes clear that in shallow water conditions ($depth/L_{wave} \leq \frac{1}{2} \rightarrow L_{wave}/depth \geq 2$) the theories converge to an approximately constant value. The theories of Wiegel, Kriebel and Bollmann, Ursell, Ruol et al. and Macagno show for wave periods larger than the natural period of the structure ($\chi > 1$) transmission coefficients larger than 50%. The theory of Kriebel and Bollmann takes wave reflection into account which is not included in the theory of Wiegel. The effect of wave reflection between the theories of Kriebel and Bollmann and Wiegel becomes clear for values of χ smaller than 1.0, where the transmission coefficient according to Kriebel and Bollmann is smaller than the wave transmission coefficient according to Wiegel. In this figure it also becomes clear that the theory of Ruol et al. differs from Macagno for χ -values between 0.5 and 1.5.

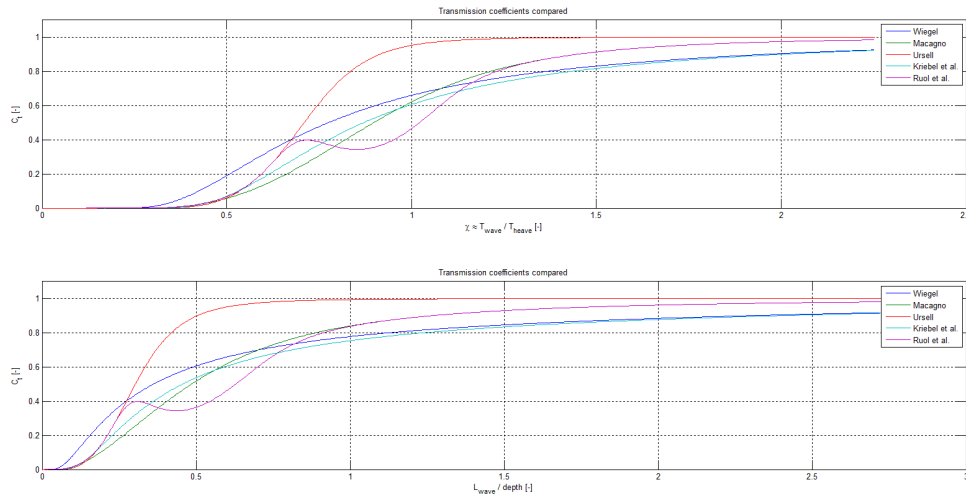


Figure 5.9: Wave transmission theories compared for T_{wave}/T_{heave} and $L_{wave}/waterdepth$. The boundary conditions used for the calculations are: $d=25m$, $T=[0 - 7]$ s, $D=1m$, $B=4m$, $Th=3.1$ s.

When the phenomenon of wave energy is considered, it is clear that most wave energy is presented in the upper part of the water column. Therefore, it is expected that the draft of the structure plays an important role for the blockage of wave energy. Besides this, the width of the structure will have an effect on wave energy dissipation. It should be obvious that when the draft of the structure equals the water depth ($D/d = 1$), there will be no wave transmission. In this case all the wave energy in the entire water column is blocked. To illustrate this a calculation is performed. The calculation results are shown in Figure 5.10 which shows the influence of the relative draft of the structure on the wave transmission coefficient. The values used to perform this calculation are typical values for a floating breakwater located in a lake. It is remarkable that the theories of Macagno and Ruol et al. predicting wave transmission for the case when the water depth equals the draft of the floating structure, the other theories do not predict wave transmission in this case. A remark related to this figure is that formula of Ruol et al. is applicable for values of D/d between 0.2 and 0.6 Ruol et al. [2013b].

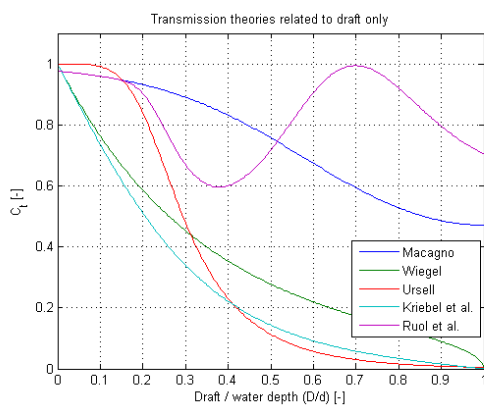


Figure 5.10: Wave transmission theories compared for draft vs. water depth, D/d . The boundary conditions used for the calculations are: $d=25m$, $T=6s$, $D=[0 - d]m$, $B=4m$, $Th=[2.3 - 10.3]s$

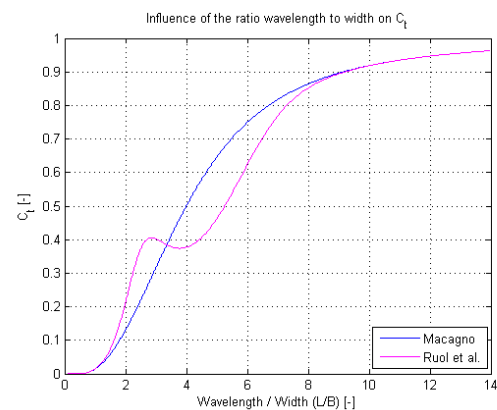


Figure 5.11: Wave transmission theory of Macagno and Ruol et al. as function of wavelength over width (L_{wave}/B). The boundary conditions used for the calculations are: $d=25m$, $T=[0 - 6]s$, $L_{wave}=[0 - 55.8]m$, $D=2m$, $B=4m$

In the theories discussed above, Macagno and Ruol et al. are the only theories which takes the draft and the width of the structure into account. Figure 5.11 shows the influence of the ratio of the wavelength to the width of the structure on the transmission coefficient. From this figure it can be seen that the transmission coefficient increases rapidly for $0 < L/B < 6.0$. For $L/B > 6.0$ the increase of the wave transmission coefficient goes is more slowly. Figure 5.12 shows the influence of the draft and the width of the structure on the wave transmission coefficient for the formula of Macagno, which is the only formula for fixed structures which takes both the draft and the width of the structure into account. The lower panel in this figure shows the contours of the upper panel.

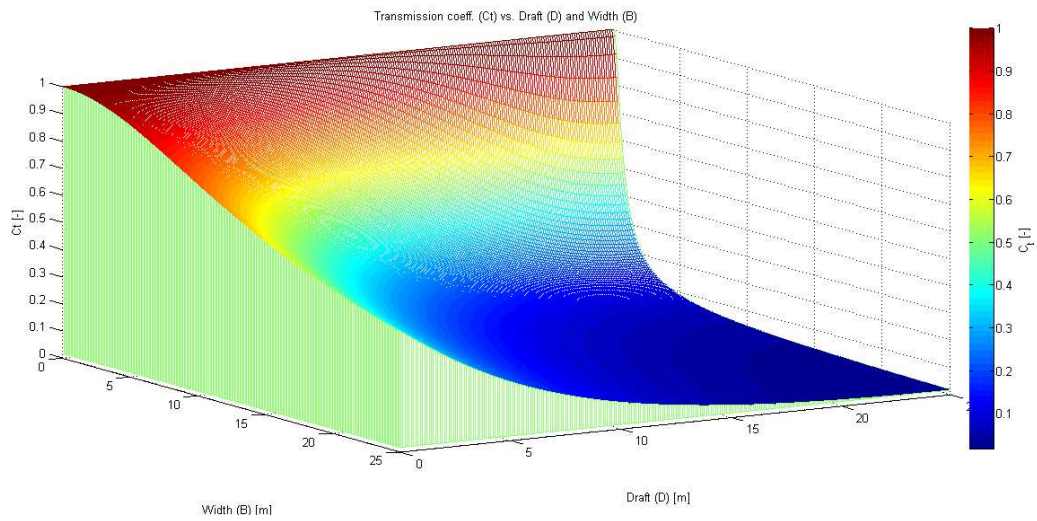


Figure 5.12: Wave transmission theory of Macagno as function of width (B) and draft (D). The boundary conditions used for the calculations are: $d=25\text{m}$, $T=5\text{s}$, $D=[0 - 25]\text{m}$, $B=[0 - 25]\text{m}$, deep water $depth/L_{wave} = 0.64$.

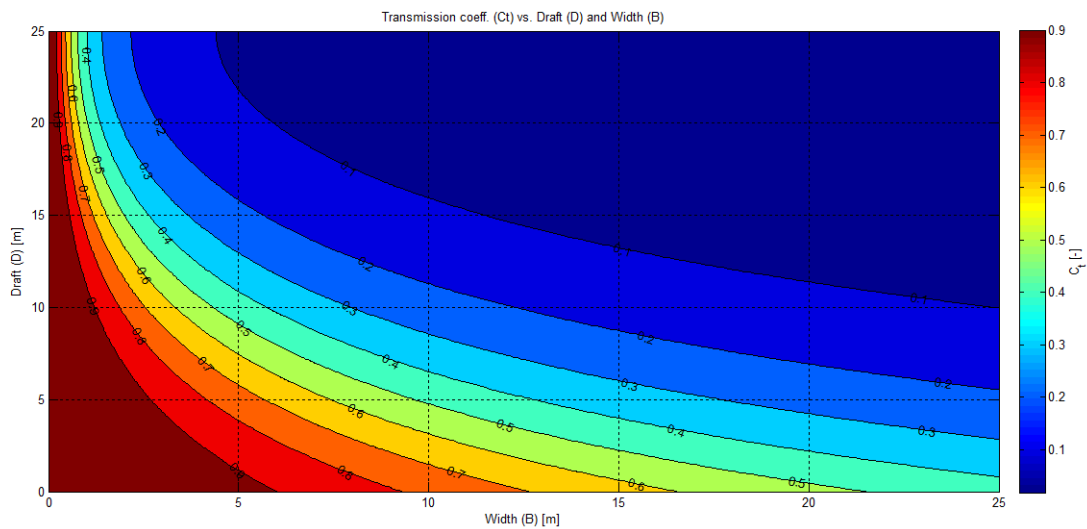


Figure 5.13: Contour plot of Figure 5.12

Conclusions

- There are a number of wave transmission theories available and there is a large difference between the theories, which can be seen in Figure 5.9. The largest differences between the theories occur for deep water situations ($L/d \leq 2$). Because of the large differences between the theories it is unclear for the designer when to use which theory.
- The difference between the theory of Wiegel and Kriebel and Bollmann is that Kriebel and Bollmann takes wave reflection into account. This effect becomes clear for short waves. For long waves this effect is negligible small.
- A large draft results in a low transmission coefficient, see Figure 5.10. When the draft of the structure equals the water depth it is expected that there is no wave transmission. The theory of Macagno and Ruol et al. shows wave transmission for this case while the other theories do not show any wave transmission.
- The formula of Macagno and Ruol et al. are the only formulas which takes the draft and the width of the structure into account.

5.2 Wave transmission theories compared with experimental data

There are a number of wave transmission theories available which are discussed in the previous section. Nearly all these theories are valid for fixed structures in deep water where linear wave theory holds. In order to investigate how well these theories are applicable for floating and non-floating (fixed) structures, these theories are compared with experimental data. The aim of this comparison is to conclude which theory is appropriate to apply under which condition.

The experimental datasets are obtained from literature and are shown in the sections below. Distinction is made between three types of anchorage systems, namely: anchorage for fixed structures, anchorage by piles (one degree of freedom) and anchorage by chains (six degrees of freedom), see also Figure 5.14. This distinction is made because the dynamics is different between these three systems. The wave steepness (H/L) in the experimental models is approximately between the 1% and 6%. The experiments obtained from literature are performed with a horizontal bottom and no overtopping is included.

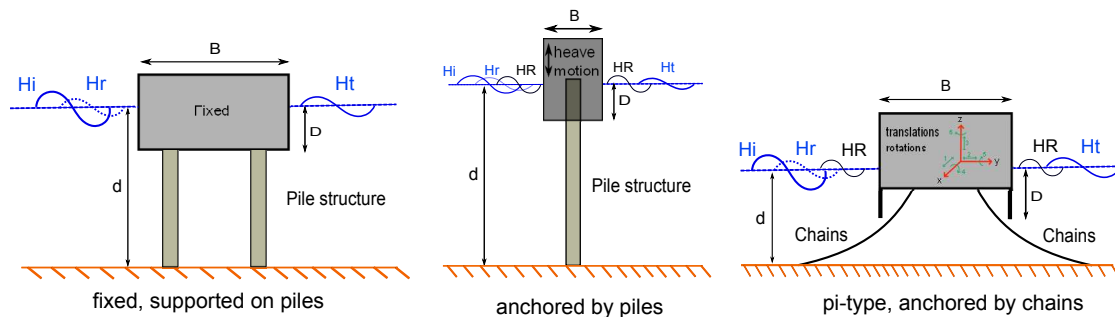


Figure 5.14: Different types of anchorage for floating breakwaters

For each experimental dataset the wave transmission theories are plotted together with the experimental data. In these graphs the y-axis represents the transmission coefficient and the x-axis represents different dimensions, which depends on the type of anchoring system. For fixed breakwaters the x-axis represent the wavelength over draft (L/D) and for floating breakwaters anchored

by piles or by chains the x-axis represents the relative period $\chi \approx T_p/T_h$ or wavelength over width (L/B). These ratios are all dimensionless in order to compare different datasets with each other. The reason for applying different ratios on the x-axis for different types of anchoring systems has to do with the dynamics which is totally different for each type of anchoring system, e.g. it is not useful to use the relative period χ for fixed structures since their natural heave period is zero. The difference of the wave transmission coefficient between each theory and each experimental data point is shown in a bar plot to identify where the largest differences occur. The Root Mean Square Error (RMSE, shown as Eq.5.15) is determined for each theory to see how well the theories compared to each other approximate the experimental data. The RMSE applied in this case is a measure of the spread of the experimental data (measured transmission coefficients) about the predicted transmission coefficients (wave transmission theories). The RMSE presents the same units which are used to calculate RMSE, i.e. when the RMSE is calculated with transmission coefficients defined as percentages, the RMSE will indicate the spread of the experimental data around the theories in percentages as well. The plots for each experimental dataset and the tables which show the RMSE are shown in Appendix C.1. In this section the conclusion of each comparison will be discussed.

$$RMSE = \sqrt{\frac{\sum_{i=1}^N (Ct_{;theory} - Ct_{;exp})^2}{N}} \quad (5.15)$$

Below an example is shown of one experimental dataset where the theories and the measured data points are plotted in Figure 5.15. The difference between each theory and experimental data point is plotted in Figure 5.16. The RMSE for each theory for this particular dataset is shown in Table 5.2. From this table it can be seen that the theory of Ruol has the smallest RMSE and this theory might be the most appropriate one to apply for this dataset.

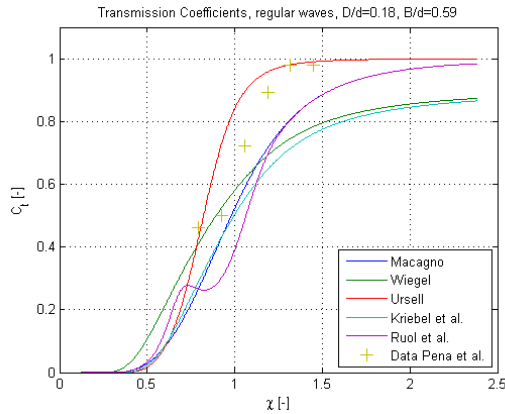


Figure 5.15: Experimental data from Peña et al. [2011], (d) = 6.75m, (B) = 4.0m and (D) = 1.2m. FB anchored by chains/cables

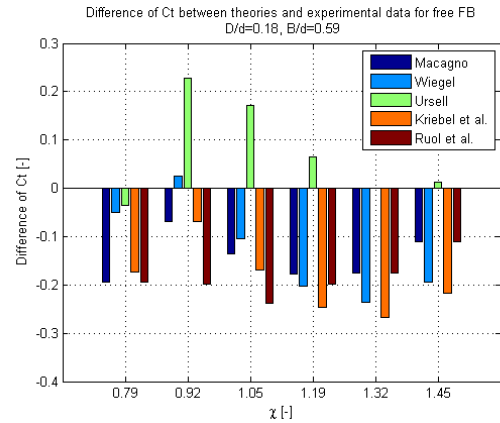


Figure 5.16: Differences between theories and experimental data of Figure 5.15

| Formula | RMSE: $D/d=0.18$, $B/d=0.59$ |
|----------------------|-------------------------------|
| Macagno | 0.1694 |
| Wiegel | 0.1606 |
| Ursell | 0.2110 |
| Kriebel and Bollmann | 0.2476 |
| Ruol et al. | 0.1570 |

Table 5.2: Root mean square errors between theories and experimental data of Peña et al. [2011], regular waves, FB anchored by chains

5.2.1 Fixed breakwaters

Experimental data for fixed breakwaters (partially submerged rigid structures) is obtained from Koutandos et al. [2005] and from Gesraha [2006]. The formulas for fixed breakwaters which are discussed above are compared with these experimental datasets. For all the comparisons reference is made to Appendix C.1.1. In Table 5.3 the characteristics of each used dataset is shown.

| Dataset | Waves | Range T [s] | D/d [-] | B/d [-] | d [m] |
|-------------------------|-----------|-------------|-----------------|-----------|-------|
| Koutandos et al. [2005] | Regular | 2.4 - 10.5 | 0.2; 0.25; 0.33 | 1.00 | 2.00 |
| Koutandos et al. [2005] | Irregular | 2.8 - 5.5 | 0.2; 0.25; 0.33 | 1.00 | 2.00 |
| Gesraha [2006] | Irregular | 0.6 - 1.8 | 0.4 | 0.75 | 0.43 |

Table 5.3: Experimental data fixed floating breakwaters

The largest difference of these two datasets are the wave periods and thus the wavelengths. The ratios D/d are in the same order of magnitude. In order to compare these datasets well, the dimensionless ratio L/D is considered, shown in Table 5.4. This ratio represents the wavelength to draft. The draft has a large influence on the blockage of wave energy in the water column. When the waves are long relative to the draft the wave transmission coefficients increases.

| L/D range Gesraha irregular waves | L/D range Koutan- dos regular waves | L/D range Koutan- dos irregular waves |
|--------------------------------------|--|--|
| 3.3 - 19.6 | 12.3 - 114.7 | 15.13 - 58.2 |

Table 5.4: Ratios of wavelength to water depth

When the dataset of Koutandos et al. is compared with the theories it becomes clear that for long waves, thus large L/D -values the theory of Kriebel and Bollmann (one theory) and the theory of Wiegel are the most appropriate one to apply. For very long waves the results of these two theories are the same because wave reflection becomes negligible small. In this dataset it is observed that all the theories are overestimating the transmission coefficient.

| Dataset | RMSE: | RMSE: | RMSE: |
|--|--------------------|---------------------|---------------------|
| | D/d=0.2 B/d=1.0 | D/d=0.25 B/d=1.0 | D/d=0.33 B/d=1.0 |
| Koutandos et al. [2005] regular waves | 0.1500 | 0.1500 | 0.1500 |
| Koutandos et al. [2005] irregular waves | 0.1500 | 0.1000 | 0.0500 |

Table 5.5: RMSE for Kriebel and Bollmann

The dataset of Gesraha relates to shorter waves and contains smaller L/D -ratios, see Table 5.4. According to this dataset the theory of Macagno approximates the data the best compared to the other theories. In this dataset it is observed that all the theories are underestimating the wave transmission.

| Dataset | RMSE: |
|-----------------------------------|---------------------|
| | D/d=0.4 B/d=0.75 |
| Gesraha [2006] irregular waves | 0.1500 |

Table 5.6: RMSE for Macagno

Conclusions

Based on experimental data obtained from different researchers a number of conclusions can be drawn for fixed breakwaters. These conclusions holds for the ranges $0.75 < B/D < 1.0$ and for $0.20 < D/d < 0.4$.

- In general it can be concluded that the RMSE is large and there is a poor agreement between the theories and experimental data, see Table 5.5 and Table 5.6. The dataset of Koutandos et al. is overestimated by all the theories. This overestimation becomes larger when the L/D -values decreases, hence shorter waves.
- For values $L/D < 5$ the transmission coefficient is smaller than 0.3 for both datasets.
- Notwithstanding the large RSME, there are two different theories applicable for fixed structures which can be used during the preliminary design stage, namely: Kriebel and Bollmann (1) and Macagno (2). For $5 < L/D < 15$ the theory of Macagno can be applied. For $15 < L/D < 95$ the theory of Kriebel and Bollmann can be applied. When the above theories are applied the wave transmission will be overestimated in general, but for a preliminary design the theories will give a good estimation regarding the effectiveness of the fixed structure.

5.2.2 Floating breakwaters anchored by piles

The experimental data for heave floating breakwaters obtained from literature is shown below in Table 5.7. The heave floating breakwater tested by Deltares differs from the other heave floating breakwaters shown in Table 5.7 in the sense of an additional fixed vertical screen between the piles. On these piles a floating caisson is located which is able to move up and downwards on the waves. The advantage of this screen is that a larger part of the water column is blocked, resulting in lower transmitted waves. For the calculation of the transmission coefficients the draft includes the length of the vertical screen. The dimensionless parameter set on the x-axis is the ratio wavelength to

draft L/D and not the dimensionless period χ . This is because the dimensionless period χ includes the draft of the floating structure. For the dataset of Deltares the draft of the floating structure is not equal to the draft of the floating breakwater in total, which includes the vertical screen. Therefore, the applicability of χ is not appropriate in this case.

| Dataset | Waves | Range χ [-] or L/D [-] | D/d [-] | B/d [-] | d [m] |
|-------------------------|-----------|-------------------------------|-----------|-----------|---------|
| Cox et al., 2007 | Irregular | $\chi = 0.94 - 1.56$ | 0.40 | 0.57 | 4.20 |
| Deltares | Irregular | $L/D = 2.07 - 11.06$ | 0.38 | 0.12 | |
| Deltares | Irregular | $L/D = 1.46 - 7.71$ | 0.54 | 0.12 | |
| Deltares | Irregular | $L/D = 2.60 - 7.16$ | 0.41 | 0.13 | |
| Deltares | Irregular | $L/D = 1.82 - 5.06$ | 0.58 | 0.13 | |
| Koutandos et al., 2005 | Irregular | $\chi = 1.12 - 3.51$ | 0.20 | 1.00 | 2.00 |
| Martinelli et al., 2008 | Irregular | $\chi = 0.77 - 1.38$ | 0.20 | 0.49 | 0.52 |
| Cox et al., 2007 | Regular | $\chi = 0.76 - 1.90$ | 0.40 | 0.57 | 4.20 |
| Deltares | Regular | $L/D = 1.49 - 11.85$ | 0.38 | 0.12 | |
| Deltares | Regular | $L/D = 1.04 - 8.33$ | 0.54 | 0.12 | |
| Deltares | Regular | $L/D = 2.64 - 7.79$ | 0.41 | 0.13 | |
| Deltares | Regular | $L/D = 1.86 - 5.48$ | 0.58 | 0.13 | |
| Koutandos et al., 2005 | Regular | 1.32 - 2.62 | 0.20 | 1.00 | 2.00 |

Table 5.7: Experimental data floating breakwaters anchored by piles

In Appendix C.1.2 plots are shown for each dataset where the experimental data is compared to the theories. According to these plots it can be concluded that the theory of Wiegel approximates this dataset the best in comparison with the other theories. This is the case for both regular and irregular waves. For all the data points the theory of Wiegel is underestimating the wave transmission coefficient with more or less the same deviation for each L/D -value set on the x-axis. Table 5.8 shows the RMSE for the theory of Wiegel which has the best agreement with the experimental data. The effect of the length of the vertical screen becomes also clear in these plots.

| Dataset | RMSE: | RMSE: | RMSE: | RMSE: |
|--------------------------|--------------------------|--------------------------|--------------------------|--------------------------|
| | $D/d=0.38$ $B/d=0.12$ | $D/d=0.54$ $B/d=0.12$ | $D/d=0.41$ $B/d=0.13$ | $D/d=0.58$ $B/d=0.13$ |
| Deltares regular waves | 0.1531 | 0.2204 | 0.1273 | 0.1961 |
| Deltares irregular waves | 0.1250 | 0.2213 | 0.0952 | 0.1642 |

Table 5.8: RMSE for the theory of Wiegel for the dataset of Deltares

The RMSE for the theory of Wiegel is large and a very poor agreement is found with the experimental data. When the theory of Wiegel is used for this type of structures (heave floating breakwater including vertical screen) the wave transmission coefficient is always underestimated. When the vertical screen is neglected the wave transmission is overestimated by the theories.

In Section 5.1.3 the wave transmission theories are compared with each other and it is concluded that a large draft results in a low transmission coefficient. When the ratio wavelength to breakwater width (L/B) is large, the wave transmission coefficient will be large as well. This is because the floating breakwater moves upwards and downwards on the waves and reflects very little wave energy, hence a large transmission coefficient. From this it can be concluded that the parameters wave period (which is related to the wavelength), draft and breakwater width influence the effectiveness of floating breakwaters with one degree of freedom. These three parameters are all

combined in the dimensionless period χ , shown as Eq.5.16. From this equation it becomes clear that when the width (B) and the draft (D) are large, χ will be small. From all the figures shown in Appendix C.1.2, in which experimental data is compared with the theories, it can be seen that for small χ -values the wave transmission coefficient is small. Therefore, this parameter will be used to set on the x-axis for floating breakwaters anchored by piles (without fixed vertical screen) because all the parameters which influence the transmission coefficient are included in χ .

$$\frac{T_p}{T_h} \approx \chi = \frac{T_p}{2\pi} \sqrt{\frac{g}{D + 0.35B}} \quad (5.16)$$

The dataset of Cox et al. is well approximated by the theory of Kriebel and Bollmann, see Table 5.9 for the RMSE. This is remarkable since the difference of the relative draft between the dataset of Deltares and Cox et al. is small. This difference can be explained by the vertical screen used in the experiments of Deltares, which is not used by Cox et al. Cox et al. performed their experiments with two different wave heights. From Table 5.9 it can be seen that the influence of the wave height on the wave transmission coefficient is very small.

| Dataset | RMSE: D/d=0.40 B/d=0.57 Hs=0.4m | RMSE: D/d=0.40 B/d=0.57 Hs=0.8m |
|---------------------|------------------------------------|------------------------------------|
| Cox regular waves | 0.1026 | 0.0959 |
| Cox irregular waves | 0.0360 | 0.0309 |

Table 5.9: RMSE for the theory of Kriebel and Bollmann for the dataset of Cox et al. [2007]

The tests executed by Koutandos et al. for regular waves are performed for a wide range of χ -values. The relative draft used by Koutandos et al. is smaller than the relative draft of the tests performed by Cox et al.. The smallest RMSE for this dataset is obtained with the theory of Kriebel and Bollmann, shown in Table 5.10. For χ -values smaller than 1.3 it can be seen that the theory of Macagno approximates the experimental data better than Kriebel and Bollmann. This is probably due to the combination of a small D/d -ratio and a large B/d -ratio, which holds for the dataset of Koutandos et al. and not for the other datasets. However, for a wide range of χ -values the theory of Kriebel and Bollmann is suitable to apply and the differences between the theory of Kriebel and Bollmann and Wiegel are small. The table below shows the RMSE for the theory of Kriebel and Bollmann.

| Dataset | RMSE: D/d=0.20 B/d=1.0 |
|----------------------------------|------------------------------|
| Koutandos et al. regular waves | 0.1230 |
| Koutandos et al. irregular waves | 0.1417 |

Table 5.10: RMSE for the theory of Kriebel and Bollmann for the dataset of Koutandos et al. [2005]

The dataset of Martinelli et al. contains low χ -values and has the same relative draft as the experiments performed by Koutandos et al. and by Cox et al.. When considering the RMSE it can be seen that the theory of Kriebel and Bollmann approximates this dataset the best. Besides this, the differences between the theories of Kriebel and Bollmann and Wiegel are larger than for the datasets of Koutandos et al. and Cox et al., implying that for this dataset wave reflection has a larger effect than for the datasets of Cox et al. and Koutandos et al.. Table 5.11 shows the RMSE for the theory of Kriebel and Bollmann for the dataset of Martinelli et al.

| Dataset | RMSE: D/d=0.20 B/d=0.48 |
|-----------------------------------|-------------------------------|
| Martinelli et al. irregular waves | 0.1013 |

Table 5.11: RMSE for the theory of Kriebel and Bollmann for the dataset of Martinelli et al. [2008]

Conclusions

- Although all the theories used for the comparisons with experimental data are derived for fixed structures, a reasonable agreement is found for floating breakwaters with one degree of freedom without a fixed vertical screen for the theory of Kriebel and Bollmann.
- Floating breakwaters anchored by piles which includes a fixed vertical screen between the piles show a very poor agreement with the theories. With the aid of physical models the wave transmission can be determined for this type of structure. For the dataset of Deltares (includes a fixed vertical screen) it is concluded that the theories of Kriebel and Bollmann and Wiegel are showing more or less the same trend as the experimental data points, but the deviation is very large. When the length of the fixed vertical screen is taken into account as draft, the wave transmission theories of Kriebel and Bollmann and Wiegel are underestimating the effectiveness. If the length of the vertical screen is neglected in the wave transmission theories, the theories of Kriebel and Bollmann and Wiegel are overestimating the effectiveness. Because of the very poor agreement between the experimental data and theories, this type of floating breakwater is not taken into account regarding the conclusions in the next sections of this report.
- The relative period χ is an appropriate value to set on the x-axis for floating breakwaters anchored by piles without a fixed vertical screen between the piles. The ratio χ contains all the parameters which influence the wave transmission coefficient. For floating breakwaters anchored by piles with a fixed vertical screen between the piles, where the length of the vertical screen is included in the draft, the ratio L/D is appropriate to apply.
- Based on the experimental datasets of Cox et al. and Koutandos et al. it is concluded that for values of $0.6 < \chi < 3.5$ the theory of Kriebel and Bollmann is good applicable. For $\chi < 0.6$ the wave transmission coefficient is smaller than 0.3. When the value of χ increases the differences between the theories of Kriebel and Bollmann and Wiegel becomes smaller. Based on the dataset of Cox et al. it can be concluded that the influence of the wave height on the wave transmission coefficient is small.
- When the ratio D/d is small and the ratio B/d is large, it is observed that for the dataset of Koutandos et al. the theory of Macagno shows a good agreement when the theory of Kriebel and Bollmann becomes larger than the theory of Macagno. This occurs for small χ -values representing short waves.

5.2.3 Floating breakwaters anchored by chains

Floating breakwaters anchored by chains have a different behaviour than floating breakwaters anchored by piles. Instead of one degree of freedom there are six degrees of freedom and some motions are coupled, such as sway and roll. Table 5.12 shows the datasets which are used for the comparisons.

| Dataset | Waves | Range χ [-] | D/d [-] | B/d [-] | d [m] |
|---------------------------------|-----------|------------------|---------|---------|-------|
| Gesraha, 2006 | Irregular | 0.56 - 1.67 | 0.4 | 0.75 | 0.43 |
| Martinelli et al., 2008 (flume) | Irregular | 0.78 - 1.23 | 0.13 | 0.40 | 0.50 |
| Martinelli et al., 2008 (basin) | Irregular | 0.78 - 1.20 | 0.13 | 0.40 | 0.50 |
| Brebner and Ofuya, 1968 | Regular | 0.69 - 1.03 | 0.15 | 1.10 | 0.45 |
| Brebner and Ofuya, 1968 | Regular | 0.66 - 0.99 | 0.19 | 1.10 | 0.45 |
| Brebner and Ofuya, 1968 | Regular | 0.61 - 0.86 | 0.30 | 1.10 | 0.45 |
| Peña et al., 2011 | Regular | 0.80 - 1.45 | 0.18 | 0.60 | 6.75 |
| Peña et al., 2011 | Regular | 0.80 - 1.20 | 0.18 | 0.57 | 6.75 |
| Peña et al., 2011 | Regular | 0.60 - 1.10 | 0.32 | 0.60 | 6.75 |

Table 5.12: Experimental data floating breakwaters anchored by chains

Peña et al. performed tests for pi-type floating breakwaters anchored by chains for deep and intermediate water depths. In their experiments they changed the length of the vertical plates and the width of the structure, resulting in different D/d and B/d ratios. When the RMSE is considered (Table 5.13) for this dataset, it is remarkable to see that for each test there is another theory which shows a good agreement with the data, while the changes they made are relatively small.

| Dataset | RMSE: D/d=0.17 B/d=0.53 | RMSE: D/d=0.32 B/d=0.59 | RMSE: D/d=0.18 B/d=0.59 |
|----------------------------------|-------------------------------|-------------------------------|----------------------------|
| Peña et al. [2011] regular waves | Ursell = 0.1206 | Macagno = 0.0488 | Ruol et al. = 0.1570 |

Table 5.13: Lowest RMSE for different theories for the dataset of Martinelli et al. [2008]

The experiments by Brebner and Ofuya are performed for pontoon floating breakwaters where the D/d ratios are nearly the same as for the experiments performed by Peña et al.. When these two datasets are compared with each other, the differences are the ratios B/d and L/B . The B/d ratio in the experiments of Brebner and Ofuya are twice as large as in the experiments of Peña et al. and the ratio L/B is in the experiments of Peña et al. twice as large as in the experiments of Brebner and Ofuya. The ratio L/B plays a significant role for floating breakwaters with one degree of freedom, which is mentioned in the previous section. Again this ratio is considered (Table 5.14) and it can be concluded that for large L/B ratios the transmission is large as well. This can be seen in the plots for the data of Brebner and Ofuya and Gesraha, see Figures 5.17 and 5.18.

| Dataset | L/B range regular waves | L/B range irregular waves |
|-----------------------------|-------------------------|---------------------------|
| Gesraha [2006] | - | 1.32 - 7.87 |
| Martinelli et al. [2008] 2D | - | 0.84 - 2.01 |
| Martinelli et al. [2008] 3D | - | 0.84 - 2.00 |
| Brebner and Ofuya [1968] | 1.3 - 3.3 | - |
| Peña et al. [2011] | 2.60 - 6.60 | - |

Table 5.14: Ratios of wavelength to breakwater width

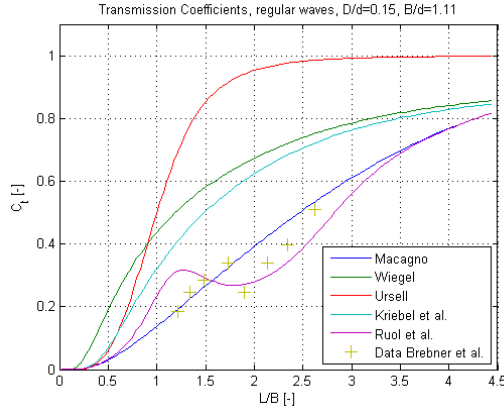


Figure 5.17: Data from Brebner and Ofuya [1968], regular waves (d) = 0.46m and heave period (Th) = 1.12s

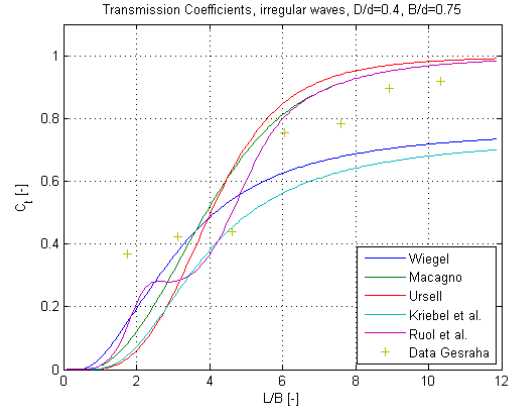


Figure 5.18: Data from Gesraha [2006], irregular waves (d) = 0.43m and heave period (Th) = 5.89s

Ruol et al. [2013a] developed a modification factor for the formula of Macagno in order to take the motions of the floating breakwater into account. Ruol et al. [2013b] investigated between which ranges of χ and D/d their formula is applicable. They concluded that for χ -values between 0.5 and 1.5 and for D/d -values between 0.20 and 0.60 their formula is suitable to apply for both pi-types and pontoon types floating breakwaters.

When the data of Brebner and Ofuya is compared with the formula of Ruol et al. a good agreement is found between the experimental data and the predicted values. For the dataset of Brebner and Ofuya with a D/d -value of 0.15, the formula of Macagno gives a good agreement and the formula of Ruol et al. as well, see Figure 5.17.

| Dataset | RMSE: | RMSE: | RMSE: |
|--|----------------------|----------------------|----------------------|
| | D/d=0.15 B/d=1.11 | D/d=0.19 B/d=1.11 | D/d=0.30 B/d=1.11 |
| Brebner and Ofuya [1968] regular waves | Macagno = 0.0593 | Ruol et al. = 0.0592 | Ruol et al. = 0.0615 |

Table 5.15: Lowest RMSE for different theories for the dataset of Brebner and Ofuya [1968]

Martinelli et al. [2008] performed experiments in a flume (two-dimensional) and performed experiments in a basin (three-dimensional). Both experiments are performed with a D/d ratio equal to 0.13. For the two-dimensional dataset a good agreement is found for the theory of Macagno. For the three-dimensional dataset a good agreement is found for the theory of Ruol et al. and the wave transmission coefficients are for this dataset smaller than for the two-dimensional dataset. In this chapter only two-dimensional datasets are considered and therefore the three-dimensional dataset is neglected here.

| Dataset | RMSE: $2D$, $D/d=0.13$ $B/d=0.4$ |
|--------------------------------------|---|
| Martinelli et al. irregular waves | 0.0411 |

Table 5.16: RMSE for different theories for the dataset of Martinelli et al. [2008]

The experiments performed by Gesraha [2006] for the free floating breakwater are executed under the conditions where the formula of Ruol et al. is applicable. When the RMSE is considered, it is concluded that the formula of Ruol et al. is the most suitable one to apply.

| Dataset | RMSE: $D/d=0.4$ $B/d=0.75$ |
|------------------------------|----------------------------------|
| Gesraha irregu- lar waves | 0.1107 |

Table 5.17: RMSE for different theories for the dataset of Gesraha [2006]

Conclusions

- Three dimensionless ratios are considered in order to make distinction between the applicability of the different theories. These ratios are: width over water depth (B/d), draft over water depth (D/d) and the relative period (χ). For long wave periods the dimensionless values χ and L/B becomes large and the wave transmission coefficient becomes large as well.
- According to the datasets of Peña et al. and Brebner and Ofuya the formula of Ruol et al. is applicable. This holds for the following ranges: $0.5 < B/d < 1.10$ and $0.20 < D/d < 0.60$ and $0.60 < \chi < 1.70$.
- According to the datasets of Martinelli et al. and Brebner and Ofuya the formula of Macagno is applicable. This holds for the following ranges: $0.4 < B/d < 1.10$ and $D/d < 0.20$ and $0.60 < \chi < 1.20$.
- Areas of interest where experimental data is missing holds for the ratio of $B/d < 0.5$ where D/d and χ are in the range where the formula of Ruol et al. is applicable. Another area of interest is for the ratio $B/d < 0.4$ where the formula of Macagno is applicable. These areas will be investigated with a numerical model in the next chapter.

5.2.4 Oblique incident waves

Till so far all the presented experimental data is related to normal incident waves, i.e. waves normal to the breakwater. In more realistic situations waves will approach the breakwater not only perpendicular, but also under an angle (oblique incident waves). Therefore it is important to know what the transmission coefficient will be for oblique incident waves in order to model more realistic situations. Only a few experiments are conducted in wave basins where transmission coefficients are measured for oblique incident waves. Figure 5.19 shows results of an experiment performed in a wave basin. From this figure it can be seen that the transmission coefficient decreases when the wave angle increases relative to the normal of the breakwater.

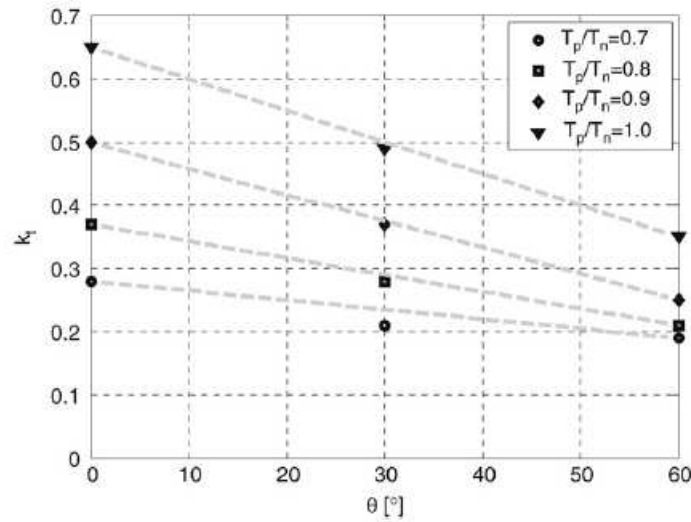


Figure 5.19: Transmission coefficient for oblique incident waves, $\theta = 0^\circ$ implies normal incident waves, [Martinelli et al., 2008]

The decrease of the wave transmission coefficient for oblique incident waves can be taken into account when the above theories are used for a specific type of breakwater. This figure only shows data for relative periods between 0.7 and 1.0. In the next chapter a numerical model will be used in order to investigate the effect of oblique incident waves for larger values of T_p/T_h .

5.3 Conclusion

In this chapter the performance of floating breakwaters is discussed together with the available theories to predict the wave transmission. Based on literature and experimental data a number of conclusions are drawn. With these conclusions a flowchart is constructed which indicates the applicability of the different theories for wave transmission. In this flowchart three different types of floating breakwaters are considered, namely: fixed breakwaters (partially submerged), floating breakwaters anchored by piles and floating breakwaters anchored by chains/cables. The wave steepness (H/L) of the experimental models is approximately between the 1% and 6% for both regular waves and irregular waves. Besides this, the experiments are performed with a horizontal bottom and no overtopping is included.

In order to compare experimental data with the theories for wave transmission, there are a number of relevant dimensionless parameters available to set on the x-axis. For fixed breakwaters and floating breakwaters anchored by piles with a vertical fixed screen between the piles, the dimensionless value wavelength over draft L/D is suggested. For floating breakwaters anchored by piles (without a fixed vertical screen) and floating breakwaters anchored by chains/cables the dimensionless value peak period over natural heave period $\chi = T_p/T_h$ is suggested. A conclusion which holds for all the considered structures is that the wave transmission coefficient is small for short waves. It is observed that the transmission coefficient is smaller than 30% for $L/D < 5$ and for $\chi < 0.6$.

Fixed breakwaters

For values of $L/D < 5$ the wave transmission coefficient is smaller than 30%. For $5 < L/D < 15$

the theory of Macagno is suitable to apply. For $15 < L/D < 95$ the theory of Kriebel and Bollmann is suitable to apply. For $L/D > 95$ there is no experimental data available. Data for this area of interest will be generated with a numerical model, which is discussed in the next chapter. For large L/D -values all the theories are underestimating the wave transmission. For small L/D -values all the theories are overestimating the wave transmission coefficients. The RMSE for these theories is approximately 0.15 in the order of magnitude. This implies that there is a poor agreement between the theories and experiments. When the above theories are applied, the wave transmission will be overestimated in general. For a preliminary design these theories can be applied and will give a good estimation regarding the effectiveness of the fixed breakwater.

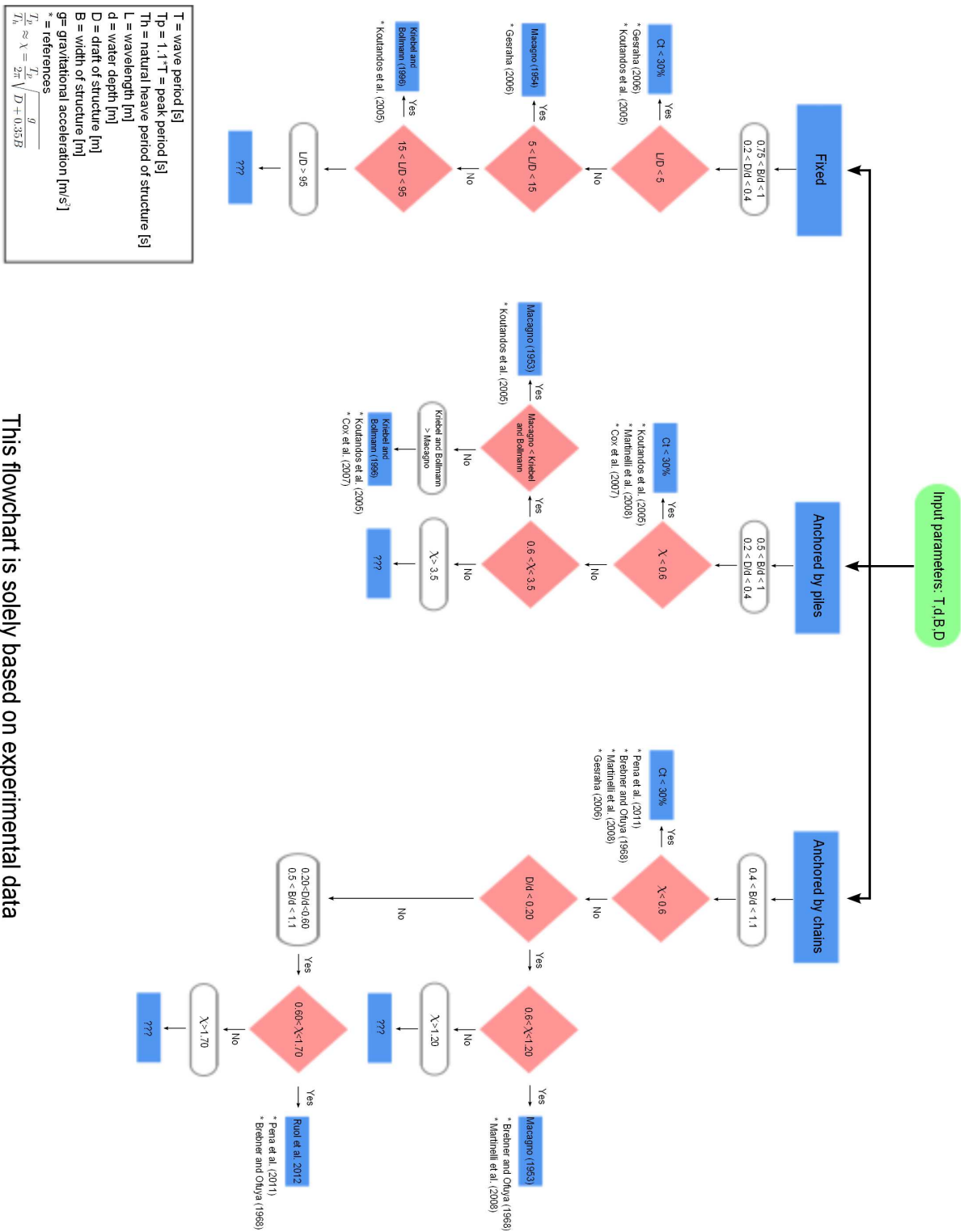
Floating breakwaters anchored by piles

Although all the theories used for the comparisons with experimental data are derived for fixed structures, a reasonable agreement is found for floating breakwaters with one degree of freedom without a fixed vertical screen for the theory of Kriebel and Bollmann. For $\chi < 0.6$ the wave transmission coefficient is smaller than 30%. Based on the experimental datasets of Cox et al., Martinelli et al. and Koutandos et al. it is concluded that for values of $0.6 < \chi < 3.5$ the theory of Kriebel and Bollmann is good applicable. When the theory of Macagno becomes smaller than the theory of Kriebel and Bollmann it is observed that Macagno is suitable to apply, according to the dataset of Koutandos et al. Cox et al. performed experiments with two different wave heights. From these experiments it becomes clear that the influence of the wave height on the wave transmission coefficient is very small compared to the influence of wave period. The RMSE for these datasets are approximately 0.10 in the order of magnitude, meaning a reasonable agreement is found. When the theories discussed above are applied, the wave transmission is slightly overestimated. For a preliminary design this overestimation is not very relevant and a good estimation is obtained regarding the effectiveness of the floating breakwater.

Floating breakwaters anchored by chains

The dimensionless ratios considered in order to make distinction between the applicability of the different theories are: width over water depth (B/d), draft over water depth (D/d) and the relative period (χ). The formula of Ruol et al. is applicable for the following ranges: $0.5 < B/d < 1.10$ and $0.20 < D/d < 0.60$ and $0.60 < \chi < 1.70$. The formula of Macagno is applicable for the following ranges: $0.4 < B/d < 1.10$ and $D/d < 0.20$ and $0.60 < \chi < 1.20$. Areas of interest where experimental data is missing are the ratio of $B/d < 0.5$ where D/d and χ are in the range where the formula of Ruol et al. is applicable. Another area of interest is for the ratio $B/d < 0.4$ where the formula of Macagno is applicable.

Below the flowchart is shown which can be constructed with the conclusions drawn above. In this flowchart there are several question marks shown, this implies that there is no experimental data available. Data can be obtained by performing physical models or by making numerical simulations. The flow chart includes references of authors from which experimental data is obtained. The plots which shows the comparisons between the experimental data and theories are enclosed as Appendix C. From these plots the conclusions becomes visible. Oblique incident waves are not taken into account in this flow chart. The next chapter discusses a numerical model which is used to generate additional data for the areas of interest. This model will also be used to investigate the effect of the ratios, χ , D/d , L/D and B/d .



This flowchart is solely based on experimental data

Figure 5.20: Flow chart of application for wave transmission theories

Modelling of Floating Breakwaters

In the previous section a number of formulas which predicts the wave transmission are compared with experimental data. From this a conclusion is drawn regarding to the applicability of these formulas, which is graphically displayed as a flow chart (Fig. 5.20). From this flow chart it can be observed that there are areas where question marks are present. This implies that there is no experimental data available. Besides this, there are also areas where a bad agreement is found between theory and experimental data. In order to answer these question marks additional data has to be generated by physical modelling or by numerical modelling.

This chapter discusses the numerical model which is used to generate data in order to complete the flow chart shown in the previous section. Numerical data is generated for fixed floating breakwaters, floating breakwaters anchored by piles and anchored by chains.

6.1 Approach

There are several software programs available which are able to compute motions of floating structures. In this thesis the program AQWA is used, which is developed by the company Ansys. The reason for using AQWA is because the program is user friendly and the Delft University of Technology has the program available for students. AQWA is a diffraction and radiation model used to investigate effects of waves, wind and currents on floating structures such as ships and offshore platforms. The program is able to calculate the motions of the floating body and pressures on the floating body and its surrounding. When the surface elevation in front of the structure is known and behind the structure, the wave transmission coefficient can be determined.

Before AQWA will be used to model floating breakwaters, it will be investigated which equations the model solves and which theories are behind these equations. The aim of this is to understand how the model works and to explain the results. The next step is to set up a model which is equal to the physical models performed for the different type of breakwaters and to validate the applicability of the model. Because most of the physical model data is obtained in wave flumes, i.e. two-dimensional experiments, it will be investigated how these two-dimensional situations can be modelled in AQWA since AQWA is a three-dimensional model. The final step is to model the areas of interest where experimental data is missing or where a bad agreement is found for the theories.

6.1.1 Theory used in AQWA

Setting up a model in AQWA is relatively easy and user friendly. Often this means that the user does not know what the program is doing and the model can be seen as a 'blackbox model', meaning that it is difficult to judge the output of the model. Below the theory which is used by AQWA is briefly discussed in order to gain more insight in what the program is doing and when the program is not suitable to use. In Appendix D the theory behind AQWA is discussed into more detail.

AQWA is based on the 3D panel method and on the linear three-dimensional potential flow theory. This implies that viscous forces are not taken into account, the wave elevation is small and the fluid is assumed as incompressible and irrotational. The boundary condition problem is solved by satisfying the body boundary condition (Timman-Newman relations), linearised free surface condition and radiation condition. This theory applies to finite depth and the diffraction problem is solved in the frequency domain.

Calculations can be performed in frequency domain and in time domain. Analyses in the frequency domain implies that the system is linear, i.e. there is a linear relationship regarding displacement, velocity and acceleration. For a linear system it also means that when the input is doubled the output of the system will be doubled as well. In this case the superposition principle holds, which is discussed in section 4.3.1. A nice result of linear theory is that the resulting motions in irregular waves can be obtained by adding the results of regular waves. The output of AQWA are Response Amplitude Operators (RAO's), wave spreading and 2D spectra as a function of wave frequency.

Analyses in time domain implies time/history analyses for (multiple) structures with irregular waves. In this case linear assumptions are not valid and therefore the superposition principle can not be used any more. This is the case for non-linear viscous damping, forces and moments due to currents and wind. The output of the analyses in the time domain are the motions of the structure and forces as a function of time. The calculations performed for this thesis are executed in the frequency domain, since wind and currents are not taken into account and the system can be assumed as linear system.

Waves

All the calculations are performed with the default value of 1.0 for the wave amplitude. The required value for the amplitude is obtained by AQWA by multiplying the default value of 1.0 by the user defined value for the amplitude. The regular waves in AQWA are described by linear wave theory, see Eq.(4.10) and by second order Stokes waves. The theory of Stokes adds corrections to the harmonic wave profile by adding extra harmonic waves to the basic harmonic. Stokes' theory approximates waves which are slightly steeper than harmonic waves and this theory is applicable in deep waters. In AQWA where 2nd order Stokes waves are applied only one 'extra' harmonic wave is added to the basic harmonic with the wave steepness raised to the second order. If the wave steepness is defined as $\epsilon = ak$, then the basic harmonic can be written as:

$$\eta(x, t) = a \cos(\omega t - kx) = \epsilon \eta_1(x, t) \quad \text{with} \quad \eta_1(x, t) = k^{-1} \cos(\omega t - kx) \quad (6.1)$$

In the equation above $\eta_1(x, t) = k^{-1} \cos(\omega t - kx)$ represents the basic harmonic. The first correction in the Stokes theory is adding a harmonic wave to the basic harmonic with the wave steepness squared:

$$\eta(x, t) = \epsilon \eta_1(x, t) + \epsilon^2 \eta_2(x, t) = a \cos(\omega t - kx) + 0.5ka^2 \cos 2(\omega t - kx) \quad (6.2)$$

Figure 6.1 shows the result of the 2nd order Stokes theory. From this figure it becomes clear that the 2nd order Stokes wave has a sharper crest and a flatter trough than a harmonic wave.

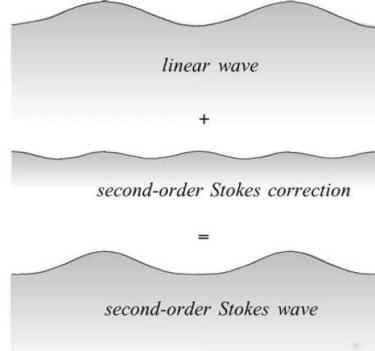


Figure 6.1: 2nd order Stokes waves, [Holthuijsen, 2007]

Potential flow

A velocity potential of a flow is a mathematical expression which has the useful property that the velocity component in a point in the fluid in any chosen direction is the derivative of the potential function [Journée and Massie, 2001]. Potential lines are curves where the potential value is constant. If the potential function is defined as ϕ , then this implies that $\phi = \text{constant}$. When substituting these velocity potentials in the continuity equation the Laplace equation is obtained. The advantage of this theory is that the velocity problem with three unknowns, u_x, u_y and u_z , is reduced to a problem of one unknown, ϕ . When the Laplace equation is solved a solution for ϕ is obtained. The Laplace equation can be solved with the kinematic boundary conditions, which are discussed in Section 4.1 and in Appendix D.2.

Potential flow around floating structures

The pressures on and around the floating body are determined by splitting the linear fluid velocity potential ϕ into three parts:

- Radiation potential (ϕ_r) potential of the oscillations of the body in still water
- Wave potential (ϕ_w) potential of the incoming waves
- Diffraction potential (ϕ_d) potential of the waves diffracting around the restrained body

The resulting fluid velocity potential then becomes:

$$\phi(x,y,z,t) = \phi_r + \phi_w + \phi_d \quad (6.3)$$

When the six degrees of motion are taken into account of the floating body, the radiation potential consist of six parts. Each part belongs to an specific type of motion, represented as $\phi_{r,j}$ where $j = 1, \dots, 6$. The potential of the floating body then becomes:

$$\phi = \sum_{j=1}^6 \phi_{r,j} + \phi_w + \phi_d \quad (6.4)$$

This equation is numerically solved by AQWA which results in potential values from which velocities and pressures are obtained. In total there are seven boundary conditions used to solve the potential of the floating body (Eq.6.4). Three of these seven boundary conditions are discussed in Section 4.1 and are the continuity condition, the kinematic boundary conditions at the seabed and at the surface. These boundary conditions are used to solve the velocity potential without a

floating structure. Besides these three boundary conditions, four additional boundary conditions are used to solve the potential when of floating body is included. These four additional boundary conditions are discussed below.

1. Dynamic boundary condition :
$$\frac{\partial^2 \phi}{\partial t^2} + g \frac{\partial \phi}{\partial z} = 0 \quad \text{at } z=0 \quad (6.5)$$

2. Kinematic boundary of oscillating body :
$$\frac{\partial \phi}{\partial n} = v_n(x, y, z, t) = \sum_{j=1}^6 v_j f_j(x, y, z) \quad (6.6)$$

3. Radiation condition :
$$\lim_{R \rightarrow \infty} \phi = 0 \quad (6.7)$$

4. Symmetric and anti-symmetric conditions :
$$\begin{aligned} \phi_2(-x, z) &= -\phi_2(+x, z) && \text{Sway} \\ \phi_3(-x, z) &= +\phi_3(+x, z) && \text{Heave} \\ \phi_4(-x, z) &= -\phi_4(+x, z) && \text{Roll} \end{aligned} \quad (6.8)$$

Dynamic boundary condition, Eq.(6.5):

The requirement for this condition is that the pressure at the surface equals the atmospheric pressure. This dynamic boundary condition is defined at the water surface and can be derived by differentiating the free surface dynamic boundary condition to t , see Appendix D.2, Eq.(D.23).

Kinematic boundary of oscillating body, Eq.(6.6):

This is the boundary condition at the surface of the floating body and implies that the velocity of the water particles at the surface of the floating body are equal to the velocity of the floating body. In Eq.(6.6) is v_n the outward normal velocity at the surface of the floating body. The subscript $j = 1, \dots, 6$ are indicating the mode of motion of the floating body.

Radiation condition, Eq.(6.7):

Far from the oscillating body the potential value has to become zero. To meet this requirement, the radiation condition states that at a large distance (R) from the floating body the potential value becomes zero.

Symmetric and anti-symmetric conditions, Eq.(6.8):

Since floating bodies, such as floating breakwaters and ships, are symmetric with respect to its middle line plane, the potential equations may be simplified to those three shown as Eq.(6.8). The indices in these equations indicate the directions. The motions for sway and roll are anti-symmetric because the horizontal velocities, $\frac{\partial \phi}{\partial x}$, of the water particles at both sides of the floating body must have the same direction at any time. The heave motions are symmetric because the horizontal velocities must be of opposite sign. The vertical velocities, $\frac{\partial \phi}{\partial z}$, must have the same direction on both sides at any time.

With potential flow theory it is possible to model flows around complex structures, e.g. a ship or circular objects by superimposing simple flow elements. This is possible since the potential flow theory is a linear theory, which allows summation of different flow elements. This principle is discussed into more detail in Appendix D.2.2.

Hydrodynamic and hydrostatic loads

When the velocity potentials are known, forces and moments can be obtained by executing the following steps:

1. Solve the potential function together with the boundary conditions. From this the stream functions and velocity potential functions are obtained.

2. Determine the pressures from the velocity potentials with the linearised Bernoulli equation (Eq.4.8) .
3. Determine the forces and moments by integrating the pressure over the submerged surface (S) of the floating body.

The equations belonging to the three steps above are not discussed into detail, only the result will be discussed. For a more detailed description reference is made to [Journee and Massie, 2001]. The forces and moments are two double integrals of the linearized Bernoulli equation:

$$\vec{F} = \rho \iint_S \left(\frac{\partial \phi_r}{\partial t} + \frac{\partial \phi_w}{\partial t} + \frac{\partial \phi_d}{\partial t} + gz \right) \vec{n} dS = \vec{F}_r + \vec{F}_w + \vec{F}_d + \vec{F}_s \quad (6.9)$$

$$\vec{M} = \rho \iint_S \left(\frac{\partial \phi_r}{\partial t} + \frac{\partial \phi_w}{\partial t} + \frac{\partial \phi_d}{\partial t} + gz \right) (\vec{n} \times \vec{r}) dS = \vec{M}_r + \vec{M}_w + \vec{M}_d + \vec{M}_s \quad (6.10)$$

In Eq.(6.9) and Eq.(6.10) is \vec{n} the outward normal vector on surface dS and \vec{r} is the position vector of surface dS . The result consists of four contributions, which are defined as follows:

1. Radiated waves generated by the oscillating body in still water, \vec{F}_r, \vec{M}_r
2. Waves which are approaching the fixed body (incident waves), \vec{F}_w, \vec{M}_w
3. Waves which are diffracting around the fixed body, \vec{F}_d, \vec{M}_d
4. Hydrostatic buoyancy in still water, \vec{F}_s, \vec{M}_s

To summarize the above, AQWA solves the potential functions (Laplace equation) and determines the pressures at the water surface and at the floating body. The pressures at the water surface can be converted to waves, shown in Figure 6.3. From the pressures on the floating body AQWA calculates the forces and moments by which the equation of motion is derived (equation in Figure 6.2). The fluid force consists of a hydrodynamic force and a hydrostatic force. The hydrodynamic force is the buoyancy force in still water. The hydrodynamic force is divided into wave forces and radiation forces. This is graphically shown below in Figure 6.2.

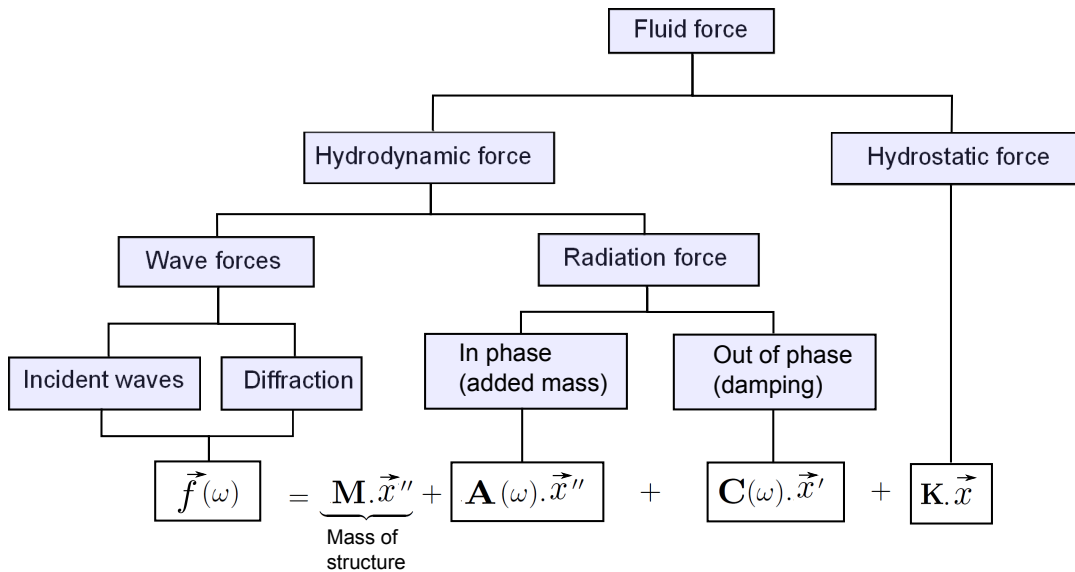


Figure 6.2: Summary of fluid forces, [partially adapted from AQWA ANSYS intro lectures presentation]

The result of the calculation by AQWA is shown in Figure 6.3, where the colours represents pressures in meters of water column.

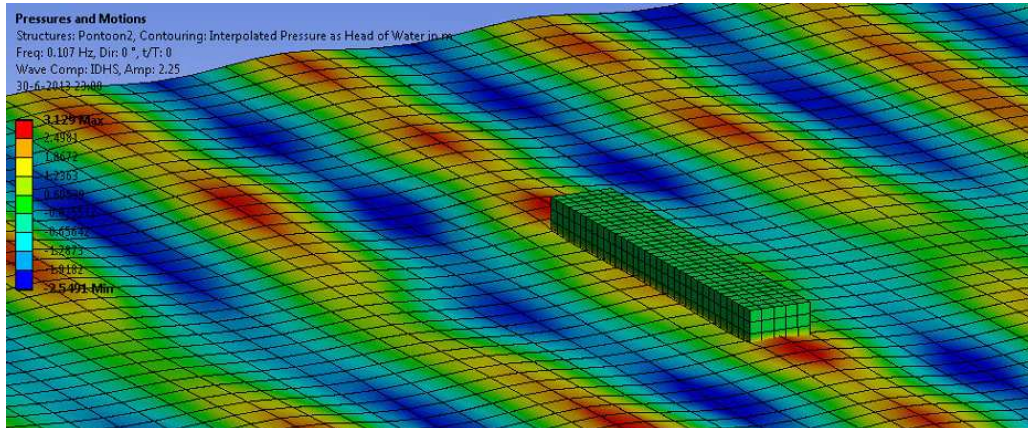


Figure 6.3: Result AQWA presented in pressures on floating structure

3D Panel method

The panel method is a suitable method for objects with zero forward speed. This method calculates the potential around the floating body based on the principle of Green's integral theorem, which states that a three-dimensional linear homogeneous differential equation can be transformed in a two-dimensional integral equation. This implies that the Laplace equation can be transformed into a surface integral, hence the three-dimensional problem becomes a two-dimensional problem. This explains why the surface of the body is divided in a number of panels (two-dimensional) and the water surface can be modelled with a two-dimensional grid. Figure 6.4 shows the panels on the surface of a floating structure.

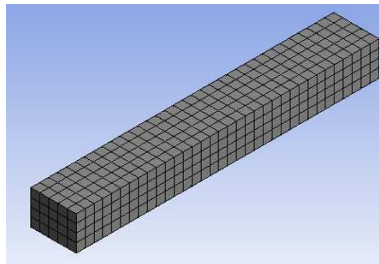


Figure 6.4: Mesh of floating breakwater

The integral obtained by Green's theory represents a number of sources or sinks and dipoles on the surface [Journée and Massie, 2001]. These sources, sinks and dipoles are potential flow elements and are discussed in Appendix D.2.2. The integral obtained by Green's theory is solved in a numerical way by dividing the surface of the body in a number of panels. The source and dipole densities are constant for each panel, resulting in a constant pressure over each element. Flow around sharp corners is not approximated well by this method. In reality flow will separate around these sharp corners, which is not included in the potential theory.

6.1.2 Model set up

Before the areas of interest where no experimental data is known can be modelled, it will be investigated how well the model performs calculations in general. Besides this, the model needs

to be validated. In order to validate the model, experimental data of Koutandos et al. [2005] is used. Koutandos et al. performed experiments with floating breakwaters in a large scale facility for regular and irregular waves for intermediate water depths. They tested floating breakwaters on a model scale of 1:15 and performed tests for fixed and heave floating breakwaters. The tests are executed in a wave flume with normal incident waves, thus no three-dimensional effects were included. AQWA is a three-dimensional model and it takes three-dimensional effects like diffraction into account. During the experiments, the transmitted waves are measured at the point which is located at halve a wavelength (L_{wg}) from the floating breakwater in the center line of the wave flume, see Figure 6.5. To compare the model results with the experimental data, three-dimensional diffraction effects at the location where the transmitted wave is calculated with AQWA needs to be very small. This is achieved by making the length of the floating breakwater long relative to the incident wavelength.

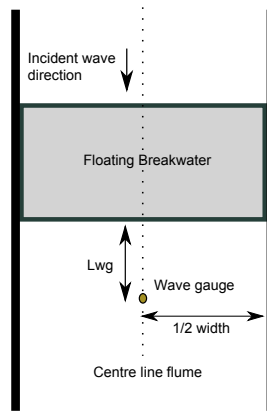


Figure 6.5: Sketch of wave flume

AQWA calculates the wave heights for each wave frequency. The incident wave height is defined in the model and the transmitted wave height is calculated by the model, hence the wave transmission coefficient can be determined. The wave transmission coefficient for each wave frequency is compared with the experimental data. In order to compare how well the model results are for all the wave frequencies, use is made of the Root Mean Square Error (RMSE):

$$RMSE = \sqrt{\frac{\sum_{i=1}^N (Ct_{;experiment} - Ct_{;model})^2}{N}} \quad (6.11)$$

The RMSE applied in this case is a measure of the spread of the experimental transmission coefficients about the modelled transmission coefficients by AQWA.

Sensitivity analyses of 3D effects

As mentioned earlier, the experiments are performed in wave flumes and three-dimensional effects such as diffraction of waves around the breakwater are not taken into account. Diffraction is the turning of waves around objects towards areas which are more sheltered against waves. The wave amplitudes will be lower in these areas due to the lateral spreading of wave energy, see also Section 2.2. AQWA is a three-dimensional model and takes effects like diffraction into account. In order to compare the calculation results with the results of the experiments, the diffraction effects should be minimized at the location where the transmitted wave is calculated. This can be achieved by increasing the length of breakwater.

Many diffraction diagrams are available for diffraction of long crested regular waves around semi-infinite breakwaters with constant water depths. Use is made of these diagrams to determine the

length of the breakwater by which the diffracted wave height is very small at the location where the transmitted wave is calculated. Sommerfeld developed in 1896 an analytical solution of the diffraction problem for light waves, which can be used for semi-infinite breakwaters as well. The Sommerfeld solution which is used for semi-infinite breakwaters is shown in Figure 6.6.

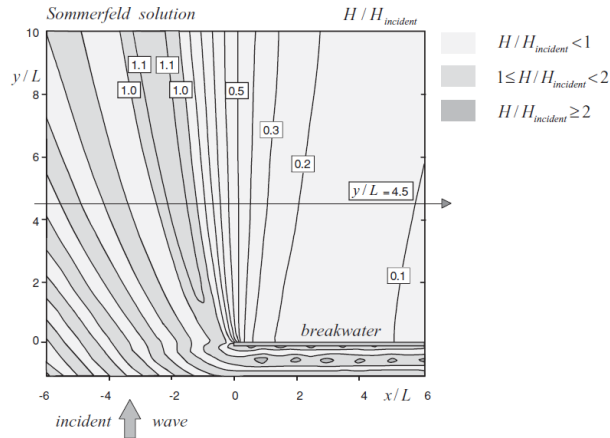


Figure 6.6: Sommerfeld solution for diffraction around an semi-infinite breakwater for normal incident waves, constant water depth, tip breakwater at $x=0$ and $y=0$, [Holthuijsen, 2007]

Bettess et al. [1984] presented a numerical code to solve the diffraction problem of waves for semi-infinite breakwaters based on finite and infinite elements. This code is based on polar coordinates and solves the diffraction problem for which no analytical solution exists. The origin of the coordinate system is located at the tip of the breakwater. This code is implemented in Matlab (which is a mathematical computer program) in order to investigate the effect of the breakwater length on diffraction. The result is shown below as Figure 6.7. From Figure 6.6 and from Figure 6.7 it can be seen that for the dimensionless value $X/L_{wave} = 5$ the diffraction coefficient is 0.1. The diffraction coefficient C_d is defined as the diffracted wave height over the incident wave height. In these figures X represents the breakwater length. At the tip of the breakwater the diffraction coefficient is for both solutions approximately 0.5. Since these solutions are valid for a semi-infinite breakwater, the diffraction coefficient and the X/L_{wave} value needs to be doubled in order to represent a finite breakwater length. Based on these results, it can be concluded that the breakwater length has to be at least ten times the wavelength ($X/L_{wave} \geq 10$) in order to have a diffraction coefficient ≤ 0.2 .

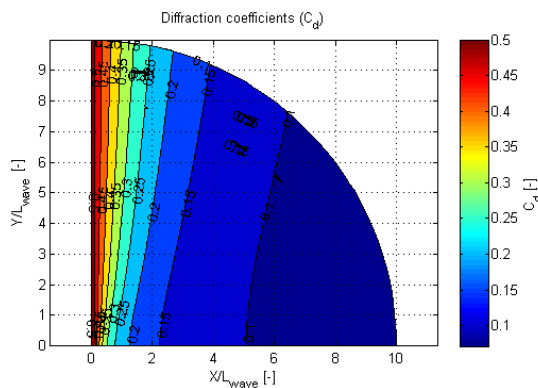


Figure 6.7: Numerical solution of diffraction according to Bettess et al. [1984]

To investigate how AQWA models diffraction, a calculation is performed in AQWA for a fixed non-floating bottom mounted breakwater. In this calculation the breakwater is defined as a fully reflective (impermeable) object. This means that there is no wave transmission because the breakwater is impermeable and there is no overtopping. In this case the calculated wave height by AQWA behind the breakwater represents the diffracted wave height. The wave input for this calculation is shown in Table 6.1. In this dataset the longest wave has a period of 6.99s and with a water depth of 2m the wavelength becomes 30.03m. In order to minimize the diffraction effects, the breakwater modelled in AQWA has to be at least 301.2 meters long according to Figure 6.7. The diffracted wave height is calculated at a distance of half the wave length from the breakwater. This distance is indicated as Lwg in Table 6.1 for each wavelength.

| Lwave [m] | T[s] | Lwg [m] | X/Lwave [-] | Cd;aqwa [-] |
|-----------|------|---------|-------------|-------------|
| 30.03 | 6.99 | 15.06 | 11.62 | 0.13 |
| 23.75 | 5.60 | 11.88 | 14.74 | 0.07 |
| 13.11 | 3.36 | 6.56 | 26.71 | 0.07 |
| 10.20 | 2.78 | 5.10 | 34.30 | 0.13 |
| 8.20 | 2.40 | 4.10 | 42.67 | 0.07 |

Table 6.1: Diffraction results of AQWA for a bottom mounted breakwater with a length (X) of 350 meter

From this table it can be seen that the diffraction coefficient is 0.13 when the breakwater is 11.62 times the wavelength. This is smaller than the expected diffraction coefficients of 0.20.

The diffraction results of the AQWA model for the bottom mounted breakwater can be represented as wave contours (snapshot), shown in Figure 6.8. From this figure it can be seen that the waves turn around the breakwater into the shadow zone. The reflected waves can be identified as well and are shown by the red colours representing high pressures.

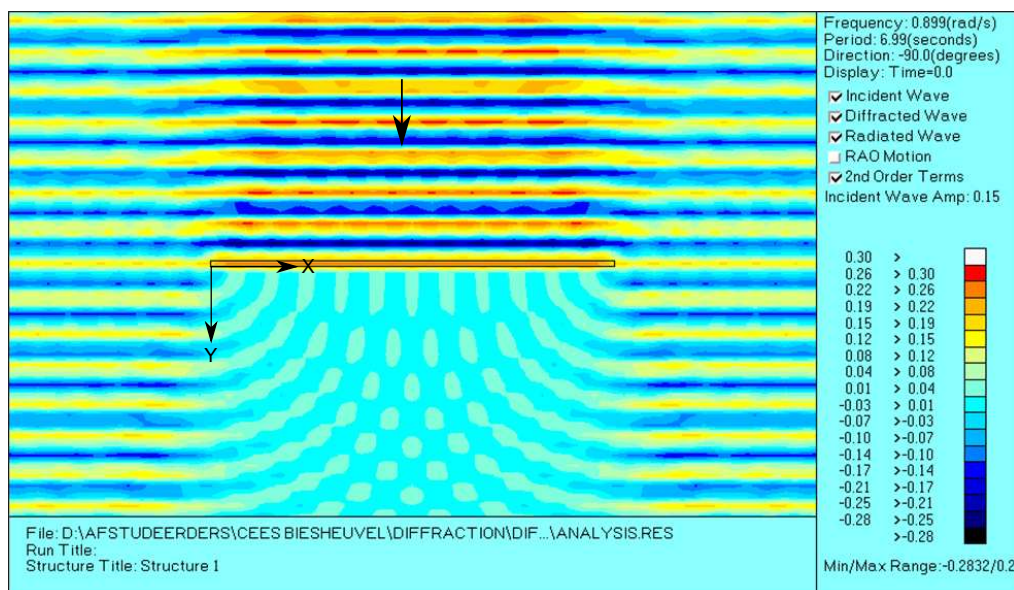


Figure 6.8: Snapshot of surface elevation of diffracted waves in AQWA for normal incident waves, $H=0.30\text{m}$ $T=6.99\text{ s}$, $d=2\text{m}$, fixed breakwater, bottom mounted (non-floating), breakwater length=350 m.

In order to gain more insight in the diffracted wave height behind the breakwater, it is investigated how the diffraction coefficient changes parallel to the breakwater and perpendicular to the breakwater. These results are shown in Figure 6.9. In the upper panel of this figure the diffraction coefficient parallel to the breakwater at a distance of half a wavelength (15m) from the breakwater in the shadow zone is shown. The breakwater in this figure is defined between $x=0$ and $x=350$. It becomes clear that outside the breakwater ($x < 0$) and ($x > 350$) the diffraction coefficient becomes 1.0, which is expected. It can also be seen that at the corners of the breakwater ($x = 0$) and ($x = 350$) the diffraction coefficient is approximately 0.5. This is also expected when making use of the diffraction diagrams (Figure 6.6 and Figure 6.7).

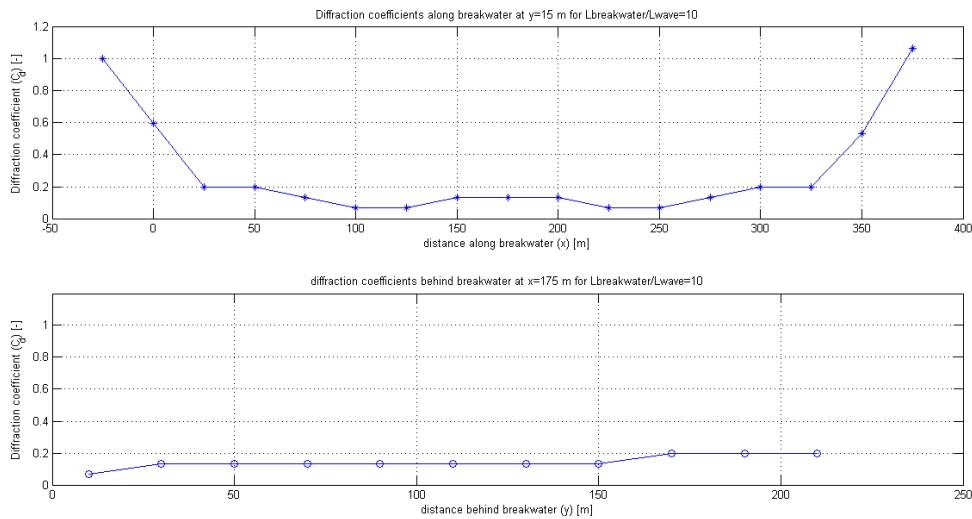


Figure 6.9: $H=0.30\text{m}$ $T=6.99\text{s}$, $d=2\text{m}$, fixed breakwater, bottom mounted (non-floating), breakwater length=350 m.

The lower panel of Figure 6.9 shows the diffraction coefficients perpendicular to the breakwater at the centre line of the breakwater ($x=175$) as a function of the distance behind the breakwater (y). This plot shows that the diffraction coefficient increases when the distance behind the breakwater increases, this is also observed in the Figures 6.6 and 6.7 where the contour lines show a small curvature. The maximum wave amplitudes are shown in Figure 6.10. From this figure it can be seen that the wave amplitude decreases towards the middle of the breakwater.

A remark regarding Figure 6.9 are the 'jumps' of the diffraction coefficients. This is due to the accuracy of the model and partially due to the amount of plotted points. It is expected when more points are plotted and the calculations are performed with a higher accuracy, the line with the diffraction coefficients will be smoother. The accuracy of the model can be explained as follows: The length scale of the model has the unit metres and the calculations are performed with an accuracy of two decimals, hence centimetres. When calculations are performed with wave heights of several metres as input, the output will be more accurate than when the input of the wave height is several centimetres. However, the trend of data points gives a good impression of the diffraction effects.

From Table 6.1 and Figure 6.9 it can be concluded that AQWA always predicts a diffracted wave height for a bottom mounted impermeable breakwater, even in the case when the length of the breakwater is approximately forty times the incident wavelength. The result of this is that the calculated wave pattern behind the floating breakwater consists of transmitted waves and

diffracted waves which reinforce each other or cancel each other out, resulting in a complex wave pattern. Due to this complex pattern it is not possible to subtract the diffracted wave height from the calculated wave height in the shadow zone of the floating breakwater in order to obtain the transmitted wave without diffraction effects. To investigate the magnitude of diffraction on the transmitted waves, wave energy behind the breakwater (in the shadow zone) is considered. The energy of a wave can be expressed as $\frac{1}{8}\rho gH^2$, see also Section 4.2. The energy balance behind the floating breakwater is:

$$H_t^2 + H_d^2 = H_{total}^2 = 1 \quad (6.12)$$

Because the diffracted wave height behind the breakwater changes in space (see Figure 6.9), the average diffracted wave height is determined for an specified area which is indicated as a grid in Figure 6.10. In each grid cell the diffracted wave height is calculated. With the diffracted wave heights calculated for this grid the average diffracted wave height is determined, which equals 0.12. Using the energy balance shown as Eq.(6.12) the following is obtained:

$$H_t^2 + H_d^2 = H_{total}^2 = 1 \quad \rightarrow \quad H_t = \sqrt{H_{total}^2 - H_d^2} \quad \rightarrow \quad H_t = \sqrt{1^2 - 0.12^2} \approx 0.993 \quad (6.13)$$

From Eq.(6.13) it becomes clear that the effect of diffraction is negligible small on the transmitted wave height. Therefore, the calculated transmission coefficients by AQWA will not be corrected in the following sections of this thesis.

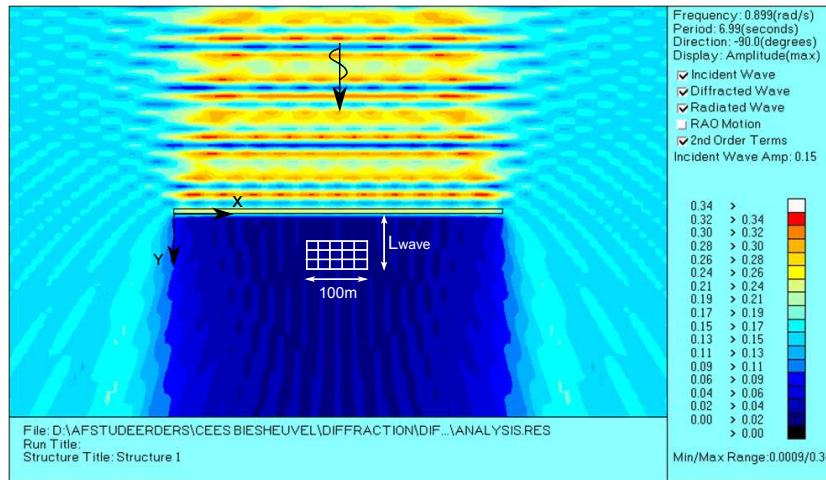


Figure 6.10: Maximum wave amplitudes solely due to diffraction and grid used to determine the average diffracted wave height due to normal incident waves, $H=0.30\text{m}$ $T=6.99\text{ s}$, $d=2\text{m}$, fixed breakwater, bottom mounted (non-floating), breakwater length=350 m.

Mesh size

Another aspect which might influence the calculation results is the mesh size and thus the number of panels. A small mesh results in a large number of panels. The mesh size relates to the maximum wave frequency which can be calculated by the model. A small mesh size allows high wave frequencies to be modelled. This can be explained because high wave frequencies represents short waves. In order to model short waves well a number of grid cells needs to be available which is achieved with a small mesh size. Depending on the mesh size which has to be defined by the user, AQWA will specify the highest wave frequency which can be modelled. When the mesh size

is too coarse to model an specified frequency, AQWA will give an error. The longest wave which can be modelled in AQWA depends on the water depth. To gain insight in the effect of the mesh size a number of models with the same wave input are made where the mesh size increases from a coarse mesh to a fine mesh.

The model used for the comparison is a fixed structure located in a water depth of 2m. The dimensions of the structure are as follows: length = 350m, width=2m and the draft=0.67m. The wave periods used for the calculations together with the calculated transmission coefficients are shown in Table 6.3. The coarsest mesh size used for the calculations has 5862 panels and the finest mesh has 17550 panels. The maximum number of panels in AQWA is 18000. With the coarsest mesh size AQWA was just able to model the shortest wave period. In total six calculations are performed where the mesh size of each calculation decreased and the number of panels increased, see Table 6.2. For all the calculations the same input (T) is used, shown in Table 6.3. The result is that the calculation results (Ct) did not change when the mesh size decreased. From this it is concluded that the mesh size does not influence the calculation results as long as the mesh is fine enough to model the shortest waves.

| Calculation | Number of panels |
|-------------|------------------|
| 1 | 5862 |
| 2 | 11722 |
| 3 | 12622 |
| 4 | 14650 |
| 5 | 16730 |
| 6 | 17550 |

Table 6.2: Number of panels used for the calculations to investigate the effect of the mesh size

| T [s] | Ct [-] |
|-------|--------|
| 6.97 | 0.87 |
| 5.60 | 0.87 |
| 3.36 | 0.67 |
| 2.78 | 0.53 |
| 2.40 | 0.33 |

Table 6.3: Input (T) and the computed output (Ct) used for the model to investigate influence of mesh size

6.1.3 Model calibration and validation

Now the diffraction effects and the influence of the mesh size are investigated, the data of the two-dimensional experiments performed by Koutandos et al. [2005] can be used to compare how well AQWA can model the transmitted waves of floating breakwaters. Since AQWA is based on potential flow theory it takes no turbulence into account and therefore no energy losses. When energy losses are taken into account the transmitted wave height will be lower. Because of this it is expected that AQWA predicts higher transmission coefficients than are observed during the experiments. The remark made for Figure 6.9, regarding the 'jumps' of the numerical data points and model accuracy, also holds for the figures shown below where numerical data points are plotted.

Model validation for fixed breakwaters

In AQWA three different simulations are performed for fixed breakwaters. The difference between the simulations is the draft of the breakwater. For each simulation the transmission coefficient is determined at the point which is located at half a wavelength from the breakwater. The table below shows the simulation results for the fixed breakwater with a draft of 0.5m ($D/d=0.25$). The results for the fixed breakwaters with a draft of 0.4m and 0.67m are shown in Appendix D.3.1 in Table D.2 and D.3. The RMSE for these two fixed floating breakwater are 0.07 and 0.03 respectively.

| T [s] | Ct _{AQWA} [-] | Ct _{exp} [-] | Ct _{exp} - Ct _{AQWA} |
|-------------|------------------------|-----------------------|--|
| 5.50 | 0.87 | 0.81 | -0.05 |
| 3.33 | 0.73 | 0.73 | -0.01 |
| 2.77 | 0.60 | 0.56 | -0.04 |
| 2.50 | 0.53 | 0.48 | -0.05 |
| 2.20 | 0.40 | 0.38 | -0.02 |
| RMSE | | | 0.04 |

Table 6.4: Results AQWA compared with data obtained from Koutandos et al. [2005] for a fixed floating breakwater, regular waves, $D=0.5m$, $L=350m$, $d=2m$

In the Figures 6.11 and 6.12 the results of the numerical models are shown together with the experimental data and the theories for wave transmission. From these figures it can be concluded that the numerical model approximates the experimental data very well. The transmission coefficients obtained from AQWA are larger than the transmission coefficients measured during the experiments, which is expected because turbulence is not included in AQWA. This is also observed in Table 6.4. There is no experimental data available for shorter wave periods. When these shorter wave periods are modelled, it can be seen that these results follow the same trend line which one could draw through the experimental data points.

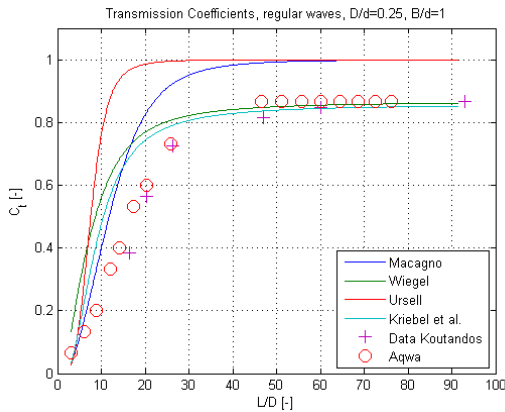


Figure 6.11: Experimental data from Koutandos et al. [2005] for fixed breakwater compared with numerical model AQWA, regular waves ($d = 2m$, $(B) = 2m$)

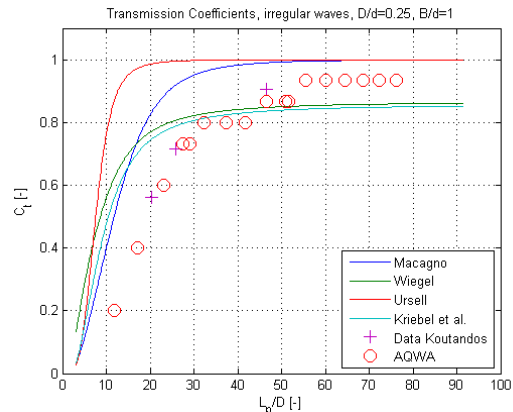


Figure 6.12: Experimental data from Koutandos et al. [2005] for fixed breakwater compared with numerical model AQWA, irregular waves, ($d = 2m$, $(B) = 2m$)

Irregular wave input

The input for AQWA consists of regular waves with a wave period T for each wave. Irregular waves are often presented in literature as waves with a peak period and a significant wave height. The peak period is the period which corresponds with the frequency in the spectrum for which the spectrum has a maximum. The proper manner to model irregular waves in AQWA is to decompose a wave spectrum into a number of regular waves with different frequencies and amplitudes, see also Section 4.1.2. In the case of a two-dimensional spectrum, the wave direction should be taken into account as well. Regular waves with different frequencies and amplitudes (and directions) can be used as input for AQWA. AQWA calculates for each wave period and for each wave direction the transmitted wave. With the transmitted wave heights and periods, a new wave spectrum can be generated. This wave spectrum represents the wave spectrum of the transmitted waves. When

the significant wave height of the transmitted spectrum is divided by the significant wave height of the incident wave spectrum the transmission coefficient is obtained.

A more simplified method to estimate the effect of irregular waves in AQWA is considering the peak period T_p as input for a regular wave. The difference between the peak period and the mean period is that the mean period approximately 10% smaller is than the peak period. The advantage of using the peak period of spectrum as input for the period of a regular wave is that the calculation time is less than when a number of periods are modelled in order to represent a spectrum. This method is applied to model irregular waves in AQWA, the results are shown in the table below. From this table it becomes clear that when a regular wave is modelled with a peak period and a significant wave height, the differences between results of AQWA and the experiments for irregular waves are small. In order to draw proper conclusions regarding irregular wave input, the calculations results of a decomposed spectrum should be compared with the calculation results shown in Table 6.5 (regular wave with a peak period). Because the limited amount of time, no calculations with AQWA are performed for a decomposed spectrum. In the next sections a regular wave with a period equal to the peak period will be used to model irregular waves because the differences are small between AQWA and the experiments.

| Tp [s] | T_{in;aqwa} [s] | Ct_{AQWA} [-] | Ct_{exp} [-] | Ct_{exp} - Ct_{AQWA} |
|---------------|--------------------------------|------------------------------|-----------------------------|---|
| 5.50 | 5.50 | 0.87 | 0.92 | 0.05 |
| 3.34 | 3.34 | 0.73 | 0.76 | 0.03 |
| 2.78 | 2.78 | 0.60 | 0.59 | -0.01 |
| RMSE | | | | 0.03 |

Table 6.5: Peak wave period as input for wave periods in AQWA

Model validation for heave floating breakwaters

Floating breakwaters which are for instance anchored by piles have one degree of freedom, which are only vertical translations called heave. Due to the vertical motions of the floating breakwater, waves are generated which are radiating away from the structure (radiated waves). The larger the vertical motions are, the larger the radiated waves are, hence the larger the transmission coefficient will be. Therefore it is important to model the heave motion well in order to obtain the transmission coefficient.

AQWA is able to model fixed structures and structures with six degrees of freedom. In order to model one degree of freedom use is made of springs with a very large spring stiffness. Additional springs are defined for all the degrees of freedom except for heave. These springs contains very large spring stiffness values in order to prevent motions. The heave floating breakwater used in the experiments of Koutandos et al. contained wheels at the corners of the floating structure. These wheels are running in rails which are attached to the walls of the flume. This combination of wheels and rails allows unrestricted vertical motions. In this experiment some mechanical friction was present due to the horizontal wave forces on the floating breakwater. Beside mechanical friction, viscous effects were present. The mechanical friction and viscous effects limits the heave motion and are not taken into account by AQWA. Because the radiated waves and thus the heave motions influence the wave transmission coefficient, it is important that the heave motions in the model are the same as the heave motions measured during the experiments.

The heave floating breakwater modelled in AQWA is calibrated with the heave motion observed during the experiments, shown in Figure 6.13. The maximum amplitude of this record is 0.129m

for a wave height of 0.2m and a period of 2.65s. This implies that the Response Amplitude Operator (RAO) should be 0.645 meter for this period. The RAO is the response motion of a floating object for an incoming wave height of 1m.

Initially, the heave motions modelled by AQWA were larger than the observed motions during the experiments. In order to obtain the same heave motion in the model as in the experiments, additional hydrodynamic damping is used. This damping represents mechanical friction between the pontoon and the anchoring system and viscous effects. With trial and error the necessary additional damping constant for heave was found of 1600000 N s/m, for a floating breakwater with a length of 350m, a width of 2m and a draft of 0.4m. This additional damping is assumed to be independent of the wave frequency. The RAO of the heave floating breakwater with this damping constant is shown in Figure 6.14.

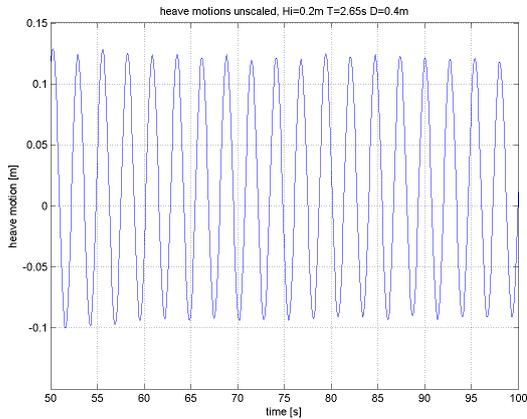


Figure 6.13: Measured heave motion of experiments for regular waves with $T=2.65s$ obtained from Koutandos

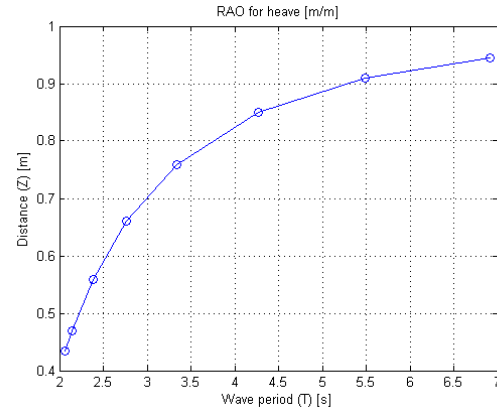


Figure 6.14: Response Amplitude Operator (RAO) for floating breakwater anchored by piles, obtained from the AQWA calculations

The same value for the damping is used for the other frequencies. Furthermore, the AQWA model equals the input of the experimental model in order to compare the results of AQWA with the experiments. The calculation results of AQWA for the floating breakwater anchored by piles are shown in Table 6.6.

| T [s] | f [Hz] | L_{wave} [m] | L_{wg} [m] | Ct_{exp} [-] | Ct_{aqwa} [-] | $Ct_{exp}-Ct_{aqwa}$ [-] |
|-------------|----------|----------------|--------------|----------------|-----------------|--------------------------|
| 6.91 | 0.14 | 28.86 | 14.43 | 0.86 | 0.89 | -0.03 |
| 5.49 | 0.18 | 29.86 | 14.93 | 0.85 | 0.89 | -0.04 |
| 4.27 | 0.23 | 30.86 | 15.43 | 0.85 | 0.89 | -0.04 |
| 3.34 | 0.30 | 31.86 | 15.93 | 0.82 | 0.79 | 0.03 |
| 2.76 | 0.36 | 32.86 | 16.43 | 0.73 | 0.69 | 0.04 |
| 2.39 | 0.42 | 33.86 | 16.93 | 0.69 | 0.49 | 0.20 |
| 2.14 | 0.47 | 34.86 | 17.43 | 0.47 | 0.39 | 0.08 |
| 2.06 | 0.49 | 35.86 | 17.93 | 0.41 | 0.40 | 0.01 |
| RMSE | | | | | | 0.08 |

Table 6.6: Results AQWA compared with data obtained from Koutandos et al. [2005] for a heave floating breakwater, $D=0.4m$, $L=350m$, $d=2m$, $Th=2.10s$

In this table large differences between the experimental transmission coefficient and the modelled transmission coefficient are observed for the wave periods of 2.14s and 2.39s. The natural heave period T_h (without damping) is 2.10s. The difference is probably due to additional damping which is present in the model, the result is that the natural heave period increases.

In Figure 6.15 it can be seen that the results of AQWA show a good agreement with the experimental data. For the value $\chi \approx 1$ ($L/B \approx 4$) a large deviation is observed in this figure. This deviation can be explained because of the additional damping used in the AQWA model. A 'jump' in the numerical data points is observed for $\chi \approx 4.3$ ($L/B \approx 19$). This can be explained by the accuracy of the model, which is explained in Section 6.1.2. When numerical data is generated for the areas where no experimental data is available, it can be concluded that these results follow the same trend line which one could draw through the experimental data points. Therefore it is concluded that AQWA is suitable to model floating breakwaters with one degree of freedom.

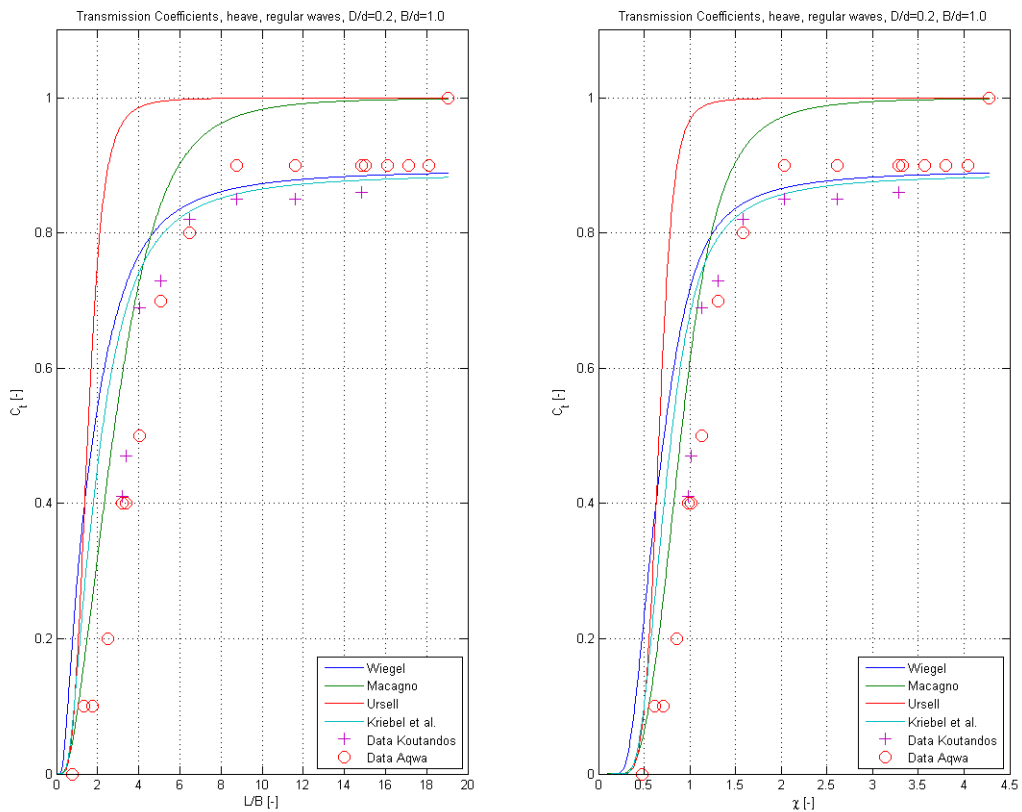


Figure 6.15: Experimental data from Koutandos et al. [2005] for heave floating breakwater compared with numerical model AQWA, regular waves, (d) = 2m, (B) = 2m, T_h = 2.10s

Model validation for floating breakwaters anchored by chains

AQWA is initially designed to determine the motions of floating structures with six degrees of freedom and takes hydrodynamic damping into account. Therefore it is expected that AQWA is suitable to model floating breakwaters with six degrees of freedom. The floating breakwater modelled in AQWA is described by Martinelli et al. [2008]. This is a pi-type floating breakwater, which is in fact a pontoon with two vertical screens on both sides. Because these vertical plates are

very thin, it is not possible in AQWA to model these plates because the amount of panels exceeds the maximum of 18000. In AQWA this floating breakwater is modelled as a pontoon (rectangular box) with the same draft as the the length of the vertical plates of the pi-type floating breakwater.

In order to model a floating breakwater anchored by piles well, additional damping is needed which represents mechanical friction between the pontoon and the anchoring system and represents the viscous effects, this is discussed above. For floating breakwaters anchored by chains, it is also expected that additional damping needs to be included in the model. The chains or cables by which the floating breakwater is anchored will behave like a spring, which is attached below the floating structure. To investigate how large this effect is, two simulations are performed. One simulation does not include additional damping and the other simulation only includes additional damping for the heave motion. The results are shown below in the Figures 6.16 and 6.17.

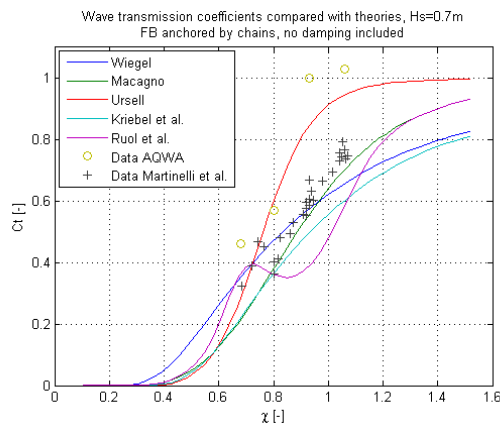


Figure 6.16: Comparison between experimental data and numerical data no damping included

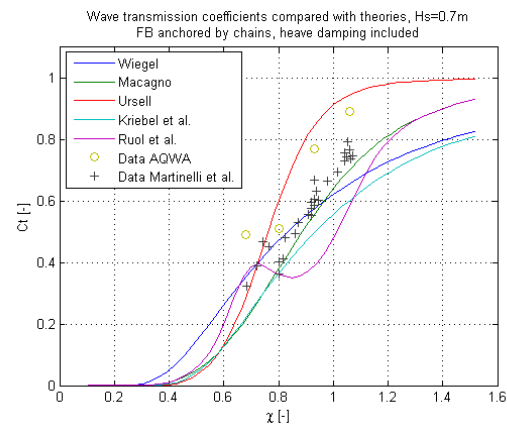


Figure 6.17: Comparison between experimental data and numerical data where heave damping is included

From Figure 6.16 it becomes clear that the transmission coefficients modelled by AQWA are much larger than the transmission coefficients of the experimental data. When the RAO's are considered, which are shown in Figure 6.18 and 6.19 it can be seen that the heave motions are very large. This is expected because there is no additional damping in the model. Therefore, additional damping should be taken into account in the model. During the experiments no motions were measured of the floating breakwater. Because of this, the model can not be calibrated. In order to see what the effect will be when additional damping is included, the same additional damping coefficient used in the model of the floating breakwater anchored by piles is used. The reason why the same amount of additional damping is used, is because the floating breakwaters in both models have dimensions in the same order of magnitude. The result of this additional damping is that the transmission coefficient determined by the model where damping is included is smaller than the transmission coefficients determined by the model without damping. When the RAO's are considered of the model with additional damping, it can be seen that the heave motions are smaller. When considering the sway motions, it can be seen that these are relatively large in comparison with the heave motions. Therefore, additional damping might also be necessary for sway motions in order to calibrate the model. The roll motions are small (maximum of 3.4 degrees per meter) and does not change due to the additional damping for heave.

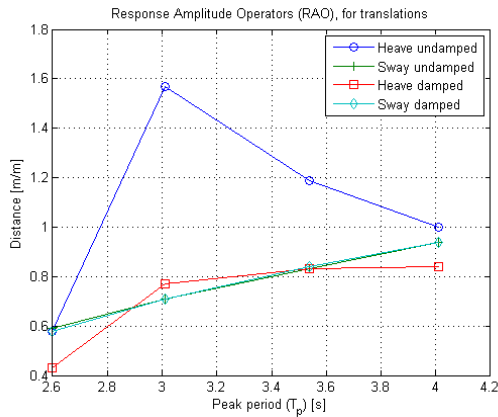


Figure 6.18: RAO's for translations of floating breakwater anchored by chains modelled with AQWA

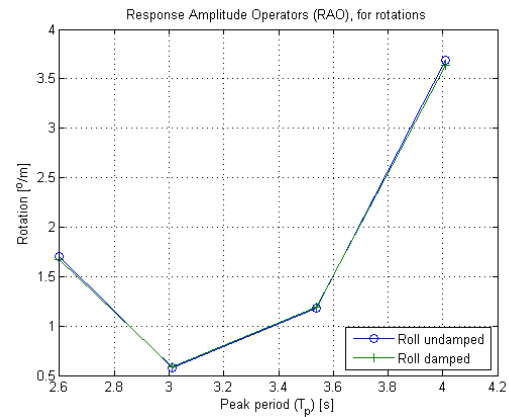


Figure 6.19: RAO's for rotations of floating breakwater anchored by chains modelled with AQWA

It can be concluded that the anchoring system of floating breakwaters with six degrees of freedom has a large influence on the effectiveness. The anchoring system can be seen as a spring. Therefore, numerical models of floating breakwaters needs to be calibrated in order to obtain realistic data. This calibration can be done by adding damping to the system. When the RAO's of the model are the same as during the experiments, the model can be used after validation. Because the experimental data of the motions of the floating breakwater is not available, the model can not be calibrated and other simulations for this type of floating breakwater are not performed.

6.2 New simulations for areas of interest

In section 5.1.3 several wave transmission theories are compared with experimental data. Based on these comparisons conclusions are drawn regarding to the applicability of the wave transmission theories. These conclusions are shown in the form of a flowchart, see Figure 5.20. In the plots below some 'jumps' can be observed in the numerical data points, this is due to the accuracy of the model which is discussed in Section 6.1.2.

The availability of experimental data is very limited and does not cover all the areas of interest. Besides this, some conclusions based on experimental data needs to be verified. In order to obtain additional data and to verify the previous conclusions, validated AQWA models are used. These validated models are discussed in the previous section. The new data obtained from the models will be compared with the wave transmission theories. Finally, a number of new conclusions are drawn and the flowchart shown in Figure 5.20 will be updated with numerical data obtained from AQWA.

6.2.1 Fixed breakwaters

There is experimental data available for fixed breakwaters for the ranges of $0.75 < B/d < 1.00$ and for $0.20 < D/d < 0.40$. From the flowchart shown in Figure 5.20, it can be seen that for fixed breakwaters for L/D values larger than 95 no experimental data is available. Besides this, the B/d ratios are large and it would be interesting to see what the influence is of smaller B/d ratios. In order to gain insight in the influence of the parameters B and D , a number of simulations are performed where these parameters are varied. The simulations are executed for the range of wave periods between 2 and 8.5 seconds, with an interval period of 0.5s.

For the area of interest in the flowchart for L/D -values larger than 95, the result is shown in Figure 6.20.

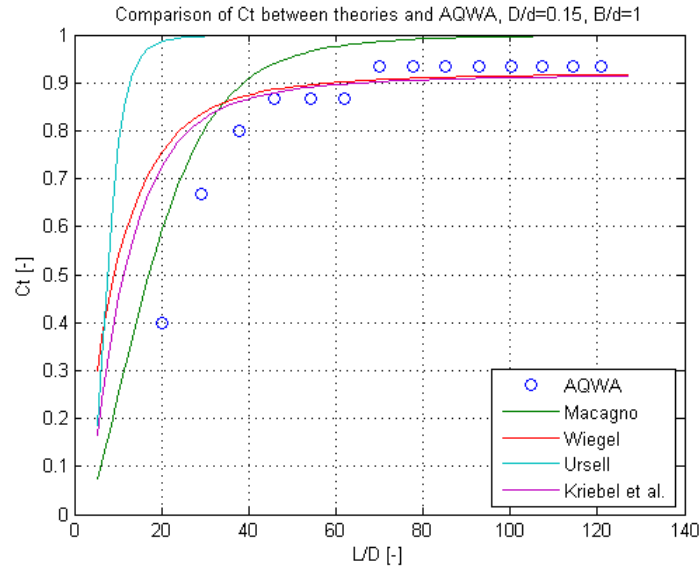


Figure 6.20: Data AQWA compared with theories for fixed breakwaters, $d=2\text{m}$, regular waves

Regarding Figure 6.20 it can be concluded that for small L/D values the theories of Wiegel and Kriebel and Bollmann are nearly the same. For large L/D -values both theories show a good agreement with the model data. When the results for the theory of Macagno becomes smaller than the theory of Kriebel and Bollmann, Macagno shows a good agreement. This is also observed with the comparisons of experimental data for fixed breakwaters and floating breakwaters anchored by piles where the D/d ratio is small compared to the B/d ratio. Whether this conclusion is due to the combination of small D/d ratios compared to the B/d ratio, will be investigated below, where the width is varied.

Variation of width and draft

In total six simulations are performed. In three simulations the draft is increased while the other parameters are constant. In the other three simulations the width is decreased while the other parameters are constant. The range of the parameters used in the calculations are outside the range of the experimental data in order to draw new conclusions. For each simulation the results are compared with the theories for wave transmission. All these comparisons are enclosed as Appendix D.4.1. Below the conclusions are discussed regarding these comparisons.

In Figure 6.22 the influence of the draft is shown. From this figure it becomes clear that when the draft increases, the transmission coefficient decreases, which is expected.

The effect of the width of the floating breakwater on the wave transmission coefficient is taken into account by the theory of Macagno for fixed breakwaters. To gain insight in the influence of the width on the wave transmission coefficient, three simulations are performed with AQWA. Figure 6.21 shows the results of these simulations for the different widths and constant drafts. From this figure it becomes clear that the width of the floating breakwater has a large effect for small wave periods. When the effect of the draft and the width are compared (see Figures 6.22 and 6.21), it is concluded that the draft has a larger effect in reducing the wave transmission coefficient than the width for this specific case. This result may vary when ratio D/d is very small compared to the B/d ratio.

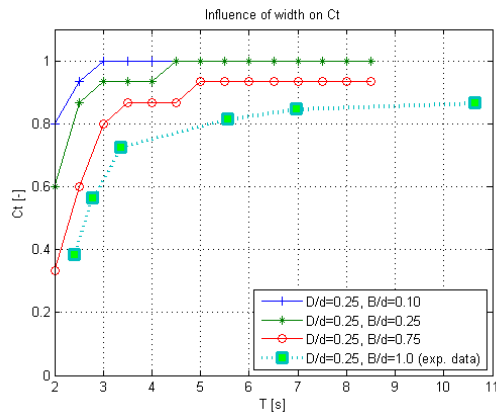


Figure 6.21: Influence of the variation of width on C_t , $d=2\text{m}$, regular waves, exp. data obtained from Koutandos et al. [2005]

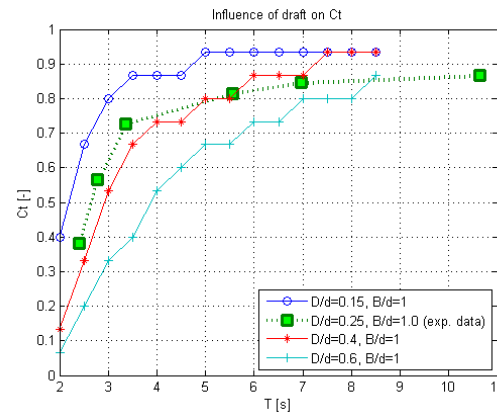


Figure 6.22: Influence of the variation of draft on C_t , $d=2\text{m}$, regular waves, exp. data obtained from Koutandos et al. [2005]

Conclusions regarding comparisons between theories and numerical model

The comparisons between the calculations performed with AQWA and the transmission theories where the draft and the width are varied can be found in Appendix D.4.1. Regarding to these comparisons the following conclusions are drawn:

- For $0.75 < B/d < 1.0$ and $0.15 < D/d < 0.4$ the theory of Kriebel and Bollmann is suitable to apply, which generally holds for large L/D values. When the theory of Macagno predicts smaller values than the theory of Kriebel and Bollmann (short waves), the theory of Macagno should be applied.
- For $0.75 < B/d < 1.0$ and $D/d > 0.4$ a poor agreement is found between the results of AQWA and the transmission theories. For this area physical or numerical models maybe suitable to apply.
- The width of the floating breakwater has a positive effect on the reduction of the wave transmission coefficient. This effect is taken into account by the theory of Macagno for fixed breakwaters. When the results of the AQWA model are considered (Appendix D.4.1), it is concluded that the theory of Macagno is suitable to apply for ratios of $B/d < 0.75$ and for a D/d ratio of 0.15.
- When the effect of the draft and the width are compared with each other, it is concluded that the draft has a larger effect in reducing the wave transmission coefficient than the width for the case which is modelled. This result may vary when the D/d ratio is small compared to the B/d ratio.

6.2.2 Floating breakwaters anchored by piles

There is experimental data available for floating breakwaters anchored by piles for the ranges $0.5 < B/d < 1.0$ and for $0.2 < D/d < 0.4$, see also the flowchart in Figure 5.20. An area of interest for this type of floating breakwater where data is missing is indicated in the flowchart as the area where the relative period $\chi > 3.5$ (long waves). A model in AQWA is made to model the areas where $\chi > 3.5$. For this calculation the validated model of Koutandos et al. is used. The mechanical friction between the floating breakwater and anchoring system is represented in this model as additional damping. The details of this validated model regarding to the motions and damping are discussed in Section 6.1.3. The results are shown in Figure 6.23. From this Figure

it can be concluded that the theories of Wiegel and Kriebel and Bollmann are suitable to apply for long waves. From this Figure it can also concluded that when the theory of Macagno predicts smaller values for the transmission coefficient than the theory of Kriebel and Bollmann, Macagno should be applied. The data point at $\chi \approx 4.3$ looks like an outlier and is due to the accuracy of the model.

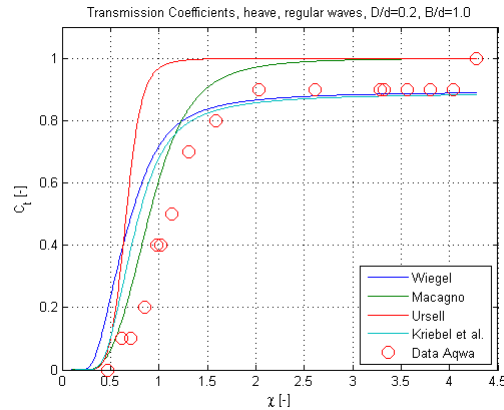


Figure 6.23: Flow chart of application for wave transmission theories

Variation of width and draft

The effect of the draft of the floating breakwater on the wave transmission coefficient is investigated by making several models where the draft varies and all the other parameters are constant for each model. The same is done for the width where the width varies and the other parameters are constant. The variation of these parameters D/d and B/d are outside the range where experimental data is available in order to draw new conclusions related to the applicability of the different transmission theories. The comparisons between the model results and the theories are enclosed as Appendix D.4.2.

Figure 6.25 shows the effect of the draft on the transmission coefficient and Figure 6.24 shows the effect of the width on the transmission coefficient. Just as for the fixed breakwater it can be concluded that the draft has larger effect on the wave transmission coefficient than the width for this specific case. Results may vary when the ratio D/d is small compared to the B/d ratio.

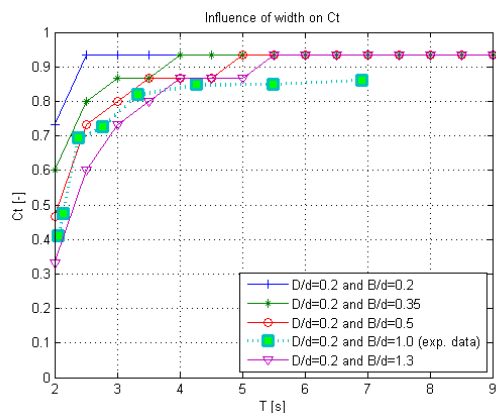


Figure 6.24: Influence of the variation of the width on C_t , $d=2m$, regular waves, exp. data obtained from Koutandos et al. [2005]

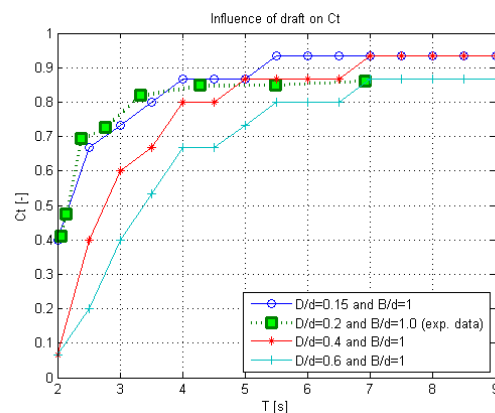


Figure 6.25: Influence of the variation of the draft on C_t , $d=2m$, regular waves, exp. data obtained from Koutandos et al. [2005]

Conclusions regarding comparisons between theories and numerical model

In Appendix D.4.2 the comparisons are shown between the model data and the theories for wave transmission. Based on these comparisons the following conclusions are drawn:

- For the ranges of $0.15 < D/d < 0.40$ and $0.2 < B/d < 1.0$ the theory of Macagno is suitable to apply and overestimates the modelled data. For χ -values smaller than 2 this overestimation becomes larger.
- For the ratios $D/d > 0.4$ and $B/d = 1.0$ a very poor agreement is found for χ -values larger than 2.0. Physical and numerical models are suitable to obtain proper transmission coefficients for this area of interest. For χ -values smaller than 2 the theory of Kriebel and Bollmann is suitable to apply.
- Both the width and the draft of the floating breakwater has an effect on the wave transmission. However, the draft has the largest effect on the wave transmission for the case which is modelled. This result may vary when the D/d ration is small compared to the B/d ratio.

6.2.3 Floating breakwaters anchored by chains

The AQWA model for floating breakwaters anchored by chains is not calibrated with the experimental data. This is because the motions of the floating breakwater observed during the experiments on which the model should be calibrated are not available. In Section 6.1.3 the calculations results of the (non-calibrated) model are compared with the experimental data. From these calculation results the conclusion can be drawn that additional damping is needed in the model to represent the effect of the anchoring system and viscous effects on the breakwater. Because the model is not calibrated, new simulations are not performed. New simulations made with a model which is not calibrated and validated are very unreliable and are often not good.

6.2.4 Oblique incident waves

Martinelli et al. [2008] performed experiments for floating breakwaters anchored by chains in a wave basin for waves which approached the breakwater under an angle, oblique incident waves. Martinelli et al. concluded that when the wave angle increases, the transmission coefficient decreases. This conclusion is drawn regarding Figure 6.26.

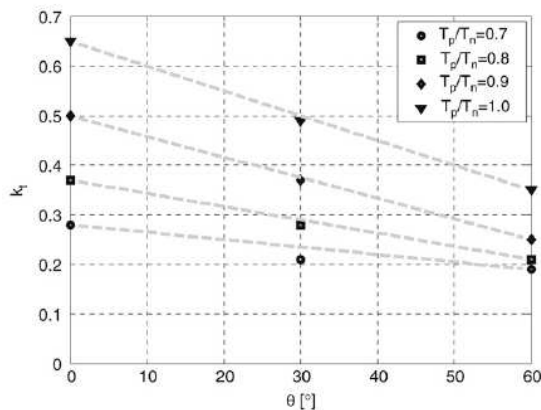


Figure 6.26: Transmission coefficient for oblique incident waves, $\theta = 0^\circ$ implies normal incident waves, [Martinelli et al., 2008]

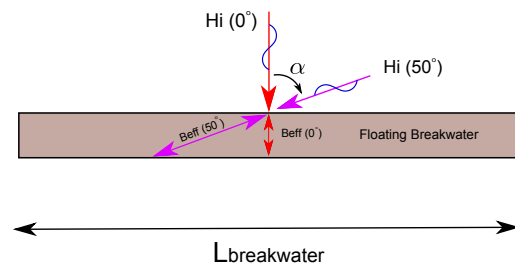


Figure 6.27: Effective width for oblique incident waves

From this figure it becomes also clear that the decrease of the transmission coefficient goes faster for larger values of T_p/T_h . The wave transmission decreases because the effective width (B_{eff}) increases for oblique incident waves, shown in Figure 6.27. In the previous sections it is concluded that when the width increases in the model, the wave transmission decreases. Therefore it is concluded that AQWA should be able to model the effect of oblique incident waves.

The calibrated models for fixed breakwaters and floating breakwaters anchored by piles are used to investigate the effect of oblique incident waves. Based on the calculation results of these models, the effect of oblique incident waves is negligible small. This is remarkable because in the previous sections it is shown that the model is able to take the width of the floating breakwater into account. An explanation for this is the accuracy of AQWA, which is two decimals when the dimension of the length scale is in meters. When the wave height is small, for instance 0.30m, small effects on wave transmission like oblique incident waves are not visible because of the accuracy of the model. To overcome this accuracy problem, the model is scaled with a scale-factor of fifteen based on the Froude scaling law. The result is that the input for the wave height can be increased (for instance to 4.5m) and the output of the model for the transmitted waves is calculated with an accuracy of two decimals (centimetres), meaning that the small effects become visible.

The length of the breakwaters in both up-scaled models is at least ten times the longest wavelength in order to minimize diffraction effects. The water depth (d) used in the model is 30m, resulting in a B/d -ratio of 1.0 and a D/d -ratio of 0.2. The incident wave steepness, defined as the incident wave height over the incident wavelength is between the 3% and 7%. The transmitted waves are calculated at one wavelength behind the breakwater, which is graphically shown in Figure 6.28. For each wave period, six incident wave angles (α) are calculated between 0 and 50 degrees, with an interval of 10 degrees. The angle of 0 degrees represents normal incident waves. In total twelve wave periods are used as input for both types of floating breakwaters. The results are shown in figures below.

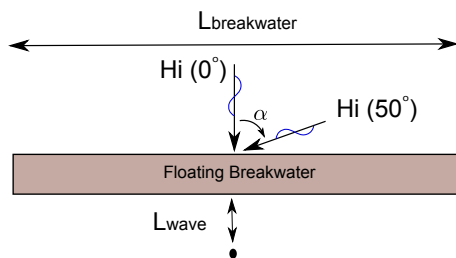


Figure 6.28: Location where the transmitted waves are calculated due to oblique incident waves (H_i)

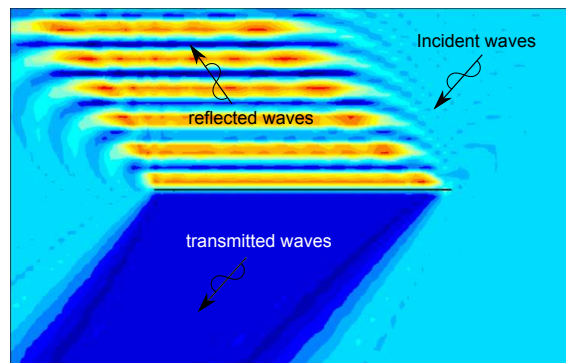


Figure 6.29: Oblique incident waves simulated by AQWA, angle of incidence is 40 degrees

Figures 6.30 and 6.31 show the results of the calculated transmitted waves due to oblique incident waves. In both figures the wave periods are between the 6.5 and 12 seconds, with an interval period of 0.5 second. For fixed breakwaters the dimensionless value L/D is used and for floating breakwaters anchored by piles the dimensionless value T/T_{heave} is used. In general the effect of oblique incident waves is small for both types of floating breakwaters. On average the decrease of the wave transmission coefficient due to oblique incident waves is 10% for an angle of 50 degrees. For an oblique incident wave angle of 50 degrees, the increase of the effective width is 55%. When the calculation results of the influence of the width (Figures 6.21 and 6.24) are compared with the calculation results of the oblique incident waves, it can be concluded that the decrease of the

transmission coefficient due to oblique incident waves with an angle of 50 degrees, is in the same order of magnitude due to an increase of the width of approximately 50%. This conclusion is based on calculations where the width of the breakwater and the natural heave period did not change, only the wave period changed. Width variations of the floating breakwater and variations of the natural heave period might influence the magnitude of the decrease of the wave transmission.

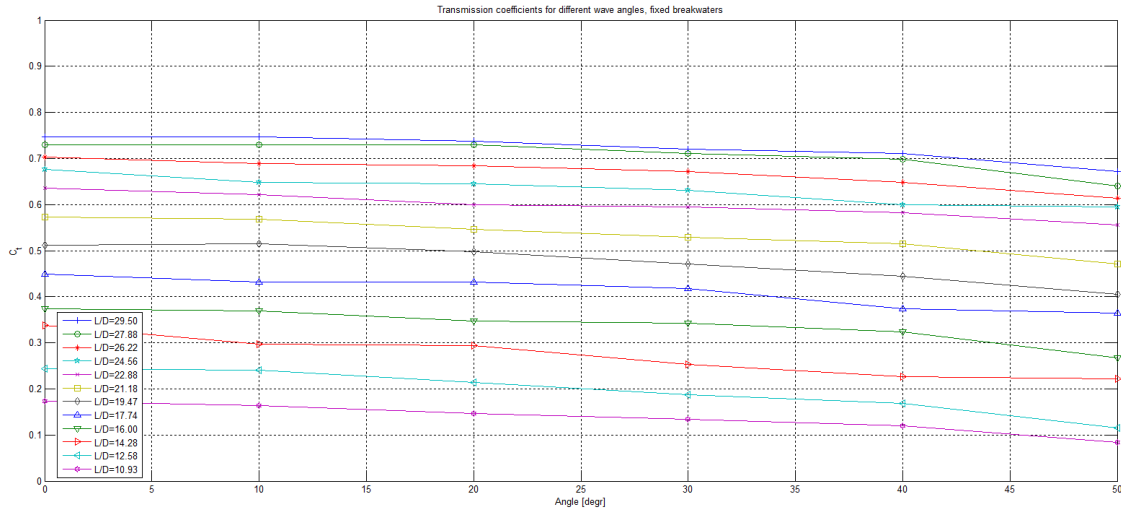


Figure 6.30: Effect of oblique incident waves on the wave transmission coefficient for fixed breakwaters, regular waves

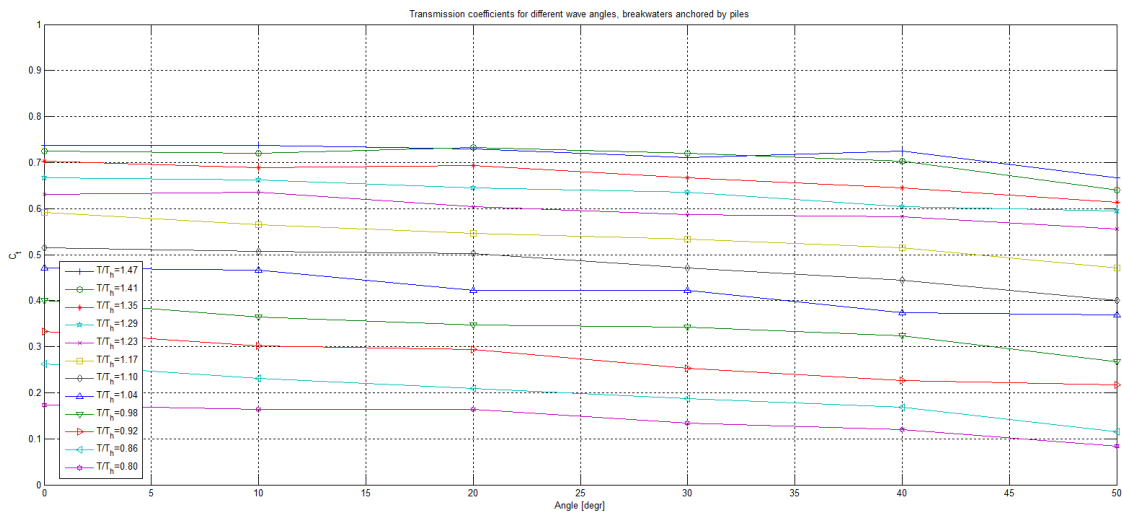


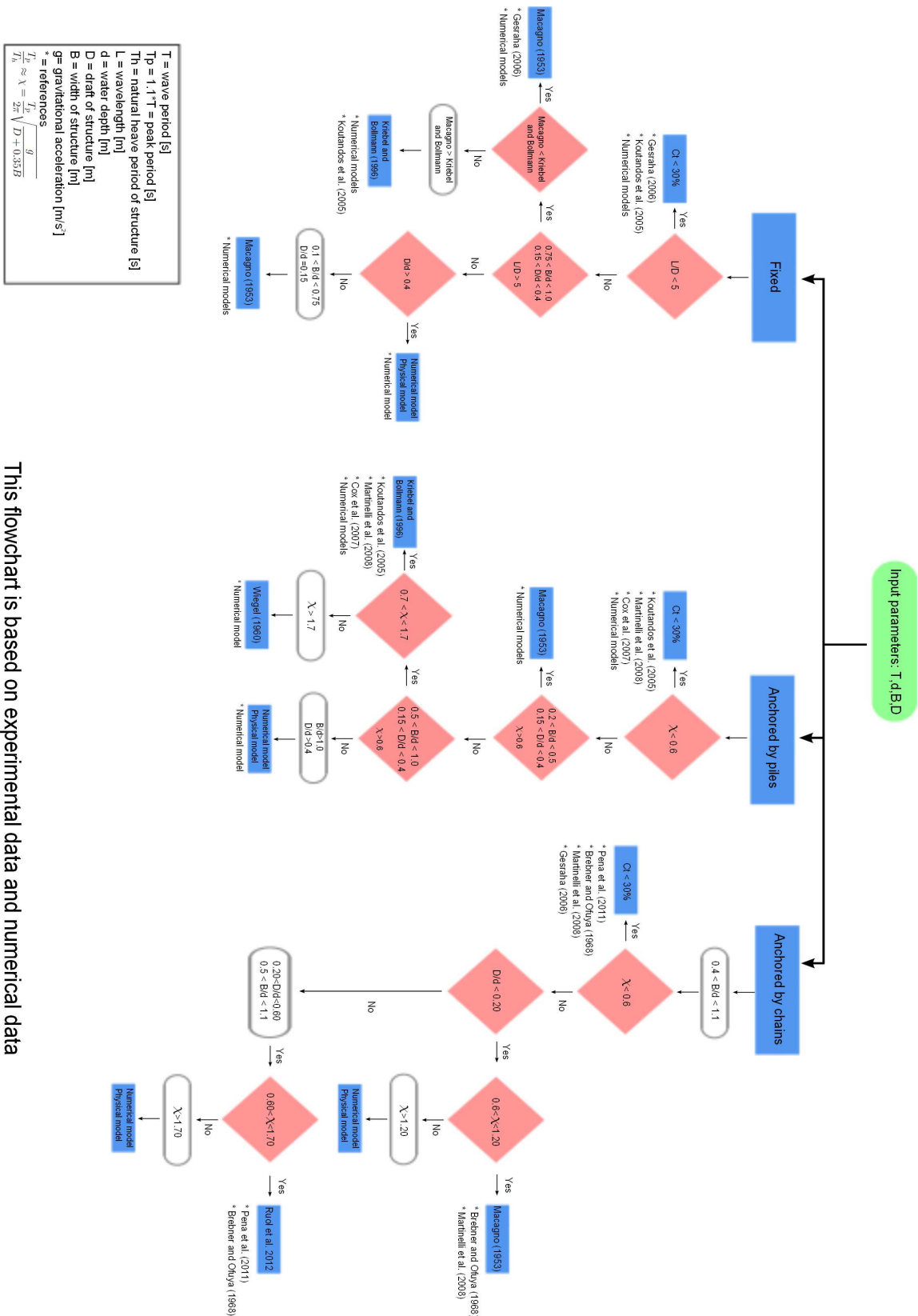
Figure 6.31: Effect of oblique incident waves on the wave transmission coefficient for floating breakwaters anchored by piles, regular waves

6.3 Conclusion

In this chapter a numerical model is discussed in order to model floating breakwaters. The numerical model is used to generate additional data in order to extend the use of the flowchart

shown in Figure 5.20, which is solely based on experimental data. The numerical computations are performed with a horizontal bottom and with a wave steepness (H/L) between the 1% and 5%. Below a number of conclusions are drawn regarding the applicability of the model and the model results for the areas of interest. The flowchart in Figure 5.20 is updated with the results of the numerical models. This updated flowchart is based on experimental data and numerical data and is shown as Figure 6.32.

- AQWA is a three-dimensional model and takes effects like diffraction around the tip of the breakwater into account. When these three dimensional effects needs to be excluded from the model, the length of the breakwater needs to be at least ten times the length of the longest incident wave. In this case the diffraction effects are negligible small on the transmitted waves in the middle of the breakwater.
- As long as the mesh size is fine enough to enable the modelling of the shortest wave, a finer mesh size has no effect on the calculation results.
- AQWA is able to model fixed breakwaters mounted on the bottom, fixed breakwaters mounted on piles (partially submerged) and floating breakwaters with one degree or more degrees of freedom. Floating breakwater models with one or more degrees of freedom needs to be calibrated. This calibration needs to be done in order to obtain the same motions in the model as in the experiments. It is concluded that the motions of the floating breakwater has a large influence on the wave transmission coefficients. Floating breakwaters anchored by chains (six degrees of freedom) could not be calibrated in this report, because the motions observed during the experiments are not available.
- The effect of the width and the draft of the floating breakwater on the wave transmission is investigated with AQWA. It is concluded that both width and draft have an effect on the wave transmission. The draft has a larger influence than the width on the wave transmission over a larger range of wave periods for the cases modelled with AQWA. This result may vary when D/d is small compared to the B/d ratio.
- Based on the new simulations which are performed in order to obtain additional data for fixed breakwaters, it is concluded that for fixed breakwaters for the ranges $0.75 < B/d < 1.0$ with $0.15 < D/d < 0.4$ the theory of Kriebel and Bollmann is applicable. When the theory of Macagno predicts smaller values for these ranges than Kriebel and Bollmann, Macagno is suitable to apply. Based on the numerical models Macagno is suitable to apply for $D/d = 0.15$ with $B/d < 0.75$.
- Based on the model results for floating breakwaters anchored by piles, it is concluded that Macagno is suitable to apply for the ranges of $0.15 < D/d < 0.40$ with $0.2 < B/d < 0.5$. For this range Macagno overestimates the modelled transmission coefficients and this overestimation becomes larger for χ -values smaller than two. For the ratios $D/d = 0.6$ and $B/d = 1.0$ a very poor agreement is found for $\chi > 2.0$. For this area a numerical model is suggested. When $\chi < 2.0$ for this area, the theory of Kriebel and Bollmann is suitable to apply.
- The effect of oblique incident waves on the wave transmission can be modelled by AQWA. It is concluded that when the angle of the incident wave increases the transmission coefficient decreases. This is due to the increase of the effective width.



T = wave period [s]
 Tp = 1.1 * T = peak period [s]
 Tn = natural heave period of structure [s]
 L = wavelength [m]
 d = water depth [m]
 D = draft of structure [m]
 B = width of structure [m]
 g = gravitational acceleration [m/s²]
 * = references
 $T_n = \chi = \frac{T_p}{2\pi} \sqrt{\frac{g}{D + 0.35B}}$

This flowchart is based on experimental data and numerical data

Figure 6.32: Flowchart with the applicable theories for wave transmission based on experimental and numerical data

Conclusions and Recommendations

In the previous chapters a number of conclusions are drawn. When these conclusions are combined, an answer for the research question is obtained. This chapter discusses the main conclusions and the answer on the research question. Besides the conclusions a number of recommendations are made for future research.

The research objective in this thesis is defined as follows:

'Identifying the steps which can be taken during the design process, in order to predict the effectiveness of floating breakwaters more accurately'

7.1 Conclusions

Floating breakwaters are suitable to apply in deep waters in combination with short waves. The wave period is the most important parameter determining the effectiveness of floating breakwaters. It is concluded from experimental data and numerical data that the effectiveness strongly decreases when the wave period increases. In order to attenuate long waves, the floating breakwater needs to have a large width and a large draft.

Wave transmission theories

The existing formulas for wave transmission are derived for fixed structures in deep water where linear wave theory is valid. When these formulas are compared with each other it is concluded that there are large differences between the theories. Because of the large differences between the theories, it becomes unclear for the designer when to use which formula. This might be a reason why the effectiveness of floating breakwaters is often overestimated.

Another reason for the differences in the expected floating breakwater performance and the achieved effectiveness of floating breakwaters, is that the available formulas to determine the wave transmission neglect a number of processes. These processes are, motions of the floating structure, overtopping and energy dissipation. Energy dissipation results in lower transmitted waves, while the motions of the floating breakwater generates waves. When the motions of the floating breakwater are large, the theories for wave transmission underestimate the wave transmission. To include all these processes in an analytical formula is a difficult task. Ruol et al. [2013a] derived a modification factor for the formula of Macagno. This modification factor is based on experimental

data and describes the difference between the formula of Macagno and the experimental data. There is not a real physical background behind this factor, but the results are suitable to use.

Fixed breakwaters

Fixed breakwaters are structures which movements relative to the bottom are negligible small and no deformations of the structure itself occur. When the wave transmission theories are compared with experimental data for fixed structures, it is concluded that nearly all theories are overestimating the wave transmission coefficient. This overestimation increases for shorter wave periods. The dimensionless values used to make distinction between the theories is the ratio wavelength to draft (L/D), ratio width to depth (B/d) and ratio draft to depth (D/d). For values of $L/D < 5$ the wave transmission coefficient is smaller than 30%. When the wave transmission predicted according to the theory of Macagno becomes smaller than the predicted wave transmission according to the theory of Kriebel and Bollmann, it is observed that Macagno is suitable to apply for $0.75 < B/d < 1.0$ and $0.15 < D/d < 0.4$. When for these same ratios the wave transmission predicted by the theory of Macagno becomes larger than the wave transmission predicted by the theory of Kriebel and Bollmann, the theory of Kriebel and Bollmann is suitable to apply. For structures with a large draft, $D/d > 0.4$, the available theories are not suitable to apply and numerical and physical models are suitable.

Floating breakwaters anchored by piles

Floating breakwaters anchored by piles are breakwaters with one degree of freedom. Only vertical translations occur which are called heave. Although all the theories used for the comparisons with experimental data are derived for fixed structures, a reasonable agreement is found for floating breakwaters with one degree of freedom for the theory of Kriebel and Bollmann. The parameter which is suggested in order to make distinction between the use of the theories for floating breakwaters with one degree of freedom is the relative period χ , representing the peak period (T_p) over the natural heave period (T_h). For $\chi < 0.6$ the wave transmission coefficient is smaller than 30%. For the ranges $0.2 < B/d < 0.5$ and $0.15 < D/d < 0.4$ the theory of Macagno is suitable to apply. For the ranges $0.5 < B/d < 1.0$ and $0.15 < D/d < 0.4$ and for $0.7 < \chi < 1.7$ the theory of Kriebel and Bollmann is applicable. For large drafts, $D/d > 0.4$, physical and numerical models need to be applied.

Floating breakwaters anchored by chains

Floating breakwaters which are anchored by chains have six degrees of freedom and have a different behaviour than floating breakwaters with one degree of freedom. The dimensionless ratios considered in order to make distinction between the applicability of the different theories are: width over water depth (B/d), draft over water depth (D/d) and the relative period (χ). The formula of Ruol et al. is applicable for the following ranges: $0.5 < B/d < 1.10$ and $0.20 < D/d < 0.60$ and $0.60 < \chi < 1.70$. The formula of Macagno is applicable for the following ranges: $0.4 < B/d < 1.10$ and $D/d < 0.20$ and $0.60 < \chi < 1.20$. Areas of interest where experimental data is missing are the ratio of $B/d < 0.5$ where D/d and χ are in the range where the formula of Ruol et al. is applicable. Another area of interest is for the ratio $B/d < 0.4$ where the formula of Macagno is applicable.

Applicability of wave transmission theories

When the theories discussed above are applied for the areas where a good/reasonable agreement is found between the theory and numerical or experimental data, the wave transmission is slightly overestimated. For a preliminary design this overestimation is not very relevant and a reasonable estimation is obtained regarding the effectiveness of the floating breakwater. Based on experimental data and numerical data a flowchart is constructed which indicates when to use which formula. This flowchart is shown as Figure 6.32. The experimental models obtained from literature are performed with a wave steepness between the 1% and 6%, a horizontal bottom and no overtopping

is included. The same holds for the numerical models, except for the maximum wave steepness, which is 5% for the numerical models.

Modelling of floating breakwaters

In this report use is made of a linear radiation and diffraction model which is based on the three-dimensional potential flow theory. This model is able to model the motions of the floating breakwater and the transmitted waves. A disadvantage of this model is that energy losses are not included and that steep waves can not be modelled.

With this model fixed breakwaters, floating breakwaters anchored by piles and floating breakwaters anchored by chains are modelled. It is concluded that the model is suitable to model fixed breakwaters well. The model is also suitable to model floating breakwaters with one or more degrees of freedom, but the model needs to be calibrated for these two types of floating breakwaters. It is important that the motions in the model are the same as the motions observed during the experiments. For floating breakwaters anchored by piles this calibration can be done by adding additional damping to the system for the heave motions. This additional damping represents mechanical friction between the pontoon and the piles and represents viscous effects. For floating breakwaters anchored by chains additional damping needs to be included for several modes of motion. It is expected that when the model is calibrated on the motions which are observed during the experiments, the model will be suitable to model wave transmission of these types of floating breakwaters.

The effect of oblique incident waves can be taken into account in the model. It is concluded that when the angle of wave incidence increases, the wave transmission decreases. This decrease is due to the increase of the effective width of the breakwater. This only holds for fixed breakwaters and floating breakwaters anchored by piles. For a floating breakwater anchored by chains the movements will also have effect on the transmission coefficient for oblique incident waves.

In general, the calibrated numerical models show a good agreement with the experimental data. When the numerical models and the available theories for wave transmission are compared with experimental data, it is concluded that the numerical models shows a better agreement with the experimental data than the available theories for wave transmission.

Answer research question

The research question is defined as follows:

'Which steps should be executed during the design process in order to predict the effectiveness of a floating breakwater more accurately?'

The answer for this question is shown in the form of a flowchart, shown as Figure 6.32. To use this flowchart the input parameters are the wave period T or peak period T_p , the water depth d , the width of the floating breakwater B and the draft of the floating breakwater D . Depending on the type of anchoring system for the floating breakwater, a number of options are available which are all based on the input parameters. If one executes all the steps in the flowchart the result is that one obtains the most suitable formula to predict the wave transmission of floating breakwaters.

7.2 Recommendations

During this thesis multiple areas are identified where additional research possibilities exists. Below these possibilities are listed:

- Investigate the influence of the anchoring system on the wave transmission.
- Obtaining a suitable method by which the additional amount of damping (effect of the anchoring system and viscous effects) can be determined which is necessary to obtain a good model for each type of floating breakwater with one or more degrees of freedom.
- Calibration and validation of the numerical model for floating breakwaters anchored by chains.
- Investigate how to model the effects of a full wave spectrum on the wave transmission.
- Extend the flowchart for floating breakwaters anchored by chains for $D/d < 0.20$ and $\chi > 1.20$ and for the ranges of $D/d > 0.20$ with $\chi > 1.70$.
- Investigate the effect of the breakwater width and the natural heave period on the wave transmission for oblique incident waves.
- Define a procedure to obtain automatically the numerical wave field computed by AQWA with sufficient accuracy.

Appendix A

Performance of floating breakwaters

This appendix shows the results of transmission coefficients obtained by physical models. Several graphs are shown for each type of floating breakwater discussed in Chapter 3, which are presenting the transmission coefficient.

A.1 Definition of Performance

The definition of performance strongly depends on the requirements the floating breakwater has to fulfil, which is in general reducing wave heights to a certain level. The transmission coefficient represents the fraction of the incident wave height which is transmitted by the floating breakwater and can be determined with the local wave conditions and the maximum allowable wave height. This implies that the transmission coefficient differs for each project and that there is no exact value which defines the performance.

A.1.1 Wave transmission theories for reflective structures

Brebner and Ofuya [1968] conducted several experiments in a wave flume for the following type of floating breakwaters: single pontoon, double pontoon and A-frame.

Single- and double Pontoon

The experiments for the single pontoon and double pontoon types are conducted with variable mass, which determines the depth of submergence. The depth of submergence has no influence on the radius of gyration but has a large influence on the metacentric height and thus the stability of the structure. The natural period of oscillation is also affected by the depth of submergence and will increase due to the increase of mass. The results and conclusions related to wave transmission are shown below. For details about the set-up of the experiments reference is made to Brebner and Ofuya [1968].

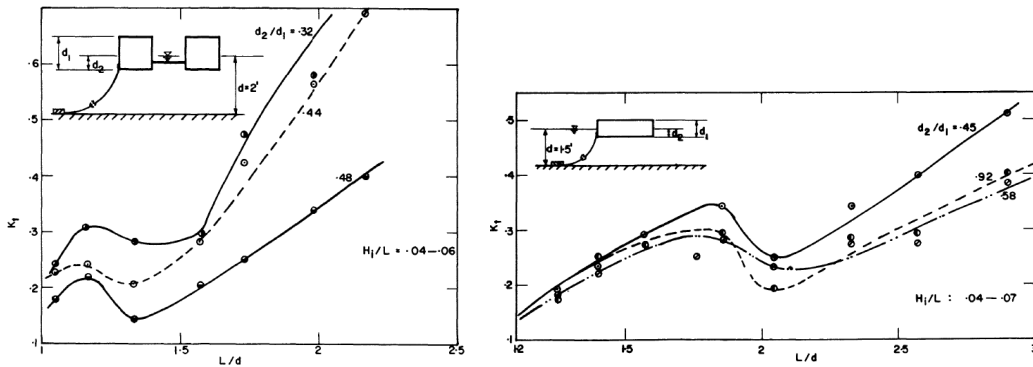


Figure A.1: Transmission coefficient for single and double pontoon for different depths of submergence, d_2 , [Brebner and Ofuya, 1968]

From Figure A.1 it can be concluded that the structure is effective in attenuating waves over a wide range of values for L/d , where in this figure d represents the water depth. The effect of submergence on the transmission coefficient is smaller for lower values of L/d but increases for larger L/d values. It also turns out that the depth of submergence has a positive effect on wave attenuation. When the results of a single pontoon and a double pontoon are compared to each other, it can be concluded that the single pontoon is more effective in attenuating waves than the double pontoon.

A-frame

In Canada several tests are performed to verify the effectiveness of the A-frame breakwater, see also Brebner and Ofuya [1968]. One of the most remarkable things related to the A-frame is its large radius of gyration, which can easily be increased with only a little increase of mass.

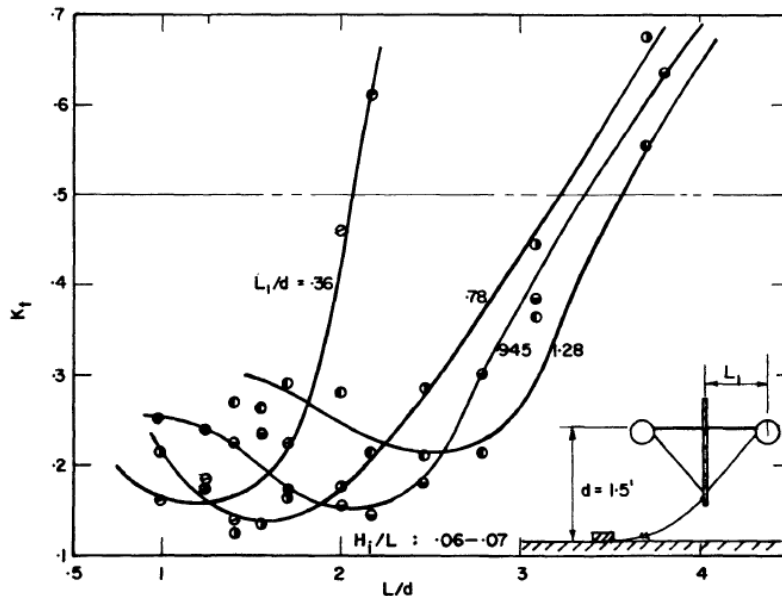


Figure A.2: Transmission coefficient for A-frame type of breakwater, for different relative breakwater widths (radius of gyration), L_1/d [Brebner and Ofuya, 1968]

From Figure A.2 it can be concluded that the effectiveness can be increased by increasing the

distance between the cylinders. This implies an increase of the mass radius of gyration.

Hinged floating breakwater

Leach et al. [1985] performed research on developing a analytical model of rigid, hinged floating breakwater. They verified their analytical model by physical model tests and derived design curves for predicting the wave attenuating characteristics.

The result of this research is a dimensionless parameter P , which is a combination of the breakwater buoyancy, weight, center of gravity, center of buoyancy, inertia, mooring line resiliency, point of attachment an anchor point Leach et al. [1985].

$$P = \frac{1}{\rho g h^3} \left[(F_B B + 2K_L C^2 \sin^2 \alpha) - m \left(\frac{l^2 \omega^2}{3} + gG \right) \right] \quad (\text{A.1})$$

In which:

| | | |
|----------------------|---|--|
| m | = | mass of breakwater [kg] |
| l | = | height of the screen [m] |
| ω | = | wave frequency [rad/s] |
| g | = | gravitational acceleration [m/s^2] |
| ρ | = | density of water [kg/m^3] |
| F_B | = | buoyancy per unit width [N] |
| h, B, C, α, G | = | see Figure A.3 |
| K_L | = | spring stiffness of mooring line [N/m] |

The value of P in Eq.A.1 represents the relative importance of the restoring forces (positive terms) and the inertia forces (negative terms) PIANC [1994]. The value of P can vary between -0.5 and 5.0. In the absence of the mooring lines P becomes slightly negative, because the inertia terms become dominant. When the mooring lines are very stiff (practical engineering applications) the value of P will become large [Leach et al., 1985].

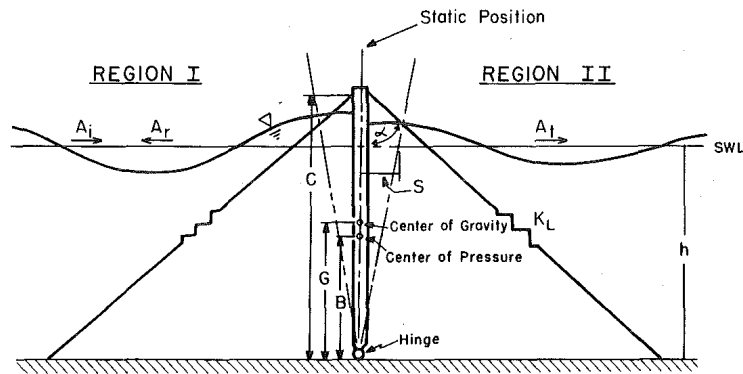
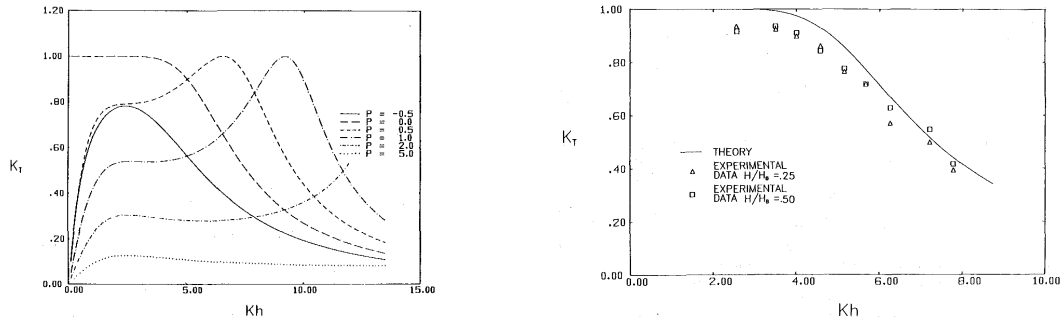


Figure A.3: Principle sketch of hinged floating breakwater, [Leach et al., 1985]



(a) Analytical behaviour of transmission coefficient as function of Kh and constant P

(b) Comparison of theoretical and experimental values of transmission coefficient

Figure A.4: Theoretical and experimental transmission coefficient for hinged type of breakwater [Leach et al., 1985]

A.1.2 Wave transmission theories for dissipative structures

Dissipation of wave energy by dissipative structures can be achieved in different ways, such as: wave breaking, generation of turbulence and friction. Depth-induced wave breaking occurs approximately around the ratio (wave height/water depth) $H/d = 0.8$. When the wave breaks, energy is converted into turbulence. Generation of turbulence can also be achieved by creating sharp edges where the flow is forced to release from. The porous walled breakwater works on this principle. Friction dominates only in situations where high velocities are achieved, which may occur in cases like resonance. This is the case for a tethered-float breakwater, see also section 3.3.2.

The amount of energy dissipation or turbulence is difficult to predict or to describe in a model. There does not exist a general formula to predict the amount of energy dissipation. Most formula's presented in literature are applicable for a specific type of energy dissipation, hence a specific type of floating breakwater. Below the formulas and graphs determining the transmission coefficient for several dissipative structures are shown.

Scrap-tire

Harms [1979] performed research on transmission coefficients for scrap-tire floating breakwaters by using linear wave theory and deep water conditions. Furthermore he considered the power required to propel a tire of negligible mass at velocity $U(t)$, unidirectionally through a viscous fluid at rest. This relationship is assumed to be applicable for a fixed tire and for an unsteady flow $U(t)$. The product of the drag force on the tire and the velocity equals the time rate of change of kinetic energy of the surrounding fluid Hales [1981]. In other words, the power (velocity \times drag force) represents the rate at which the energy is dissipated within the structure. The drag related dissipation is considered to vary only in proportion to the wave height squared (H^2). This implies that the energy dissipation along the breakwater is proportional to the wave energy along the breakwater, $1/8 \rho g H^2$. Making use of the energy flux balance, see Bouwmeester and Van der Breggen [1984] the following transmission coefficient is obtained:

$$C_t = \exp \left\{ \frac{-20\pi C_d \frac{H_t}{L}}{3 P \frac{L}{B}} \right\} \quad (\text{A.2})$$

In which:

- C_d = drag coefficient [-]
 H_i = incident wave height [m]
 L = wave length [m]
 P = porosity [-]
 B = width of structure [m]

Harms [1979] performed several experiments where he measured the transmitted wave height. From Eq.(A.2) he determined the drag coefficient for the specific structure. According to his results it turned out that the drag coefficient did not vary a lot with respect to the different structures which were tested. The value for C_d was found to be around the 0.6. From this Harms concluded that the porosity parameter primarily determines the performance of the structure. Another remarkable result is that the theoretical values of the transmitted wave heights did not vary more than 10% of the measured transmitted wave heights. Based on this, Harms concluded that Eq.(A.2) describes the wave transmission quite well.

For the Goodyear breakwater $P=0.87$ and $C_d = 0.60$. For the pile-tire breakwater $P=0.53$ and $C_d = 0.65$.

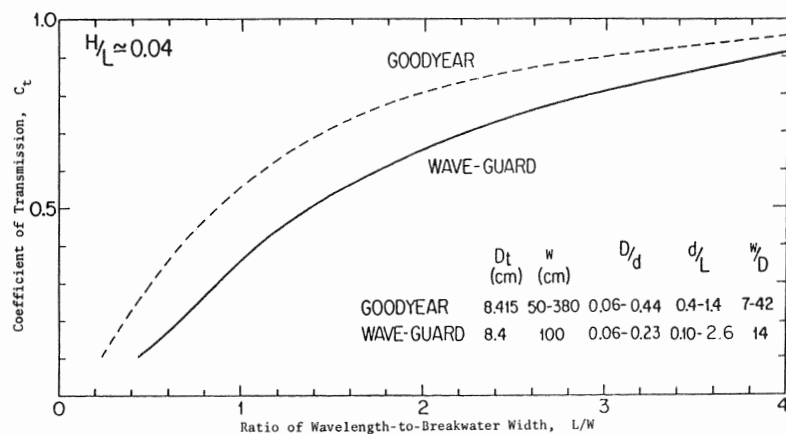


Figure A.5: Comparison of wave transmission coefficients for Goodyear and Pipe-tire (Wave-Guard) floating breakwaters, for various ratios of wavelength-to-breakwater width, L/W [Harms, 1979]

Tethered-Float

Friction or drag is proportional to the third power of the relative velocity between structure and the fluid particle. In most cases this relative velocity is very low which results in a low amount of energy dissipation. But at a high relative velocity a high drag can be achieved which results in a large amount of energy dissipation. The Tethered-float breakwater is based on this principle of high relative velocities which results into large drag.

The tethered float can be modelled as a pendulum and the responses of the floats on the wave forcing are behaving like a damped system. The float motion amplitude and phase lag increases when the frequency of the excitation is close to its own frequency. When the frequency of the excitation is close to the natural frequency of the floats, there will be large motions of the floats and hence, large relative velocities which induces a large drag. In fact, this buoy converts wave energy into turbulence and turbulence into heat. In Figure A.6 the theoretical performance is shown. Only drag dissipation is included in these results. These results are made by Seymour and Isaacs in 1974. To obtain these results a number of calculations and iterations should be executed and there does not exist a simple formula to predict the wave transmission coefficient. The details

of these calculations can be found in [Hales, 1981]. In Figure A.6 all the parameters which needs to be taken into account in order to achieve a certain transmission coefficient are shown.

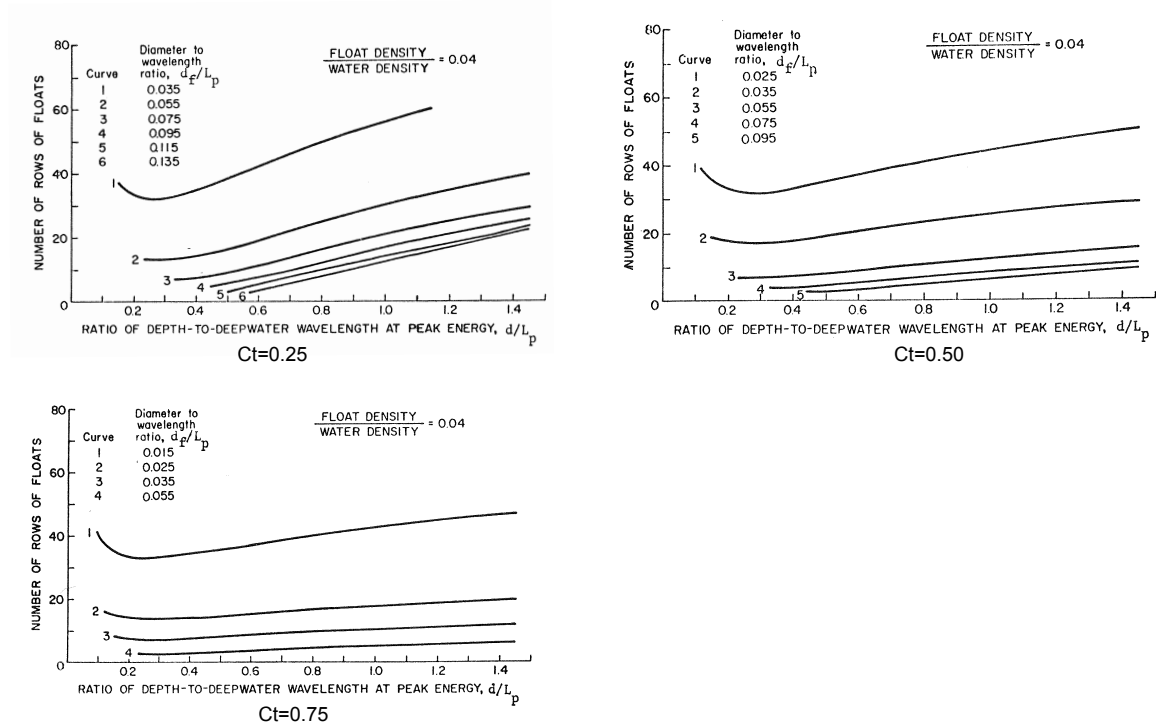


Figure A.6: Theoretical performance for three different transmission coefficients

Porous Wall

Richey and Sollitt [1969] investigated the effectiveness of the porous walled breakwater. The principle of this breakwater is as follows: As the waves approach the porous wall, part of the wave energy will be reflected and another part of the wave energy will pass through the perforations, resulting in the rise of water level a . In Figure A.7 the inner water level (a) and outer water level (n) are shown.

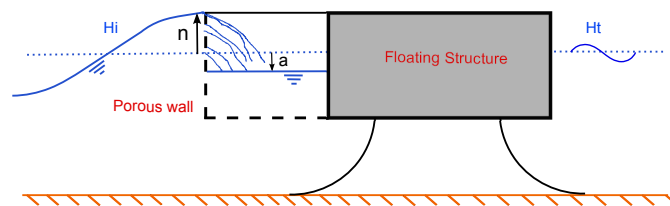


Figure A.7: Porous walled breakwater

When the outer water level is higher than the inner water level, ($n > a$), then potential wave energy will be converted into kinetic energy which will be dissipated in the chamber into turbulence. In this case the inner water level will rise. As soon as a becomes larger than n , the flow reverses and the chamber empties itself. The reversal flow encounters the next incoming wave and dissipates a part of its wave energy before the wave hits the breakwater [Hales, 1981].

The advantage of this type of breakwater is that only a part of the wave energy is reflected. In the case of a pontoon breakwater the incoming wave energy is fully reflected along the surface of the pontoon, causing higher mooring forces and larger oscillations of the breakwater.

Richey and Sollitt [1969] performed mainly research on the reflection coefficient of the porous walled breakwater. To obtain an estimation for the transmission coefficient use is made of the simple relation shown as Eq.(A.3). Note that there are no energy losses taken into account in this equation.

$$\begin{aligned} H_i^2 &= H_t^2 + H_r^2 \\ 1 &= C_t^2 + C_r^2 \quad \rightarrow \quad C_t = \sqrt{1 - C_r^2} \end{aligned} \quad (\text{A.3})$$

In which:

- H = wave energy density [J/m^3]
- C = coefficients [-]
- indices r = reflective [-]
- indices i = incident [-]
- indices t = transmitted [-]

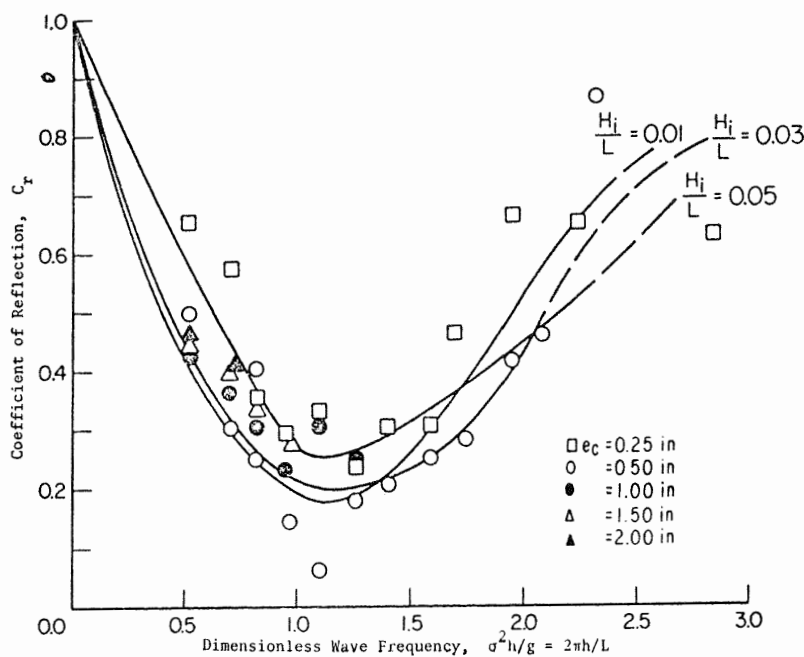


Figure A.8: Effect of incident wave steepness, H_i/L and dimensionless wave frequency, $\sigma^2 h/g$, on reflection coefficient C_r for porous walled breakwaters, e_c indicates the wave generator eccentricities [Richey and Sollitt, 1969]

In the dimensionless parameter on the x-axis of Figure A.8 is the σ the radian frequency of the wave, h is the water depth and g is the gravitational acceleration.

Flexible Membrane

The efficiency of this system was found to be good on steep waves because of the large vertical accelerations. Waves which are less steep require a longer wave trap in order to attenuate the waves effectively. Most energy is dissipated in the structure itself, causing large stresses on the structural elements.

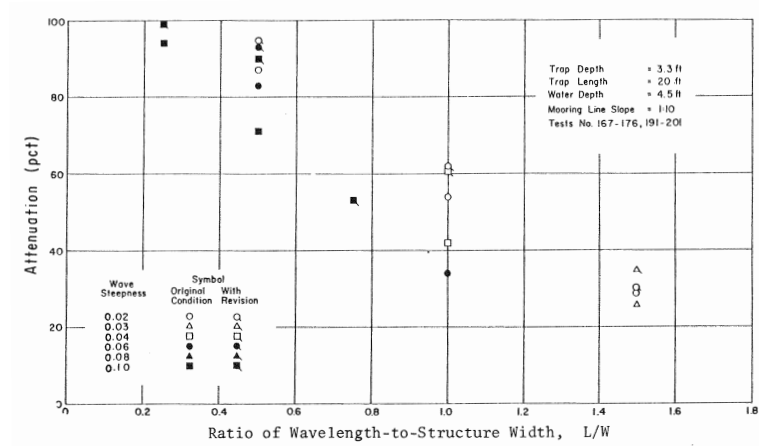


Figure A.9: Transmission coefficient for wave trap breakwater [[Ripken, 1960]]

From Figure A.9 it can be seen that good wave height attenuation is achieved for small values of wavelength over trap width (L/W). If the wave steepness increases the transmission coefficient slightly decreases. One of the conclusions of the physical model tests were the high forces on the structure and therefore it would not work in practical design cases [Hales, 1981].

Appendix B

Linear wave theory

In Chapter 4.1 linear wave theory is discussed briefly, below a more detailed description is given.

B.1 Linear wave theory

Ocean waves can be described by linear wave theory. The most interesting result of this theory is a long-crested propagating harmonic wave. Based on this theory, many wave characteristics can be derived. Besides this, most theories on wave transmission (see also Chapter 5) are based on linear wave theory. In order to understand the behaviour of waves and its characteristics, an explanation of linear wave theory is given. For more detailed information and the derivations of the formulas given below, reference is made to Holthuijsen [2007].

Linear wave theory is based on two equations: a mass balance equation and a momentum balance equation. These two equations are describing the kinematic and dynamic aspects of waves. Waves can be described by linear wave theory when the amplitude of the wave is small compared to the water depth and wavelength. In this case non-linear effects of waves are negligible. Furthermore it is assumed that water is an ideal fluid, which implies: incompressible, constant density, no viscosity and no rotation of water particles around their own axis. From the mass balance equation the continuity equation can be derived:

$$\frac{\partial u_x}{\partial x} + \frac{\partial u_y}{\partial y} + \frac{\partial u_z}{\partial z} = 0 \quad (\text{B.1})$$

In which:

- u = velocity
- x, y, z = indicating direction of a three-dimensional reference frame

The position of the reference frame is located on the mean water level surface, with the positive x-axis towards the right and the positive z-axis upwards, see also Figure B.1.

To solve this equation use is made of the velocity potential function $\phi = \phi(x, y, z, t)$, shown below as Eq.(B.2). This function is defined as a function of which the spatial derivatives are equal to the velocities of the water particles [Holthuijsen, 2007]. Substituting this in Eq.(B.1) the Laplace equation is obtained (Eq.(B.3)).

$$\text{Velocity potential function : } u_x = \frac{\partial \phi}{\partial x}, \quad u_y = \frac{\partial \phi}{\partial y}, \quad u_z = \frac{\partial \phi}{\partial z} \quad (\text{B.2})$$

$$\text{Laplace equation : } \frac{\partial^2 \phi}{\partial x^2} + \frac{\partial^2 \phi}{\partial y^2} + \frac{\partial^2 \phi}{\partial z^2} = 0 \quad (\text{B.3})$$

Boundary conditions can be defined at the water surface (η) and at the bottom in terms of the velocity potential function. The kinematic boundary conditions are:

$$\text{Kinematic boundary conditions } \begin{cases} \frac{\partial \phi}{\partial z} = \frac{\partial \eta}{\partial t} & \text{at } z=0 \\ \frac{\partial \phi}{\partial z} = 0 & \text{at } z=-d \end{cases} \quad (\text{B.4})$$

With the kinematic boundary conditions and the velocity potential function the Laplace equation can be solved. One of the analytical solutions of the Laplace equation with the kinematic boundary conditions is a long-crested harmonic wave, propagating in the positive x-direction. In fact, this wave represents the surface elevation and can be defined as:

$$\eta(x, t) = a \sin(\omega t - kx) \quad (\text{B.5})$$

In which:

$$\begin{aligned} a &= \text{wave amplitude [m]} \\ \omega &= \text{radian frequency [rad/s], defined as } \frac{2\pi}{T}, \text{ where } T \text{ is the wave period [s]} \\ t &= \text{time [s]} \\ k &= \text{wave number [rad/m], defined as } \frac{2\pi}{L}, \text{ where } L \text{ is the wave length [m]} \end{aligned}$$

The velocity potential function belonging to this equation is:

$$\phi = \hat{\phi} \cos(\omega t - kx) \quad \text{with} \quad \hat{\phi} = \frac{\omega a \cosh[k(d+z)]}{k \sinh(kd)} \quad (\text{B.6})$$

The above solution of the Laplace equation is based on a mass balance (continuity equation) and the kinematic boundary conditions only. This implies that all the kinematic aspects (velocities and accelerations) can be derived from Eq.(B.5) and Eq.(B.6). Since wave energy implies the movement of water particles, the equations above are essential for describing the distribution of wave energy in the water column.

When waves are propagating they are transporting energy in the direction of propagation. This horizontal transport of energy is due to the work done by the wave induced pressure. This wave induced pressure can be described by the dynamic aspects of waves, which are derived from the momentum balance.

Momentum is by definition the mass density of water times the velocity of the water particles. The second law of Newton states that the rate of change of momentum equals force. For momentum in the x-direction the following momentum balance equation is obtained:

$$\frac{\partial(\rho u_x)}{\partial t} + \frac{\partial u_x(\rho u_x)}{\partial x} + \frac{\partial u_y(\rho u_x)}{\partial y} + \frac{\partial u_z(\rho u_x)}{\partial z} = F_x \quad (\text{B.7})$$

$$\text{The dynamic boundary condition is defined as: } p = 0 \text{ at } z = 0 \quad (\text{B.8})$$

The pressure (p) at the water surface is assumed as zero and functions as a reference pressure since the interest is in the pressures below the water surface. In Eq.(B.7) F_x is the body force in x-direction per unit volume. The second, third and fourth terms are the advective terms and contain non-linear terms. In order to make the theory linear, these terms should be removed from the momentum equation. After applying some mathematics and ignoring the non-linear terms in Eq.(B.7) the linearised Bernoulli equation for unsteady flow is obtained, shown as Eq.(B.9).

$$\frac{\partial \phi}{\partial t} + \frac{p}{\rho} + gz = 0 \quad (\text{B.9})$$

Just as the kinematic boundary condition, it is possible to express the dynamic boundary condition in terms of the velocity potential. This implies $z = \eta$ with $p = 0$ and results in:

$$\frac{\partial \phi}{\partial t} + g\eta = 0 \quad \text{at } z=0 \quad (\text{B.10})$$

The analytical expression for the wave induced pressure is derived by substituting the solution of the velocity potential function (Eq.B.6) into the linearised Bernoulli equation (Eq.B.9). After substitution the following result is obtained:

$$P_{wave} = \hat{P}_{wave} \sin(\omega t - kx) \quad \text{with} \quad \hat{P}_{wave} = \rho g a \frac{\cosh[k(d+z)]}{\cosh(kd)} \quad (\text{B.11})$$

The equations above together with the boundary conditions are summarized in Figure B.1. In this figure the Laplace equation together with the kinematic boundary conditions and the linearised Bernoulli equation with the dynamic boundary conditions are shown.

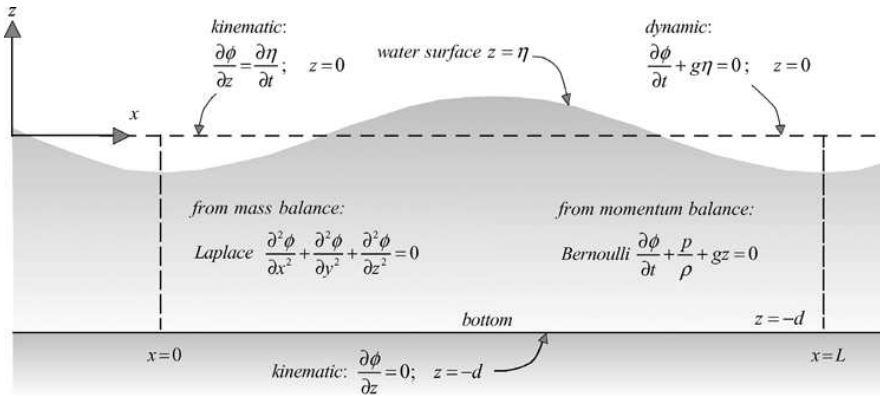


Figure B.1: Linearised basic equations and boundary conditions for the linear wave theory, in terms of velocity potential [Holthuijsen, 2007]

B.1.1 Regular waves

The most interesting result of linear wave theory is a long-crested propagating harmonic wave. This harmonic wave (regular wave) can be defined as a propagating sinusoidal wave with an amplitude (a), radian frequency (ω) and wave number (k). The equation of the sinusoidal harmonic wave is shown below.

$$\eta(x, t) = \frac{H}{2} \sin\left(\frac{2\pi}{T}t - \frac{2\pi}{L}x\right) = a \sin(\omega t - kx) \quad (\text{B.12})$$

The phase speed is the forward speed (c) by which the wave propagates while the phase ($\omega t - kx$) remains constant. Mathematically this implies that the time derivative of the phase is zero. From this the phase speed is obtained (Eq.B.13). The parameters used in the equations are shown in Figure B.2.

$$c = \frac{\omega}{k} = \frac{L}{T} \quad (\text{B.13})$$

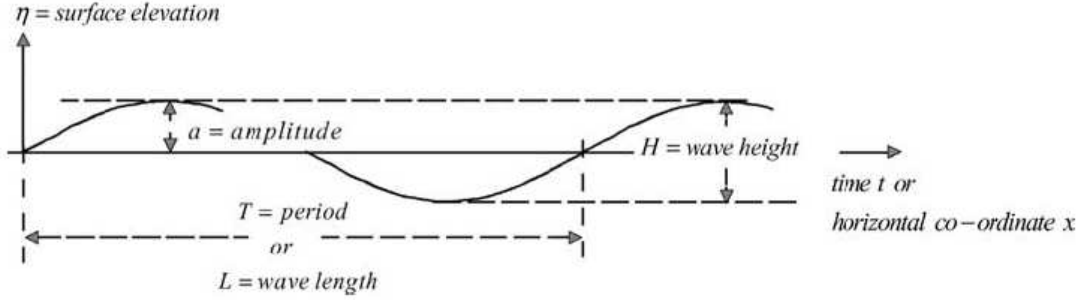


Figure B.2: Propagating harmonic sine wave, [Holthuijsen, 2007]

B.1.2 Irregular waves

If one observes the water surface, it can be seen that it continuously changes without repeating itself. When the water surface elevation is measured, the resulting signal will be like an irregular wave signal, which can be modelled by the sum of a large number of harmonic wave components:

$$\underline{\eta}(t) = \sum_{i=1}^N \underline{a}_i \cos(2\pi f_i t + \underline{\alpha}_i) \quad (\text{B.14})$$

In which:

- N = large number of frequencies
- $\underline{\alpha}_i$ = phase as a random variable
- \underline{a}_i = amplitude as a random variable
- f_i = wave frequency

Each wave component is a propagating regular wave which has a sinusoidal shape. From this it follows that the irregular wave signal, which describes the surface elevation, can be decomposed by a Fourier series into a number of harmonic waves, see Figure B.3. The result is a set of values for the amplitude (\underline{a}_i) and phase ($\underline{\alpha}_i$), where the underscores indicate that the variables are random. Each set of values of \underline{a}_i and $\underline{\alpha}_i$ belongs to the frequency f_i . This approach is called the random-phase amplitude model. The benefit of this model is that it is possible to describe the waves as a spectrum.

The random variables are characterized by their probability density functions. The phase ($\underline{\alpha}_i$) at each frequency (f_i) is uniformly distributed between 0 and 2π . The amplitude (\underline{a}_i) has at each frequency (f_i) a Rayleigh distribution [Holthuijsen, 2007].

If the expected value of the amplitude ($E\{\underline{a}_i\}$) is considered, it is possible to generate an amplitude spectrum. However, it makes more sense to consider the variance of the amplitude ($E\{\frac{1}{2}\underline{a}_i^2\}$), because the wave energy spectrum can easily be obtained by multiplying the variance spectrum

with the density of the water (ρ) and the gravitational acceleration (g). The variance spectrum is discrete, i.e., only the frequencies f_i are present. At sea all frequencies are present. In order to obtain a continuous distribution of the variance over the frequency, this approach is modified by dividing the variance of the amplitude by the frequency interval Δf_i . When the width of the frequency interval (Δf_i) approaches zero, a continuous distribution of the variance over the frequency interval is obtained. This distribution is known as the (one-dimensional) variance density spectrum:

$$E(f) = \lim_{\Delta f \rightarrow 0} \frac{1}{\Delta f} E\left\{\frac{1}{2}a^2\right\} \quad (\text{B.15})$$

The variance density spectrum gives a complete description of the surface elevation of waves in a statistical sense, under the assumption that the surface elevation can be seen as a stationary Gaussian process [Holthuijsen, 2007].

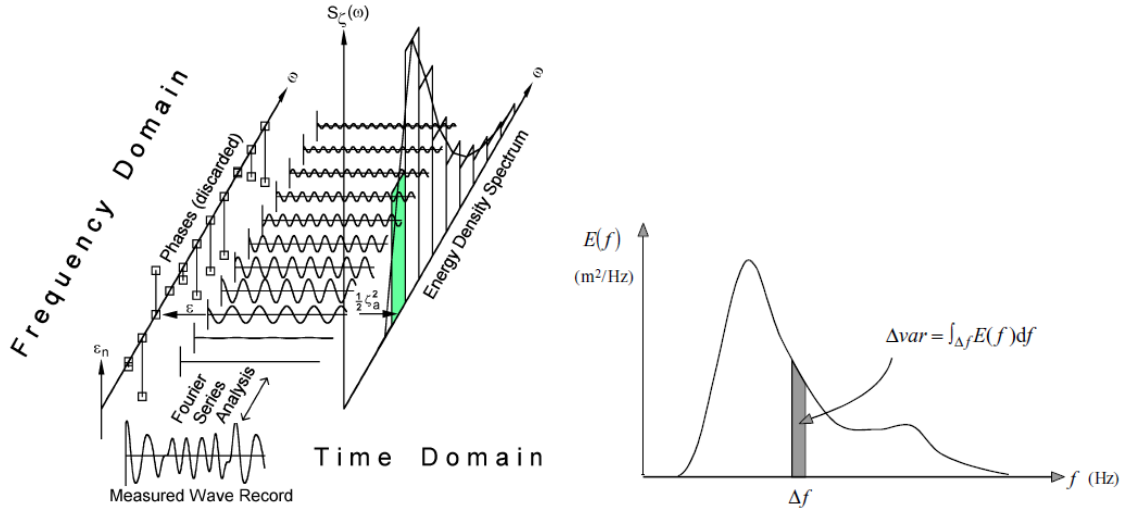


Figure B.3: Wave record analyses, ζ_a represents wave amplitude, [Journee and Massie, 2001]

Figure B.4: Interpretation of the variance density spectrum as the distribution of the total variance of the sea-surface elevation over frequencies, [Holthuijsen, 2007]

The variance density spectrum is expressed in terms of frequency (f). Since it is common to use angular arguments for sine and cosine waves, it is useful to express the variance density spectrum in terms of angular frequency (ω). This can be achieved by multiplying Eq.B.15 by $\frac{1}{2\pi}$. For details on this transformation reference is made to Holthuijsen [2007].

Waves are propagating in a certain direction, which is not taken into account in the one-dimensional variance density spectrum discussed above. The direction can be taken into account by considering the propagation of the harmonic wave in the x, y -plane. If θ is the angle relative to the positive x -axis and using the principles for the one-dimensional variance density spectrum, the two-dimensional variance density spectrum is obtained:

$$E(f, \theta) = \lim_{\Delta f \rightarrow 0} \lim_{\Delta \theta \rightarrow 0} \frac{1}{\Delta f \Delta \theta} E\left\{\frac{1}{2}a^2\right\} \quad (\text{B.16})$$

In which:
 $E(f, \theta)$ = variance density as function of frequency (f) and direction (θ) [$m^2/Hz/radian$]
 a = amplitude as a random variable [m]

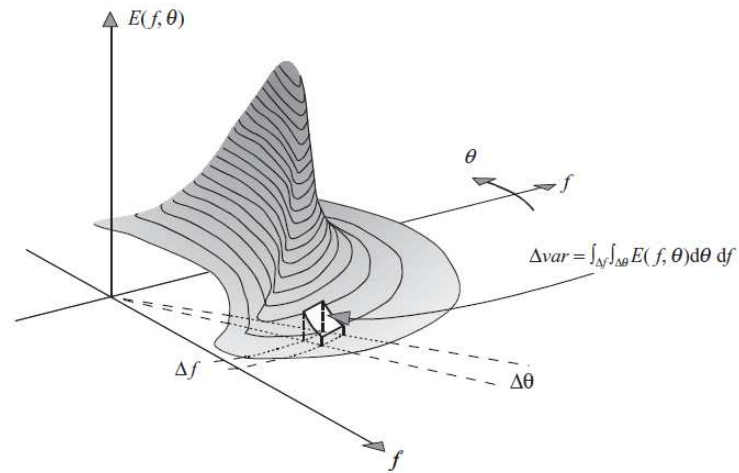


Figure B.5: Two-dimensional variance density spectrum as the distribution of the total variance of the sea-surface elevation over frequency and direction (polar coordinates), [Holthuijsen, 2007]

From the variance density spectrum it is relatively easy to obtain the wave energy density spectrum. This can be obtained by multiplying the variance density spectrum with the density of the water and with the gravitational acceleration.

Appendix C

Experimental data

This appendix shows the experimental data obtained from literature and the comparisons between experimental data and theories for wave transmission.

C.1 Experimental datasets

Distinction is made between fixed breakwaters, floating breakwaters anchored by piles and floating breakwaters anchored by chains. Furthermore, distinction is made between regular waves and irregular waves. Each dataset is compared with the existing formulas for wave transmission and based on this comparison conclusions are drawn related to the applicability of these formulas for wave transmission.

C.1.1 Fixed breakwaters

The table below shows the datasets for fixed floating breakwaters. This dataset is obtained from Koutandos et al. [2005] and from Gesraha [2006].

| Dataset | Waves | Range T [s] | D/d [-] | B/d [-] | d [m] |
|-------------------------|-----------|-------------|-----------------|---------|-------|
| Koutandos et al. [2005] | Regular | 2.4 - 10.5 | 0.2; 0.25; 0.33 | 1.00 | 2.00 |
| Koutandos et al. [2005] | Irregular | 2.8 - 5.5 | 0.2; 0.25; 0.33 | 1.00 | 2.00 |
| Gesraha [2006] | Irregular | 0.6 - 1.8 | 0.4 | 0.75 | 0.43 |

Table C.1: Experimental data fixed floating breakwaters

Comparison with experimental data obtained from Koutandos et al. [2005]

In Figure C.1 different wave transmission theories are plotted together with experimental data for regular waves for a fixed floating breakwaters. Figure C.2 shows the differences between the theories and the experimental data. From this figure it can be seen that for long wave periods the theory of Wiegel and Bollmann gives a good agreement and that all the theories are overestimating the wave transmission coefficient. When the Root Mean Square Error (RMSE) is considered (Eq.C.1) in order to judge which theory approximates the experimental data the best, it turns out that the theory of Kriebel and Bollmann is the most suitable to apply. In Table C.2 the RMSE's of the other theories are shown. From this table it can be seen that when the draft increases, the

RMSE of Macagno and Ursell increases, while the RMSE for the other theories stays more or less constant.

$$RMSE = \sqrt{\frac{\sum_{i=1}^N (C_{t,theory} - C_{t,model})^2}{N}} \quad (C.1)$$

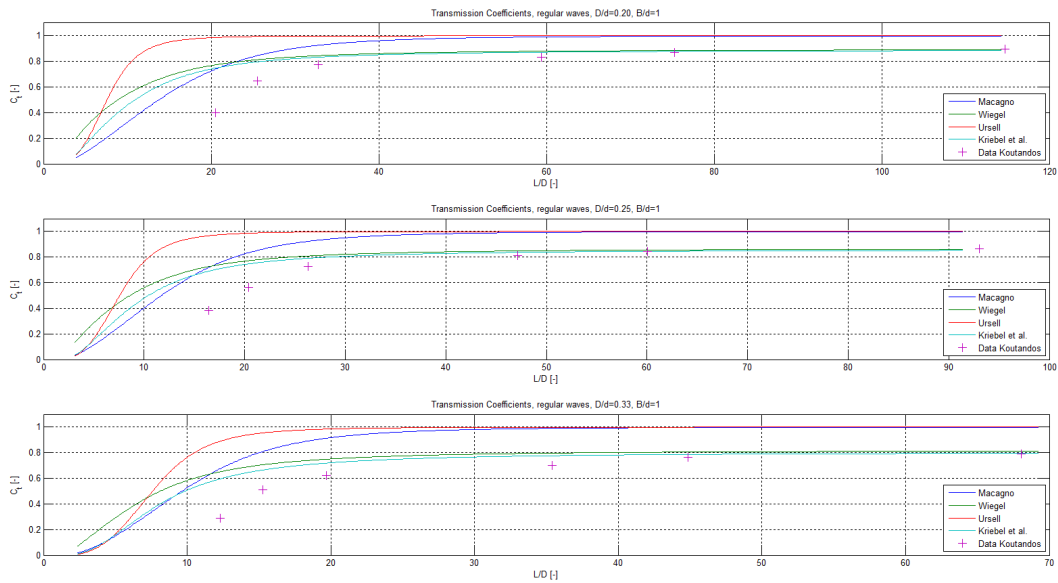


Figure C.1: Experimental data obtained from Koutandos et al. [2005] for fixed floating breakwaters compared with wave transmission theories for three different drafts and regular waves

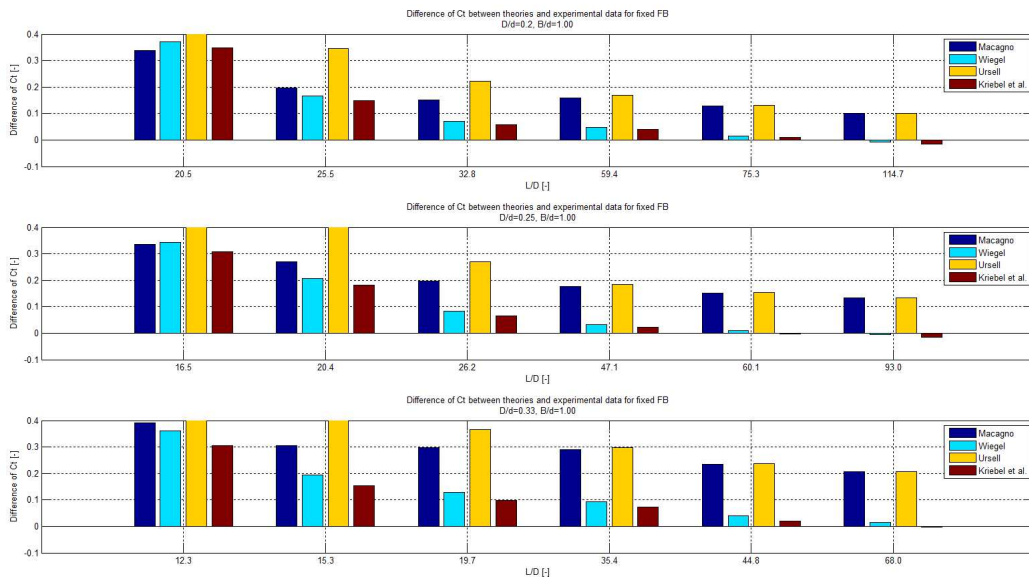


Figure C.2: Differences between wave transmission theories and experimental data obtained from Koutandos et al. [2005], regular waves. (y-axis is limited to 0.40)

| Formula | RMSE: D/d=0.2, B/d=1.0 | RMSE: D/d=0.25, B/d=1.0 | RMSE: D/d=0.33, B/d=1.0 |
|----------|------------------------------|-------------------------------|-------------------------------|
| Macagno | 0.1947 | 0.2218 | 0.2929 |
| Wiegel | 0.1699 | 0.1677 | 0.1808 |
| Ursell | 0.3081 | 0.3336 | 0.3826 |
| Bollmann | 0.1569 | 0.1486 | 0.1486 |

Table C.2: Root mean square errors between theories and experimental data of Koutandos et al. [2005], regular waves, fixed FB.

All the wave transmission theories considered are derived for regular waves. When these formulas are used for irregular waves the RMSE becomes smaller, see Table C.3. From Figure C.3 and C.4 it can be seen that for longer wave periods the wave transmission theories show a better agreement than for smaller wave periods.

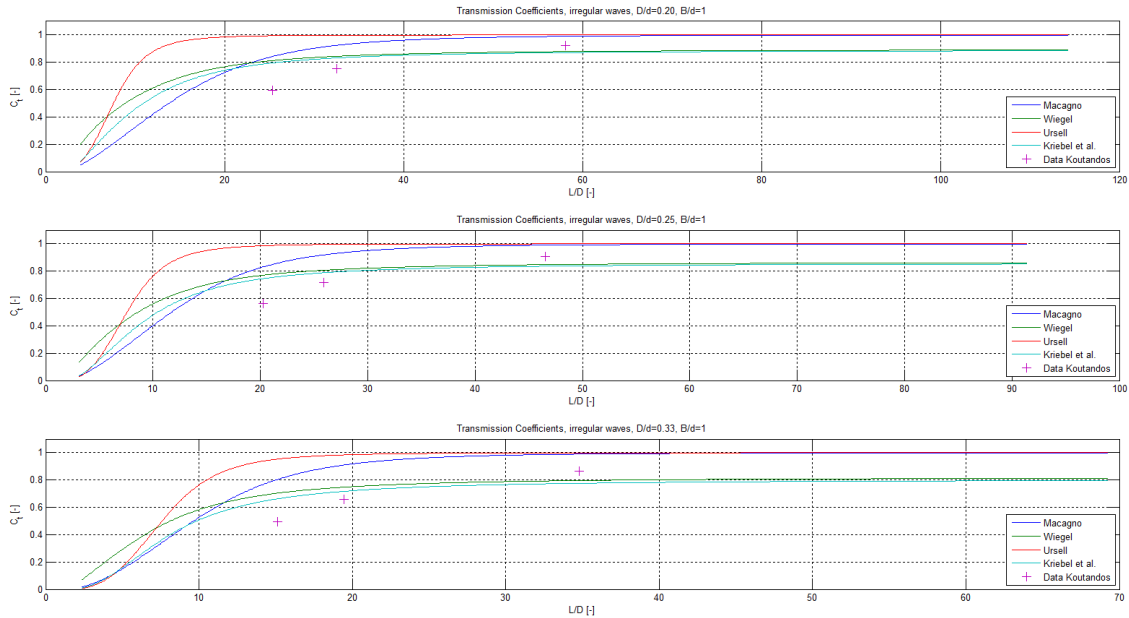


Figure C.3: Experimental data obtained from Koutandos et al. [2005] for fixed floating breakwaters compared with wave transmission theories for three different drafts and regular waves

| Formula | RMSE: D/d=0.2, B/d=1.0 | RMSE: D/d=0.25, B/d=1.0 | RMSE: D/d=0.33, B/d=1.0 |
|----------|------------------------------|-------------------------------|-------------------------------|
| Macagno | 0.2818 | 0.3224 | 0.3968 |
| Wiegel | 0.1534 | 0.1409 | 0.1257 |
| Ursell | 0.4173 | 0.4620 | 0.5259 |
| Bollmann | 0.1324 | 0.1090 | 0.0716 |

Table C.3: Root mean square errors between theories and experimental data of Koutandos et al. [2005], irregular waves, fixed FB.

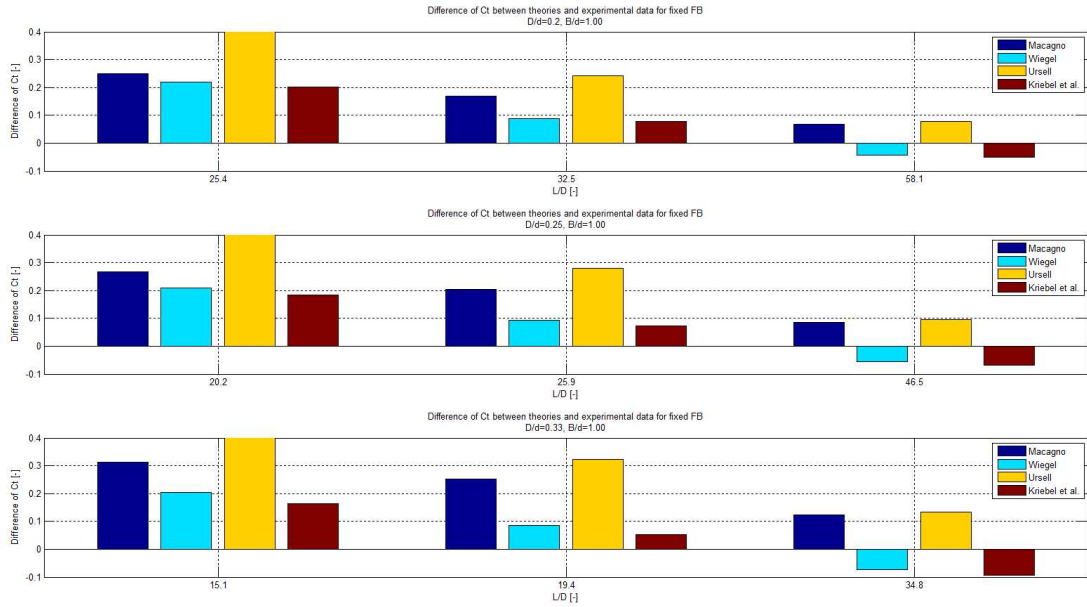


Figure C.4: Differences between wave transmission theories and experimental data obtained from Koutandos et al. [2005], irregular waves. (y-axis is limited to 0.40)

Comparison with experimental data obtained from Gesraha [2006]

Gesraha [2006] performed experiments for a fixed floating breakwater in short irregular waves. When this experimental data set is compared with the theories it can be seen that all the theories are underestimating the transmission coefficient. The major difference between this dataset and the one of Koutandos et al. [2005] are the smaller wave periods considered by Gesraha.

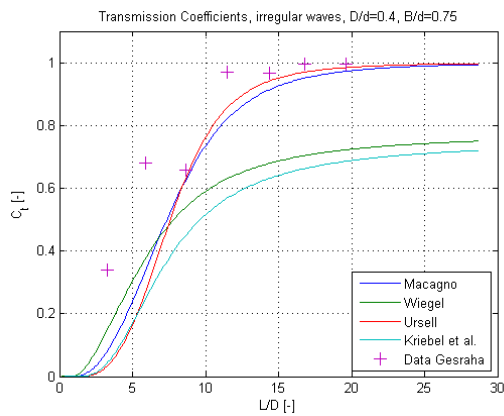


Figure C.5: Experimental data obtained from Gesraha [2006] for fixed floating breakwaters compared with wave transmission theories.

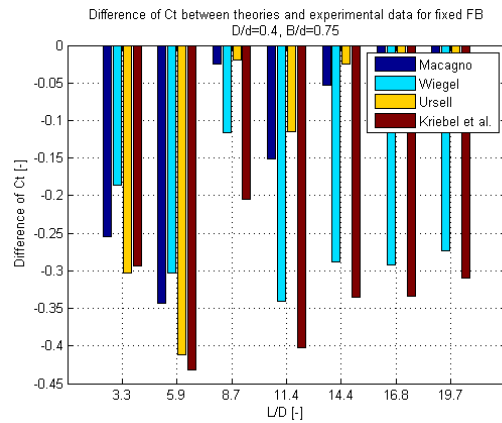


Figure C.6: Differences of C_t between theories and experimental data, fixed FB, irregular waves

| Formula | RMSE: D/d=0.4, B/d=0.75 |
|----------|-------------------------------|
| Macagno | 0.1737 |
| Wiegel | 0.2669 |
| Ursell | 0.1987 |
| Bollmann | 0.3372 |

Table C.4: Root mean square errors between theories and experimental data of Gesraha [2006], irregular waves, fixed FB.

C.1.2 Breakwaters anchored by piles

The table below shows the datasets for floating breakwaters anchored by chains. These datasets are obtained from literature, which can be seen in the first column of this table.

| Dataset | Waves | Range χ [-] or L/D [-] | D/d [-] | B/d [-] | d [m] |
|-------------------------|-----------|-----------------------------|---------|---------|-------|
| Cox et al., 2007 | Irregular | $\chi = 0.94 - 1.56$ | 0.40 | 0.57 | 4.20 |
| Deltares | Irregular | $L/D = 2.07 - 11.06$ | 0.38 | 0.12 | |
| Deltares | Irregular | $L/D = 1.46 - 7.71$ | 0.54 | 0.12 | |
| Deltares | Irregular | $L/D = 2.60 - 7.16$ | 0.41 | 0.13 | |
| Deltares | Irregular | $L/D = 1.82 - 5.06$ | 0.58 | 0.13 | |
| Koutandos et al., 2005 | Irregular | $\chi = 1.12 - 3.51$ | 0.20 | 1.00 | 2.00 |
| Martinelli et al., 2008 | Irregular | $\chi = 0.77 - 1.38$ | 0.20 | 0.49 | 0.52 |
| Cox et al., 2007 | Regular | $\chi = 0.76 - 1.90$ | 0.40 | 0.57 | 4.20 |
| Deltares | Regular | $L/D = 1.49 - 11.85$ | 0.38 | 0.12 | |
| Deltares | Regular | $L/D = 1.04 - 8.33$ | 0.54 | 0.12 | |
| Deltares | Regular | $L/D = 2.64 - 7.79$ | 0.41 | 0.13 | |
| Deltares | Regular | $L/D = 1.86 - 5.48$ | 0.58 | 0.13 | |
| Koutandos et al., 2005 | Regular | 1.32 - 2.62 | 0.20 | 1.00 | 2.00 |

Table C.5: Experimental data floating breakwaters anchored by piles

Comparison with experimental data obtained from Deltares

Deltares performed experimental scale modelling on floating breakwaters. Their model set-up is different compared to the other models of floating breakwaters anchored by piles. The main difference is the fixed screen below the water level. With this lay-out of the floating breakwater structure a large part of the water column is blocked. For the calculations the fixed vertical screen is taken into account for the draft. The dimensionless value which is used to set on the x-axis is defined as the wavelength over the draft, L/D .

Regular waves:

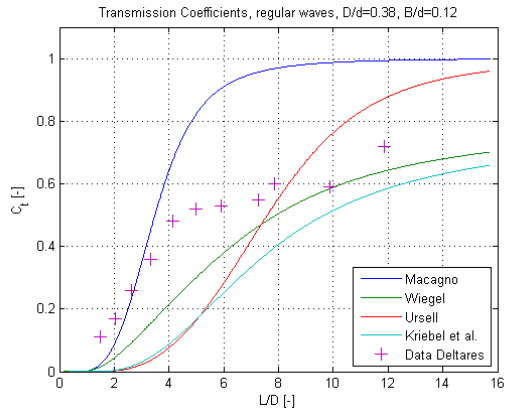


Figure C.7: Data from Deltares, regular waves

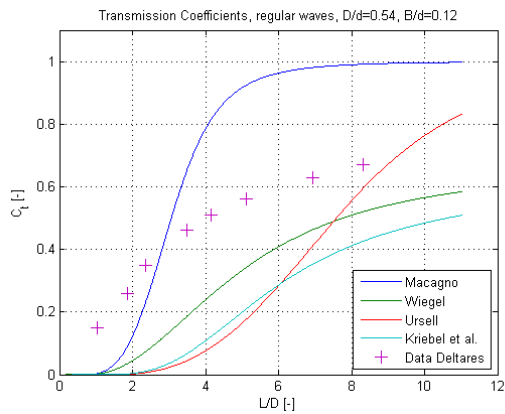


Figure C.9: Data from Deltares, regular waves

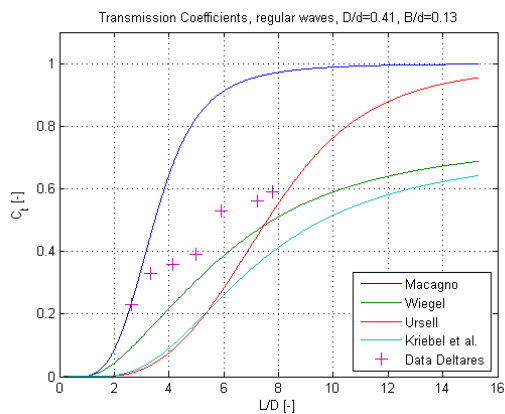


Figure C.11: Data from Deltares, regular waves

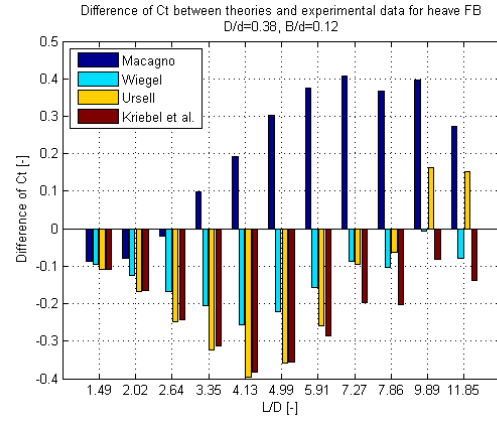


Figure C.8: Differences between theories and experimental data Figure C.7

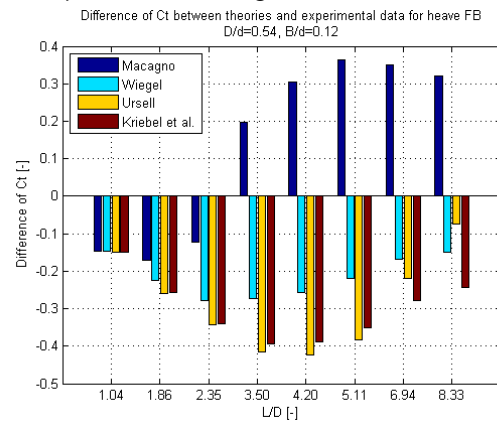


Figure C.10: Differences between theories and experimental data Figure C.9

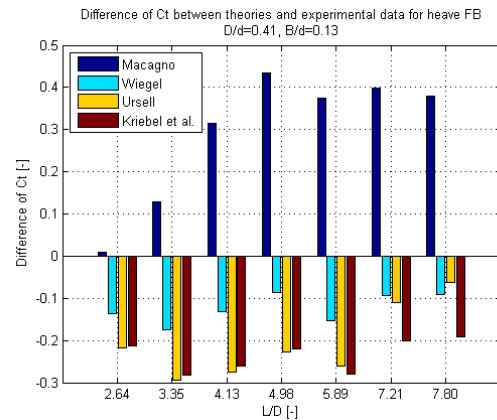


Figure C.12: Differences between theories and experimental data Figure C.11

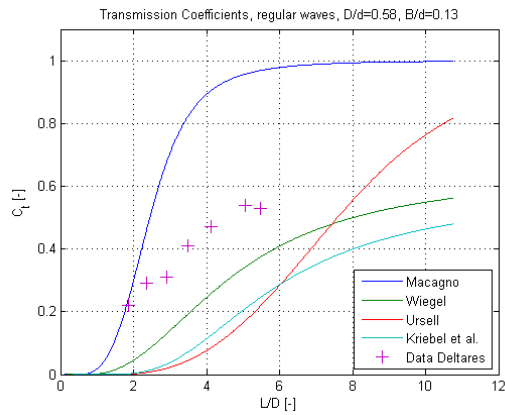


Figure C.13: Data from Deltares, regular waves

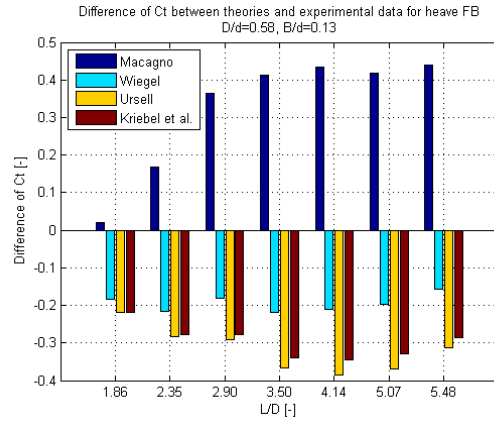


Figure C.14: Differences between theories and experimental data Figure C.13

| Formula | RMSE: D/d=0.38 B/d=0.12 | RMSE: D/d=0.54, B/d=0.12 | RMSE: D/d=0.41, B/d=0.13 | RMSE: D/d=0.58, B/d=0.13 |
|----------|-------------------------------|--------------------------------|--------------------------------|--------------------------------|
| Macagno | 0.2737 | 0.2634 | 0.3263 | 0.3562 |
| Wiegel | 0.1531 | 0.2204 | 0.1273 | 0.1961 |
| Ursell | 0.2372 | 0.3084 | 0.2222 | 0.3224 |
| Bollmann | 0.2446 | 0.3102 | 0.2381 | 0.2989 |

Table C.6: Root mean square errors between theories and experimental data of Deltares, regular waves, FB anchored by piles

Irregular waves:

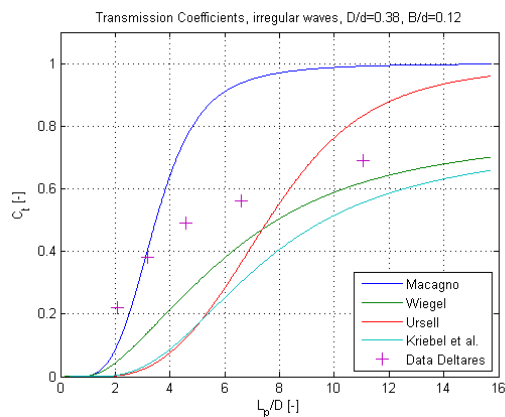


Figure C.15: Data from Deltares, irregular waves

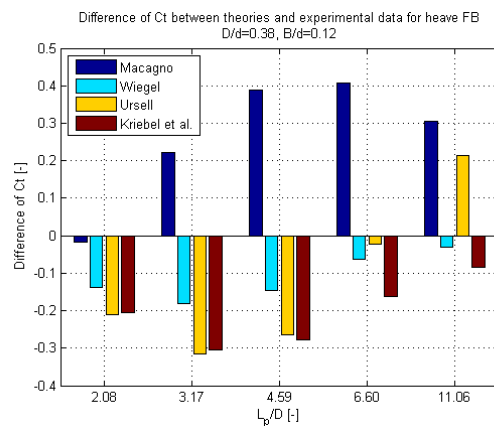


Figure C.16: Differences between theories and experimental data Figure C.15

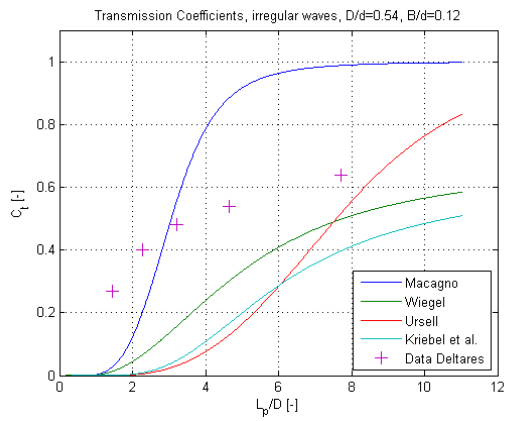


Figure C.17: Data from Deltares, irregular waves

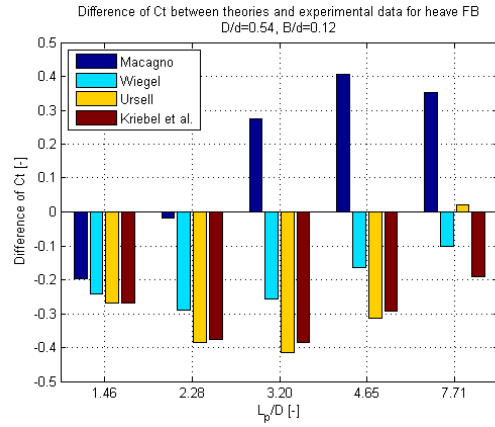


Figure C.18: Differences between theories and experimental data Figure C.17

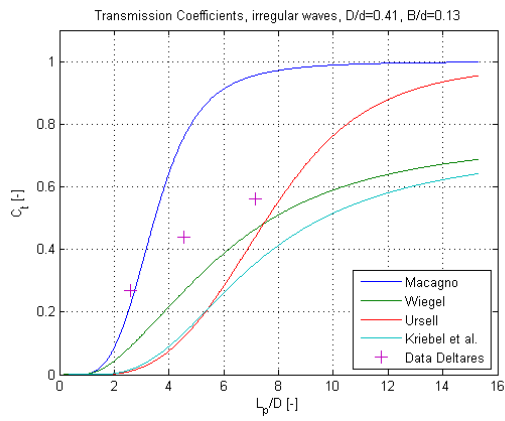


Figure C.19: Data from Deltares, irregular waves

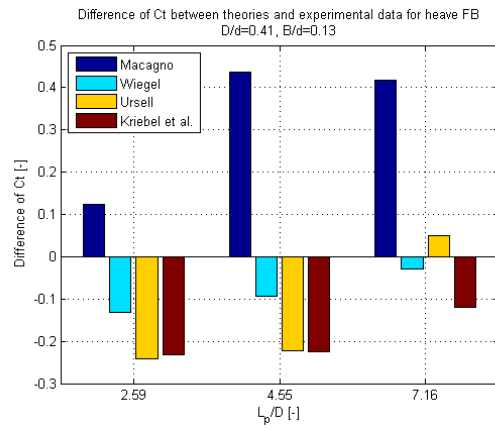


Figure C.20: Differences between theories and experimental data Figure C.19

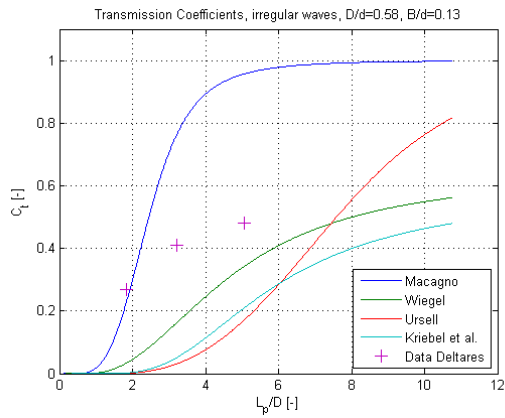


Figure C.21: Data from Deltares, irregular waves

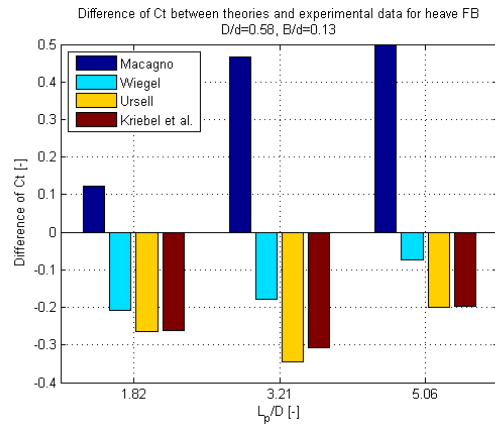


Figure C.22: Differences between theories and experimental data Figure C.21

| Formula | RMSE: D/d=0.38 B/d=0.12 | RMSE: D/d=0.54, B/d=0.12 | RMSE: D/d=0.41, B/d=0.13 | RMSE: D/d=0.58, B/d=0.13 |
|----------|-------------------------------|--------------------------------|--------------------------------|--------------------------------|
| Macagno | 0.3029 | 0.2849 | 0.3555 | 0.4005 |
| Wiegel | 0.1250 | 0.2213 | 0.0952 | 0.1642 |
| Ursell | 0.2284 | 0.3134 | 0.1916 | 0.2764 |
| Bollmann | 0.2220 | 0.3109 | 0.1997 | 0.2600 |

Table C.7: Root mean square errors between theories and experimental data of Deltares, irregular waves, FB anchored by piles

Comparison with experimental data obtained from Cox et al. [2007]

Below the experimental data of Cox et al. [2007] is shown together with the transmission theories. From these two figures it becomes clear that for $\chi \leq 0.6$ the transmission coefficient is smaller than 30%. The dataset of the regular waves is well approximated by the theory of Wiegel. The dataset of the irregular waves is well approximated till the value of $\chi = 1.0$. For higher χ -values the wave transmission is overestimated by Macagno.

| Formula | RMSE: D/d=0.40, B/d=0.57, Hs=0.4m | RMSE: D/d=0.40, B/d=0.57, Hs=0.8m |
|----------|--|--|
| Macagno | 0.2211 | 0.2260 |
| Wiegel | 0.958 | 0.0618 |
| Ursell | 0.1921 | 0.2121 |
| Bollmann | 0.1026 | 0.0959 |

Table C.8: Root mean square errors between theories and experimental data of Cox et al. [2007], regular waves, FB anchored by piles

| Formula | RMSE: D/d=0.40, B/d=0.57, Hs=0.4m | RMSE: D/d=0.40, B/d=0.57, Hs=0.8m |
|----------|--|--|
| Macagno | 0.2900 | 0.2705 |
| Wiegel | 0.0806 | 0.0472 |
| Ursell | 0.2442 | 0.2319 |
| Bollmann | 0.0360 | 0.0309 |

Table C.9: Root mean square errors between theories and experimental data of Cox et al. [2007], irregular waves, FB anchored by piles

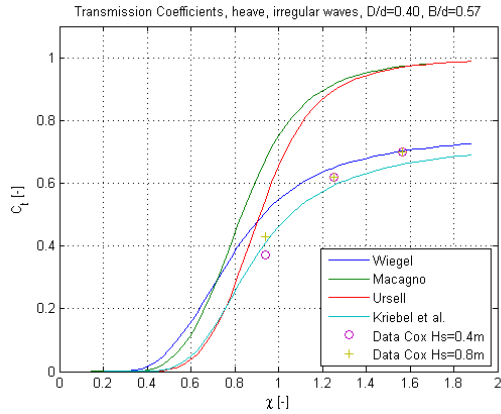


Figure C.23: Data from Cox et al. [2007], irregular waves, depth (d) = 4.20m and heave period (Th) = 3.2s

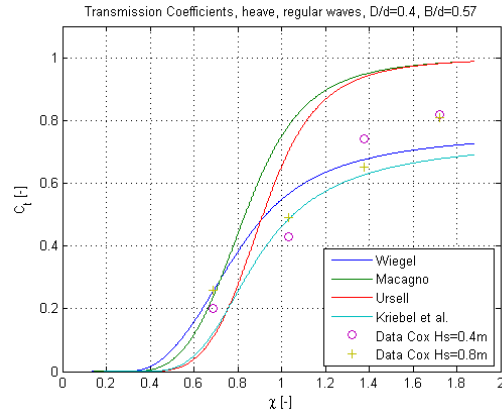


Figure C.24: Data from Cox et al. [2007], regular waves, depth (d) = 4.20m and heave period (Th) = 3.2s

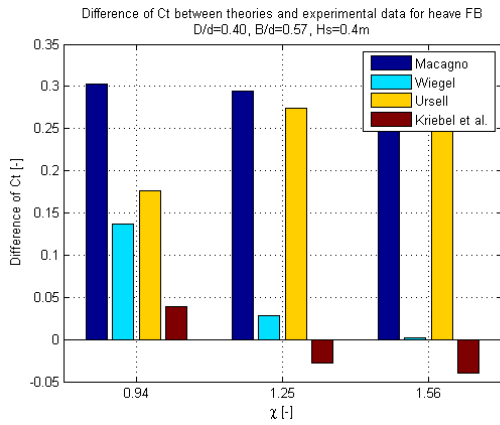


Figure C.25: Differences between theories and experimental data Figure C.23 for $H_s=0.4m$

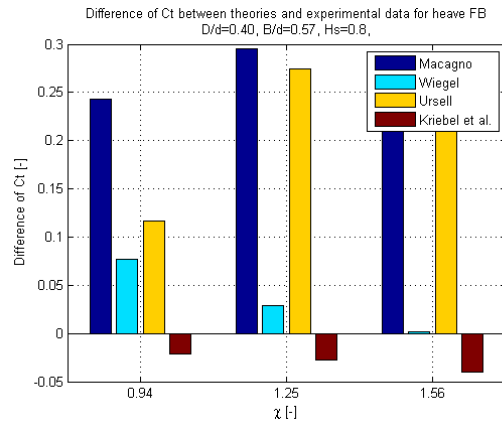


Figure C.26: Differences between theories and experimental data Figure C.23 for $H_s=0.8m$

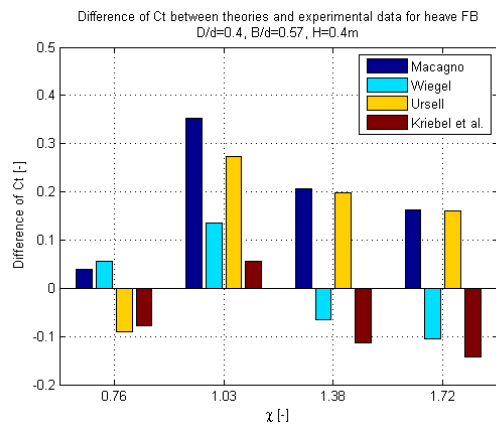


Figure C.27: Differences between theories and experimental data Figure C.24 for $H_s=0.4m$

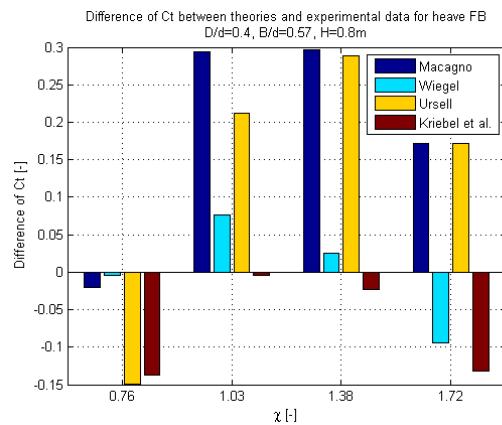


Figure C.28: Differences between theories and experimental data Figure C.24 for $H_s=0.8m$

Comparison with experimental data obtained from Koutandos et al. [2005]

Koutandos et al. [2005] performed experimental model tests for shallow- and intermediate water depths in a large scale facility. The shallow water depth, which implies relatively long waves is represented by the high χ -values. When this data is compared with the theories it becomes clear that most theories are overestimating the transmission for the case of irregular waves. When regular waves are considered, it can be seen that Macagno approximates the measured values well till the value of $\chi = 2.2$. For higher χ -values Macagno overestimates the transmission coefficients.

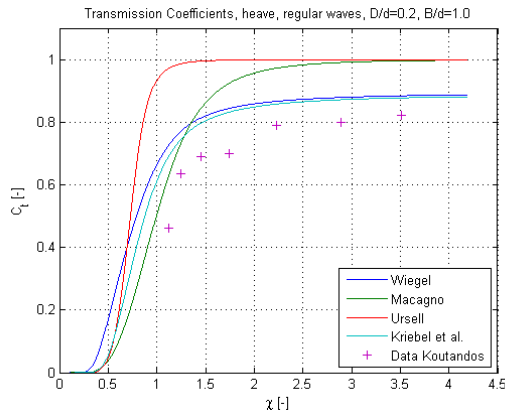


Figure C.29: Data from Koutandos et al. [2005], regular waves, depth (d) = 2.00m and heave period (Th) = 2.1s

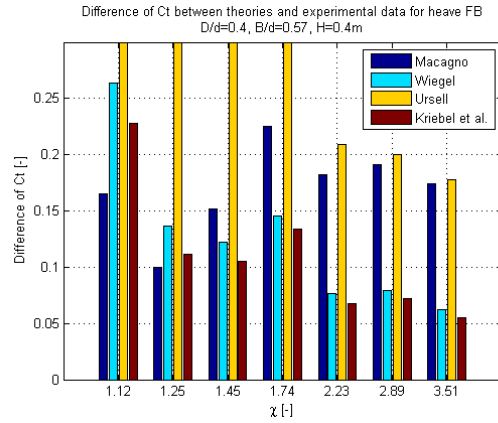


Figure C.30: Differences between theories and experimental data Figure C.29

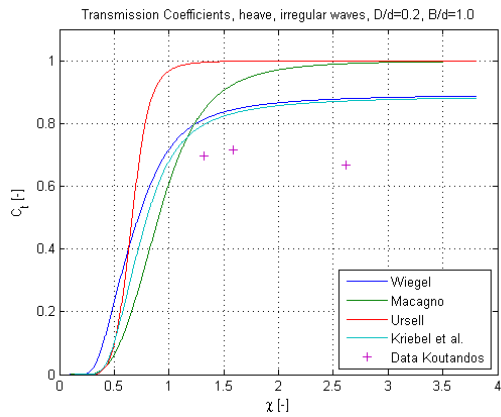


Figure C.31: Data from Koutandos et al. [2005], irregular waves, depth (d) = 2.00m and heave period (Th) = 2.1s

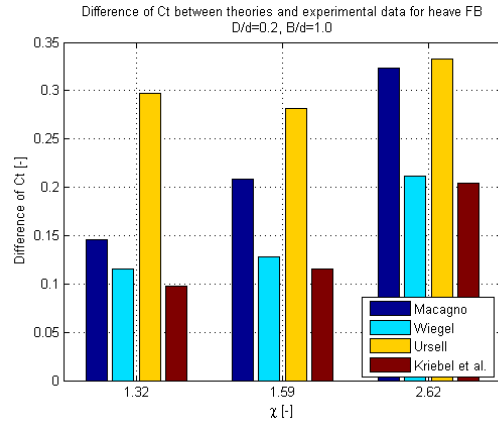


Figure C.32: Differences between theories and experimental data Figure C.31

| Formula | RMSE: D/d=0.20, B/d=1.0 |
|----------|-------------------------------|
| Macagno | 0.1738 |
| Wiegel | 0.1415 |
| Ursell | 0.3118 |
| Bollmann | 0.1230 |

Table C.10: Root mean square errors between theories and experimental data of Koutandos et al. [2005], regular waves, FB anchored by piles

| Formula | RMSE: D/d=0.20, B/d=1.0 |
|----------|-------------------------------|
| Macagno | 0.2374 |
| Wiegel | 0.1575 |
| Ursell | 0.3046 |
| Bollmann | 0.1417 |

Table C.11: Root mean square errors between theories and experimental data of Koutandos et al. [2005], irregular waves, FB anchored by piles

Comparison with experimental data obtained from Martinelli et al. [2008]

The dataset obtained from Martinelli et al. [2008] shows in general a good agreement with Macagno. For χ -values smaller than 1.0, there is a small overestimation of the transmission coefficients by Macagno. For χ -values between 1.0 and 1.5 Macagno shows a good agreement.

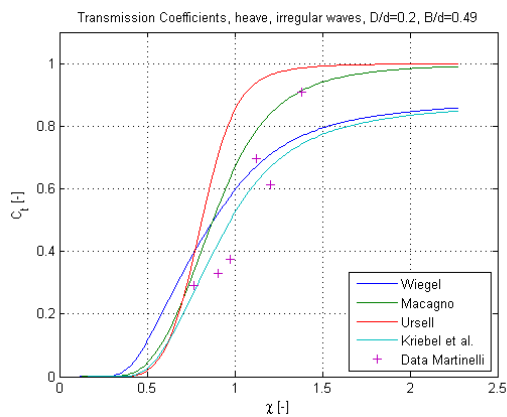


Figure C.33: Data from Martinelli et al. [2008], irregular waves, depth (d) = 0.52m and heave period (Th) = 0.88s

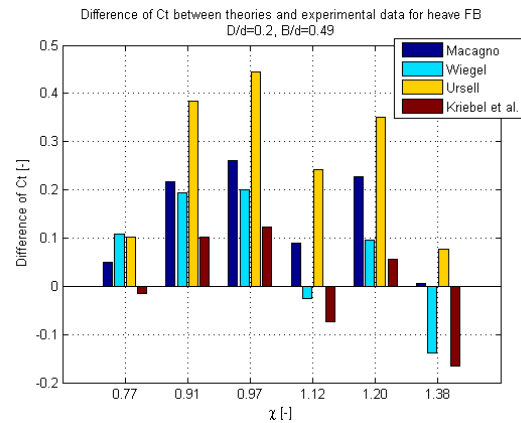


Figure C.34: Differences between theories and experimental data Figure C.33

| Formula | RMSE: D/d=0.20, B/d=0.48 |
|----------|--------------------------------|
| Macagno | 0.1717 |
| Wiegel | 0.1410 |
| Ursell | 0.3011 |
| Bollmann | 0.1013 |

Table C.12: Root mean square errors between theories and experimental data of Martinelli et al. [2008], irregular waves, FB anchored by piles

C.1.3 Breakwaters anchored by chains

Several researchers investigated the effect of wave transmission for floating breakwaters anchored by chains. The table shows the datasets which are obtained from literature.

| Dataset | Waves | Range χ [-] | D/d [-] | B/d [-] | d [m] |
|---------------------------------|-----------|------------------|---------|---------|-------|
| Gesraha, 2006 | Irregular | 0.56 - 1.67 | 0.4 | 0.75 | 0.43 |
| Martinelli et al., 2008 (flume) | Irregular | 0.78 - 1.23 | 0.13 | 0.40 | 0.50 |
| Martinelli et al., 2008 (basin) | Irregular | 0.78 - 1.20 | 0.13 | 0.40 | 0.50 |
| Brebner and Ofuya, 1968 | Regular | 0.69 - 1.03 | 0.15 | 1.10 | 0.45 |
| Brebner and Ofuya, 1968 | Regular | 0.66 - 0.99 | 0.19 | 1.10 | 0.45 |
| Brebner and Ofuya, 1968 | Regular | 0.61 - 0.86 | 0.30 | 1.10 | 0.45 |
| Peña et al., 2011 | Regular | 0.80 - 1.45 | 0.18 | 0.60 | 6.75 |
| Peña et al., 2011 | Regular | 0.80 - 1.20 | 0.18 | 0.57 | 6.75 |
| Peña et al., 2011 | Regular | 0.60 - 1.10 | 0.32 | 0.60 | 6.75 |

Table C.13: Experimental data floating breakwaters anchored by chains

Regarding to this table the following remarks are made:

- For a large part of the available datasets, the range of the relative period χ falls in the domain for which the modification factor developed by Ruol et al. [2013a] is valid, namely between 0.50 and 1.50. For χ -values larger than 1.50, the formula of Macagno holds, since the modification factor developed by Ruol et al. [2013a] becomes 1.0
- For a couple of datasets, the range of the relative draft D/d does not fall in the domain for which the formula of Ruol et al. [2013a] is valid.

Comparison with experimental data obtained from Peña et al. [2011]

The dataset obtained from Peña et al. contains values of relative draft which are just outside or inside the domain for which the formula of Ruol et al. is applicable. From the plots shown below, it can be concluded that the formula of Ruol et al. slightly underestimates the wave transmission for values close to the boundaries for which Ruol et al. is applicable. When the relative width decreases the measured values approach closer to formula proposed by Ruol et al.

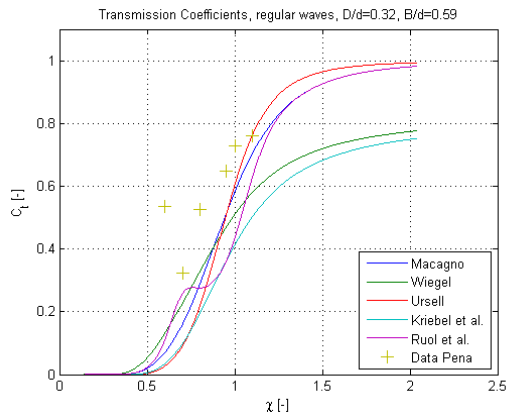


Figure C.35: Experimental data from Peña et al. [2011], (d) = 6.75m, (B) = 4.0m and (D) = 2.15m

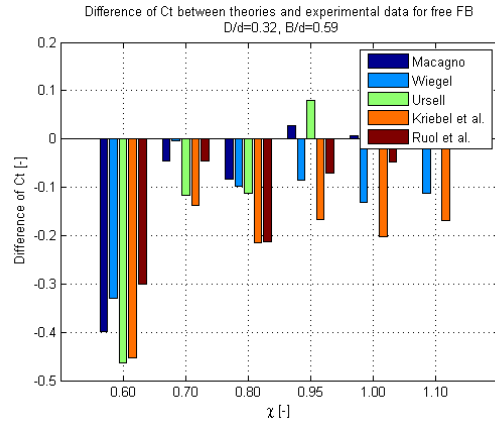


Figure C.36: Differences between theories and experimental data of Figure C.35

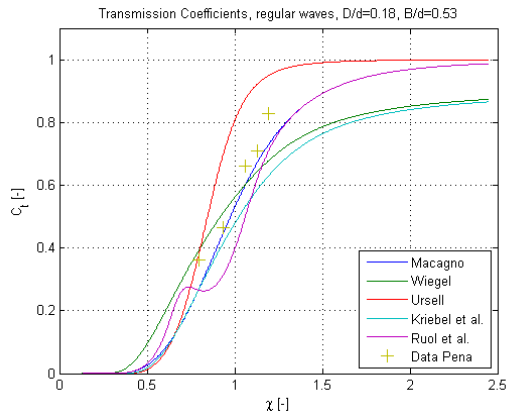


Figure C.39: Experimental data from Peña et al. [2011], (d) = 6.75m, (B) = 3.6m and (D) = 1.2m

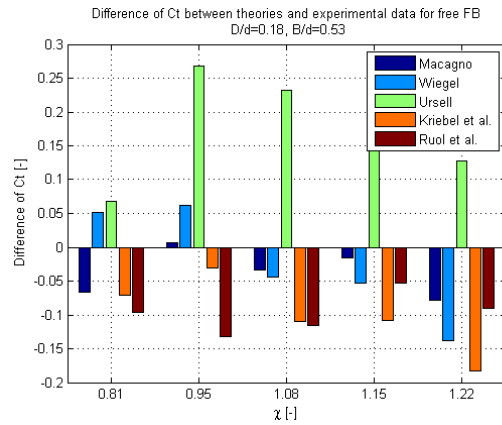


Figure C.40: Differences between theories and experimental data of Figure C.39

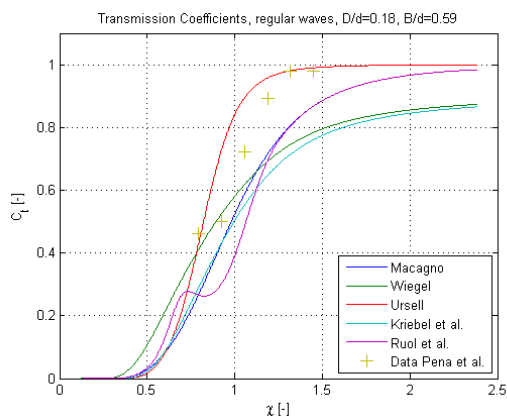


Figure C.37: Experimental data from Peña et al. [2011], (d) = 6.75m, (B) = 4.0m and (D) = 1.2m

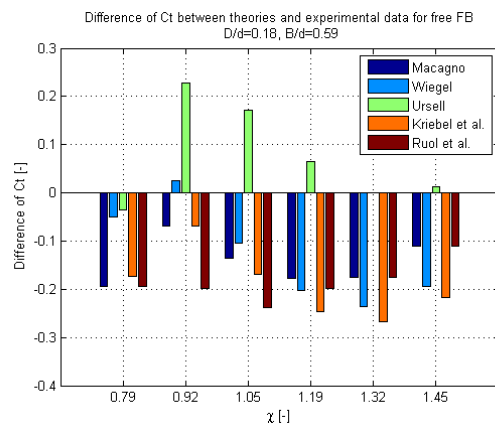


Figure C.38: Differences between theories and experimental data of Figure C.37

| Formula | RMSE: D/d=0.18, B/d=0.53 | RMSE: D/d=0.32, B/d=0.59 | RMSE: D/d=0.18, B/d=0.59 |
|----------|--------------------------------|--------------------------------|--------------------------------|
| Macagno | 0.1502 | 0.0488 | 0.1694 |
| Wiegel | 0.1571 | 0.0779 | 0.1606 |
| Ursell | 0.1206 | 0.1980 | 0.2110 |
| Bollmann | 0.2010 | 0.1121 | 0.2476 |
| Ruol | 0.1899 | 0.1011 | 0.1570 |

Table C.14: Root mean square errors between theories and experimental data of Peña et al. [2011], regular waves, floating breakwater anchored by chains

Comparison with experimental data obtained from Brebner and Ofuya [1968]

For the datasets obtained from Brebner et al., there are two datasets which contain ranges of χ and D/d for which the formula of Ruol et al. is applicable, see Figure C.41 and Figure C.43. Furthermore, it is remarkable that all the χ -values are lower than one for this dataset and that for χ -values lower than 0.7 the transmission coefficient is lower than 0.3.

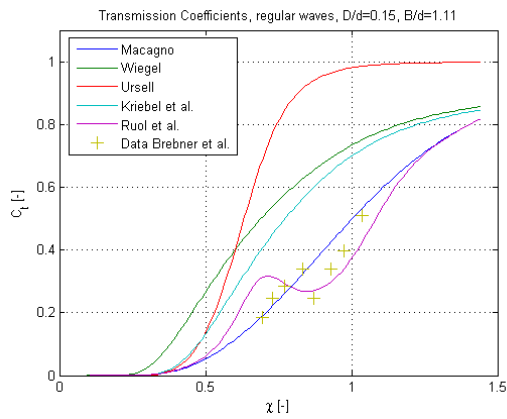


Figure C.41: Data from Brebner and Ofuya [1968], regular waves ($d = 0.46m$ and heave period ($T_h = 1.12s$))

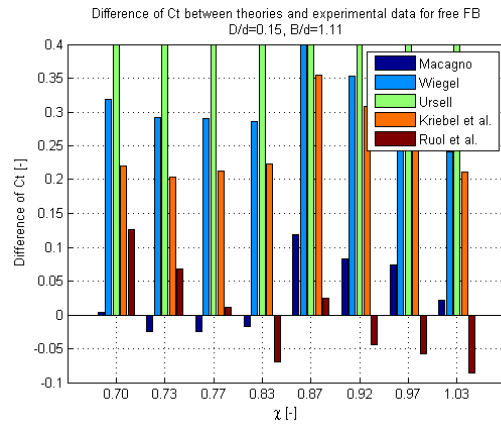


Figure C.42: Differences between theories and experimental data of Figure C.41

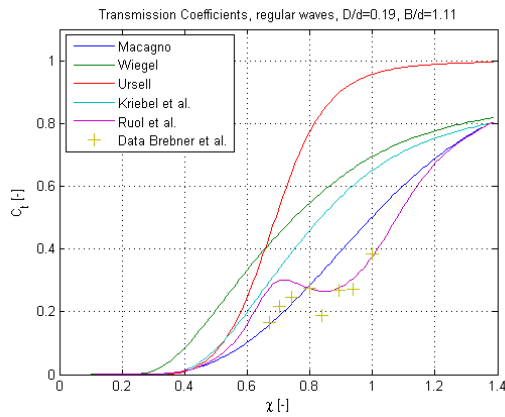


Figure C.43: Data from Brebner and Ofuya [1968], regular waves, depth (d) = 0.46m and heave period (Th) = 0.59s

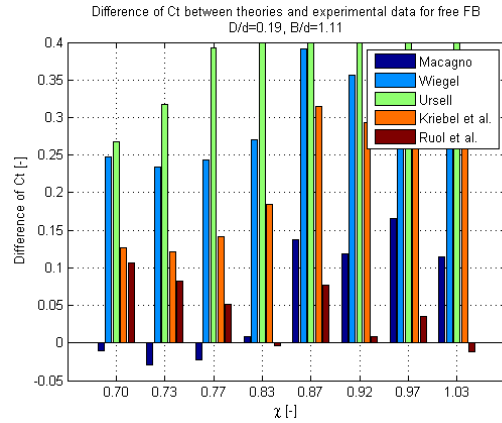


Figure C.44: Differences between theories and experimental data of Figure C.43.

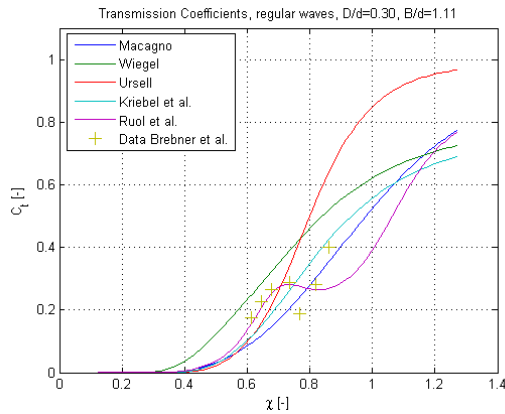


Figure C.45: Data from Brebner and Ofuya [1968], regular waves, depth (d) = 0.46m and heave period (Th) = 0.744s

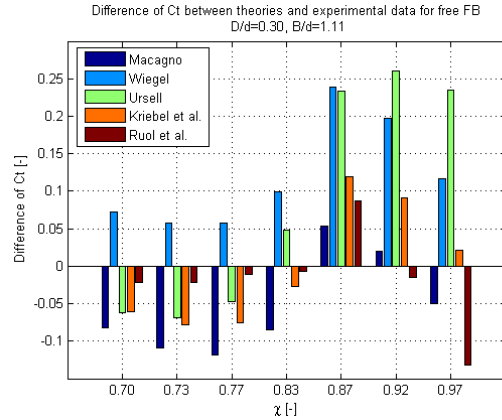


Figure C.46: Differences between theories and experimental data of Figure C.45.

| Formula | RMSE: D/d=0.2, B/d=1.0 | RMSE: D/d=0.25, B/d=1.0 | RMSE: D/d=0.33, B/d=1.0 |
|----------|------------------------------|-------------------------------|-------------------------------|
| Macagno | 0.1947 | 0.2218 | 0.2929 |
| Wiegel | 0.1699 | 0.1677 | 0.1808 |
| Ursell | 0.3081 | 0.3336 | 0.3826 |
| Bollmann | 0.1569 | 0.1486 | 0.1486 |

Table C.15: Root mean square errors between theories and experimental data of Brebner and Ofuya [1968], regular waves, floating breakwater anchored by chains

Comparison with experimental data obtained from Martinelli et al. [2008]

Martinelli et al. performed 2D experiments in a flume and 3D experiments in a wave basin. From Figure C.47 it can be seen that the wave transmission is lower for the 3D experiments, which is probably due to diffraction. The dimensionless value (D/d) for the dataset of Martinelli et al. [2008] falls outside the domain for which the formula of Ruol et al. is valid. From Figure C.47

it can be seen that the formula of Macagno approximates the 2D experiments well. The 3D experiments are good approximated by Ruol et al.

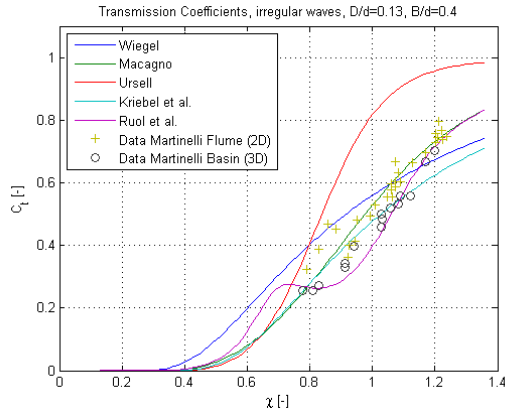


Figure C.47: Experimental data from Martinelli et al. [2008], (d) = 0.50m and (Th) = 0.83s, irregular waves

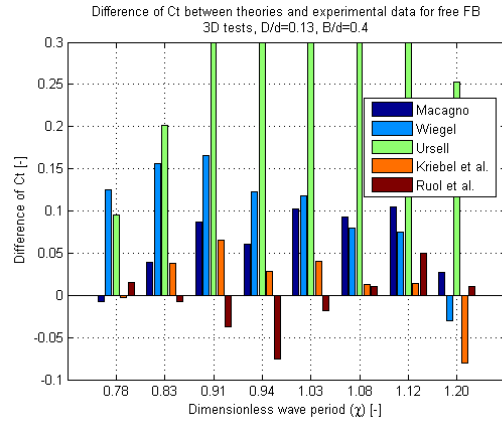


Figure C.48: Differences between theories and experimental data 3D-tests of Figure C.47,(y-axis limited to 0.3)

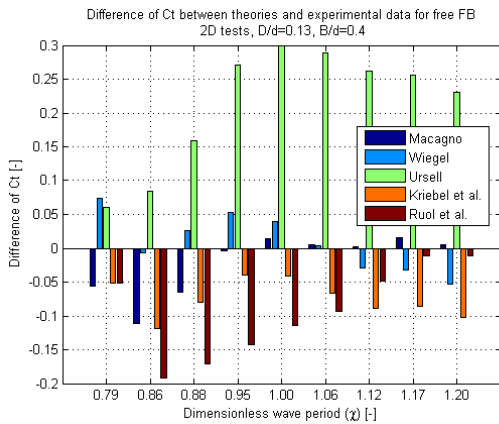


Figure C.49: Differences between theories and experimental data 2D-tests of Figure C.47,(y-axis limited to 0.3)

| Formula | RMSE: 2D, D/d=0.13, B/d=0.4 | RMSE: 3D, D/d=0.13, B/d=0.4 |
|----------|--------------------------------------|--------------------------------------|
| Macagno | 0.4760 | 0.0737 |
| Wiegel | 0.0411 | 0.1170 |
| Ursell | 0.2292 | 0.3083 |
| Bollmann | 0.0794 | 0.0431 |
| Ruol | 0.1122 | 0.0360 |

Table C.16: Root mean square errors between theories and experimental data of Martinelli et al. [2008], irregular waves, floating breakwater anchored by chains

Comparison with experimental data obtained from Gesraha [2006]

The dataset obtained from Gesraha [2006] shows a better agreement with Macagno than for Ruol et al., but the differences are small. This is remarkable because the dimensionless values χ and D/d for this dataset are in the domain for which Ruol et al. is valid. Furthermore it can be seen that for χ -values lower than 0.90 there is an overestimation of the wave transmission for both the theories of Macagno and Ruol et al.

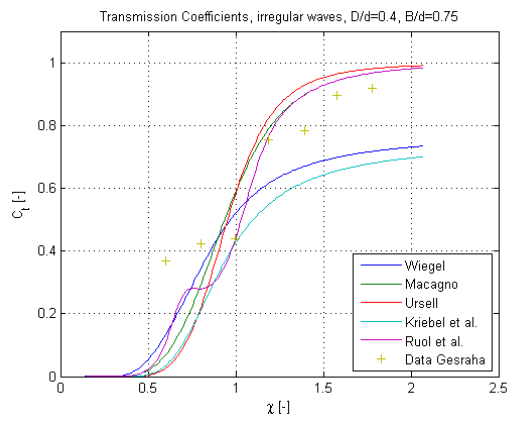


Figure C.50: Experimental data from Gesraha [2006], (d) = 0.425m and (Th) = 5.89s, irregular waves

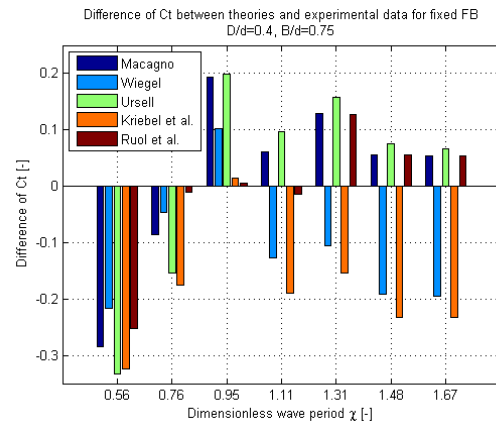


Figure C.51: Differences between theories and experimental data Figure C.50

| Formula | RMSE: D/d=0.4, B/d=0.75 |
|----------|-------------------------------|
| Macagno | 0.1478 |
| Wiegel | 0.1520 |
| Ursell | 0.1768 |
| Bollmann | 0.2082 |
| Ruol | 0.1107 |

Table C.17: Root mean square errors between theories and experimental data of Gesraha [2006], irregular waves, floating breakwater anchored by chains

Appendix D

Modelling of floating breakwaters

This appendix discusses the theory used in AQWA and the calculations results obtained by AQWA.

D.1 Theory used in AQWA

Setting up a model in AQWA is relatively easy and user friendly. Often this means that the user does not know what the program is doing and the model can be seen as a 'blackbox model'. In this section the theory which is used by AQWA is discussed into more detail.

As mentioned before, AQWA is based on a three-dimensional panel method and is based on linear three-dimensional potential theory. This implies that viscous forces are not taken into account, the wave elevation is small and the fluid is assumed as incompressible and irrotational. The boundary condition problem is solved by satisfying the body boundary condition (Timman-Newman relations), linearised free surface condition and radiation condition. This theory applies to finite depth and the diffraction problem is solved in the frequency domain.

D.1.1 Waves

The regular waves in AQWA are described by linear wave theory, see Eq.(4.10) and by second order Stokes waves. The theory of Stokes adds corrections to the harmonic wave profile by adding extra harmonic waves to the basic harmonic. Stokes' theory approximates waves which are slightly steeper than harmonic waves and this theory is applicable in deep waters. In this case (2nd order Stokes wave) only one 'extra' harmonic wave is added to the basic harmonic with the wave steepness raised to the second order. If the wave steepness is defined as $\epsilon = ak$, than the basic harmonic can be written as:

$$\eta(x, t) = a \cos(\omega t - kx) = \epsilon \eta_1(x, t) \quad \text{with} \quad \eta_1(x, t) = k^{-1} \cos(\omega t - kx) \quad (\text{D.1})$$

In the equation above $\eta_1(x, t) = k^{-1} \cos(\omega t - kx)$ represents the basic harmonic. The first correction in the Stokes theory is adding a harmonic wave to the basic harmonic with the wave steepness squared:

$$\eta(x, t) = \epsilon \eta_1(x, t) + \epsilon^2 \eta_2(x, t) = a \cos(\omega t - kx) + 0.5ka^2 \cos 2(\omega t - kx) \quad (\text{D.2})$$

Figure D.1 shows the result of the 2nd order Stokes theory. From this figure it becomes clear that the 2nd order Stokes wave has a sharper crest and a flatter trough than a harmonic wave.

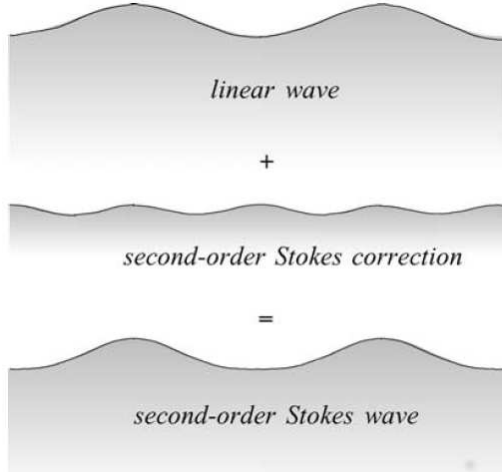


Figure D.1: 2nd order Stokes waves, [Holthuijsen, 2007]

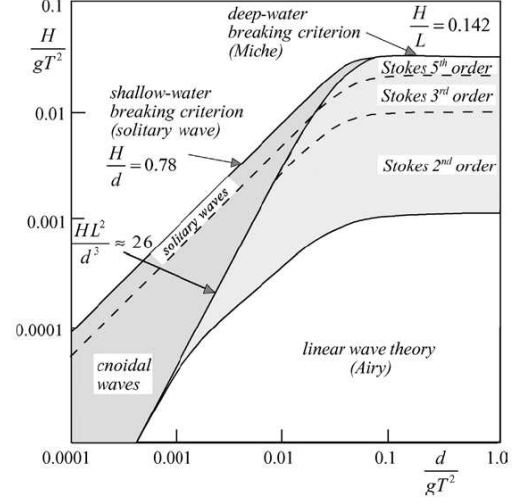


Figure D.2: Applicability for different wave theories , [Holthuijsen, 2007]

The degree of non-linearity of waves can be quantified with the Ursell number:

$$N_{Ursell} = \frac{\text{steepness}}{(\text{relative depth})^3} = \frac{\frac{H}{L}}{\frac{d}{L^3}} = \frac{HL^2}{d^3} \quad (\text{D.3})$$

In Figure D.2 the applicability for the different wave theories is shown. The input for the waves in AQWA consists of a wave frequency and a wave amplitude. The input for the frequency of the waves is limited by the water depth and by the mesh size. Long waves (low frequency) are depth limited while the short wave (high frequency) are limited by the mesh size.

D.2 Potential flow

A velocity potential of a flow is simply a mathematical expression which has the useful property that the velocity component in a point in the fluid in any chosen direction is the derivative of the potential function [Journee and Massie, 2001].

Potential lines are curves where the potential value is constant. If the potential function is defined as ϕ , than this implies that $\phi = \text{constant}$. The velocity potential function is by definition the derivative of the potential function, when substituting these velocity potentials (Eq.D.4) in the continuity equation (Eq.D.6) the Laplace equation (Eq.D.5) is obtained:

$$\text{Velocity potential function :} \quad u_x = \frac{\partial \phi}{\partial x}, \quad u_y = \frac{\partial \phi}{\partial y}, \quad u_z = \frac{\partial \phi}{\partial z} \quad (\text{D.4})$$

$$\text{Laplace equation :} \quad \frac{\partial^2 \phi}{\partial x^2} + \frac{\partial^2 \phi}{\partial y^2} + \frac{\partial^2 \phi}{\partial z^2} = 0 \quad (\text{D.5})$$

The advantage of this theory is that the velocity problem with three unknowns, u_x, u_y and u_z , represented as \vec{V} is reduced to a problem of one unknown, ϕ . All the solutions of the potential theory must fulfil the Laplace equation (D.5) and must be rotation free. This later requirement is valid outside the boundary layer. Very close to the body this requirement is not fulfilled by the potential theory. However, this boundary layer is very small compared to the dimensions of the body in the flow and the region of interest around the body, which makes this theory suitable to apply for large floating structures.

In order to obtain a solution for the velocity potential, the following boundary conditions are used, see also Section 4:

$$1. \text{ Continuity condition : } \quad \frac{\partial u_x}{\partial x} + \frac{\partial u_y}{\partial y} + \frac{\partial u_z}{\partial z} = 0 \quad (\text{D.6})$$

$$2. \text{ kinematic boundary at the sea bed : } \quad \frac{\partial \phi}{\partial z} = 0 \quad \text{for } z = -d \quad (\text{D.7})$$

$$3. \text{ kinematic boundary at the surface : } \quad \frac{\partial \phi}{\partial z} = \frac{\partial \eta}{\partial t} \quad \text{for } z = 0 \quad (\text{D.8})$$

The increase of the potential value from two points in the fluid (A and B) is defined as:

$$\begin{aligned} \Delta\phi_{A \rightarrow B} &= \int_A^B \vec{V} \cdot \vec{ds} = \int_A^B (u dx + v dy + w dz) \\ &= \int_A^B \left(\frac{\partial \phi}{\partial x} dx + \frac{\partial \phi}{\partial y} dy + \frac{\partial \phi}{\partial z} dz \right) = \phi(B) - \phi(A) \end{aligned} \quad (\text{D.9})$$

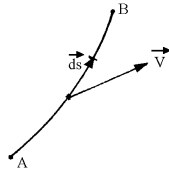


Figure D.3: Definition of velocity potential [Journee and Massie, 2001]

Besides the potential lines and potential functions, there are streamlines and stream functions. A streamline is a line which defines the flow direction. An important characteristic of the stream function is that the value of the stream function is constant along the streamline, $\psi = \text{constant}$. This implies that the rate of flow between any two streamlines remains constant when the points A and B follow their streamlines. The rate of flow between two streamlines in a 2D-plane (x,y-plane) is defined by:

$$\begin{aligned} \Delta Q &= \Delta\psi_{A \rightarrow B} = \int_A^B (\vec{V} \cdot \vec{n} ds) = \int_A^B (u dy + v dx) \\ &= \int_A^B \left(\frac{\partial \psi}{\partial y} dy + \frac{\partial \psi}{\partial x} dx \right) = \psi(B) - \psi(A) \end{aligned} \quad (\text{D.10})$$

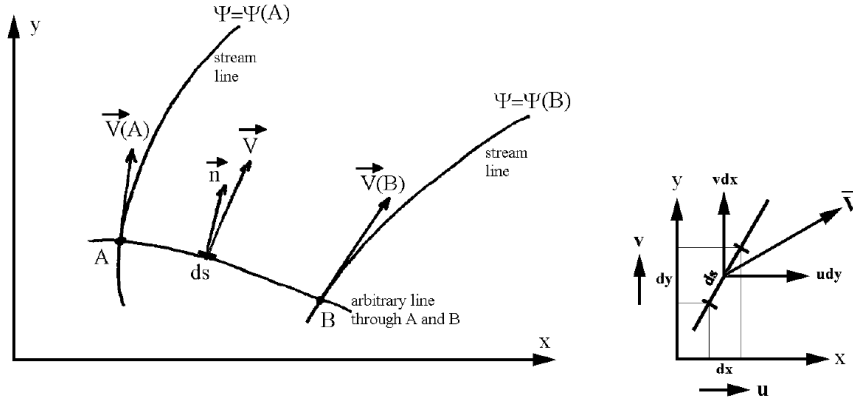


Figure D.4: Streamlines [Journee and Massie, 2001]

If the rate of flow stays constant for two streamlines which are converging or diverging, the flow velocity must increase or decrease (since the continuity condition must be fulfilled). The stream function for a 2-dimensional flow field can be defined like the potential function and must be defined such that its derivative equals the velocity component, see Eq.(D.12). For the complete derivation of this reference is made to [White, 1999]. The stream function is limited to two coordinates (x, y) unlike the velocity potential function.

$$\text{Laplace equation for } \psi : \quad \frac{\partial^2 \psi}{\partial x^2} + \frac{\partial^2 \psi}{\partial y^2} = 0 \quad (\text{D.11})$$

$$\text{Derivative of stream function } \psi : \quad u_x = \frac{\partial \psi}{\partial y} \quad \text{and} \quad u_y = -\frac{\partial \psi}{\partial x} \quad (\text{D.12})$$

With the potential lines (ϕ) and streamlines (ψ) a mesh can be generated. Since potential flow is assumed to be frictionless, energy is conserved along the streamline, hence the equation of Bernoulli may be applied. Between the streamlines the flow velocity can be determined from which pressures can be derived by the Bernoulli equation. For the equation of Bernoulli distinction is made between steady and unsteady flow.

$$\text{Velocity :} \quad \vec{V}^2 = u_x^2 + u_y^2 + u_z^2 = \left(\frac{\partial \phi}{\partial x}\right)^2 + \left(\frac{\partial \phi}{\partial y}\right)^2 + \left(\frac{\partial \phi}{\partial z}\right)^2 \quad (\text{D.13})$$

$$\text{Bernoulli unsteady flow :} \quad \frac{\partial \phi}{\partial t} + \frac{1}{2} \vec{V}^2 + \frac{p}{\rho} + gz = C(t) \quad (\text{D.14})$$

$$\text{Bernoulli steady flow :} \quad \frac{1}{2} \vec{V}^2 + \frac{p}{\rho} + gz = C \quad (\text{D.15})$$

From Figure D.5 it can be seen that the streamlines (ψ) and potential lines (ϕ) cross each other at right angles (orthogonal). Between the streamlines there is a constant discharge ΔQ . Another important characteristic is that there is no flow across a streamline. This fact can be used when structures are modelled which are impervious. The result is that any impervious flow boundary is a streamline.

Because of the orthogonality of the potential lines and stream lines the velocity components u_x and u_y can be expressed in two different ways:

$$u_x = \frac{\partial \phi}{\partial x} = \frac{\partial \psi}{\partial y} \quad \text{and} \quad u_y = \frac{\partial \phi}{\partial y} = -\frac{\partial \psi}{\partial x} \quad (\text{D.16})$$

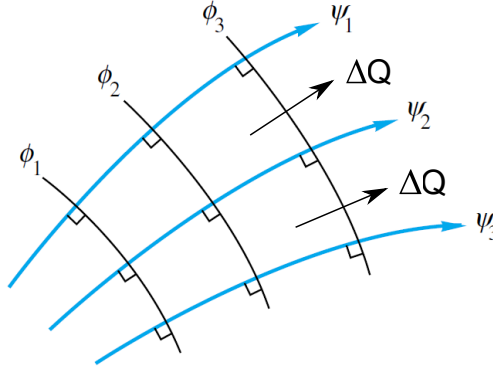


Figure D.5: Streamlines and potential lines with discharge ΔQ

D.2.1 Potential flow around floating structures

In order to determine the pressures on and around the floating body the linear fluid velocity potential can be split into three parts:

- Radiation potential (ϕ_r) potential of the oscillations of the body in still water
- Wave potential (ϕ_w) potential of the incoming waves
- Diffraction potential (ϕ_d) potential of the waves diffracting around the restrained body

The resulting fluid velocity potential then becomes:

$$\phi_{(x,y,z,t)} = \phi_r + \phi_w + \phi_d \quad (\text{D.17})$$

When the six degrees of motion are taken into account of the floating body, the radiation potential consist of six parts. Each part belongs to an specific type of motion, represented as $\phi_{r,j}$ where $j = 1, \dots, 6$. The potential of the floating body then becomes:

$$\phi = \sum_{j=1}^6 \phi_{r,j} + \phi_w + \phi_d \quad (\text{D.18})$$

This equation is numerically solved by AQWA which results in potential values from which velocities and pressures are obtained. In total there are seven boundary conditions used to solve the potential of the floating body (Eq.D.18). Three of these seven boundary conditions (Eq.D.6, Eq.(D.7) and Eq.D.8)) are used to solve the velocity potential without a floating structure and are discussed in Section D.2. Besides these three boundary conditions, four additional boundary conditions are used to solve the potential when of floating body is included. These four additional boundary conditions are discussed below.

$$4. \text{ Dynamic boundary condition : } \quad \frac{\partial^2 \phi}{\partial t^2} + g \frac{\partial \phi}{\partial z} = 0 \quad \text{at } z=0 \quad (\text{D.19})$$

$$5. \text{ Kinematic boundary of oscillating body : } \quad \frac{\partial \phi}{\partial n} = v_n(x, y, z, t) = \sum_{j=1}^6 v_j f_j(x, y, z) \quad (\text{D.20})$$

$$6. \text{ Radiation condition : } \quad \lim_{R \rightarrow \infty} \phi = 0 \quad (\text{D.21})$$

$$7. \text{ Symmetric and anti-symmetric conditions : } \quad \begin{aligned} \phi_2(-x, z) &= -\phi_2(+x, z) & \text{Sway} & (\text{D.22}) \\ \phi_3(-x, z) &= +\phi_3(+x, z) & \text{Heave} & \\ \phi_4(-x, z) &= -\phi_4(+x, z) & \text{Roll} & \end{aligned}$$

Dynamic boundary condition, Eq.(D.19):

The requirement for this condition states that the pressure at the surface equals the atmospheric pressure. This dynamic boundary condition is defined at the water surface and can be derived by differentiating the free surface dynamic boundary condition to t :

$$\frac{\partial}{\partial t} \underbrace{\left[\frac{\partial \phi}{\partial t} + g\eta = 0 \right]}_{\text{free surface dyn. b.c.}} = \frac{\partial^2 \phi}{\partial t^2} + g \frac{\partial \eta}{\partial t} = 0 \quad (\text{D.23})$$

Substituting the kinematic surface boundary condition (Eq.D.8) in Eq.D.23 for $z = 0$:

$$\underbrace{\frac{\partial \phi}{\partial z} = \frac{\partial \eta}{\partial t} = 0}_{\text{kinematic surface b.c.}} \rightarrow \frac{\partial^2 \phi}{\partial t^2} + g \frac{\partial \phi}{\partial z} = 0 \quad (\text{D.24})$$

Kinematic boundary of oscillating body, Eq.(D.20):

This is the boundary condition at the surface of the floating body and implies that the velocity of the water particles at the surface of the floating body is equal to the velocity of the floating body. In Eq.(6.6) is v_n the outward normal velocity at the surface of the floating body. The subscript $j = 1, \dots, 6$ are indicating the mode of motion of the floating body.

Radiation condition, Eq.(D.21):

Far from the oscillating body the potential value has to become zero. To meet this requirement, the radiation condition states that at a large distance (R) from the floating body the potential value becomes zero.

Symmetric and anti-symmetric conditions, Eq.(D.22):

Since floating bodies, e.g. floating breakwaters and ships, are symmetric with respect to its middle line plane, the potential equations may be simplified to those three shown as Eq.D.22. The indices in these equations indicate the directions. The motions for sway and roll are anti-symmetric because the horizontal velocities, $\frac{\partial \phi}{\partial x}$, of the water particles at both sides of the floating body must have the same direction at any time. The heave motions are symmetric because the horizontal velocities must be of opposite sign. The vertical velocities, $\frac{\partial \phi}{\partial z}$, must have the same direction on both sides at any time.

D.2.2 Potential flow elements

With potential flow it is possible to model more complex flows by superimposing simple flow elements. This is possible since the potential flow theory is a linear theory, which allows summation of different flow elements.

For an uniform flow in the x-direction $u(x, y) = U$, there is a stream function and a potential function, which are defined below. These potential functions and stream functions are shown in Figure D.7. Due to the orthogonality of the potential lines and stream lines the following two equations holds:

$$u_x = \frac{\partial \phi}{\partial x} = \frac{\partial \psi}{\partial y} \quad \text{and} \quad u_y = 0 = \frac{\partial \phi}{\partial y} = -\frac{\partial \psi}{\partial x} \quad (\text{D.25})$$

Integrating both equations with respect to x and y and omitting the integration constants (integration constants do not effect the velocity in the flow) the result is:

$$\phi = U \cdot x = u_x \cdot x \quad \text{and} \quad \psi = U \cdot y = u_x \cdot y \quad (\text{D.26})$$

These solutions satisfies the Laplace equation because the second derivatives with respect to x, y and z are all zero.

Besides the uniform flow element discussed above, there are two other common used flow elements. These two elements are source and sinks. A source is point with an outward radiating flow and sink is a negative source, thus an point with an inward radial flow. For a more detailed description about potential flow elements reference is made to [White, 1999] and [Journee and Massie, 2001]

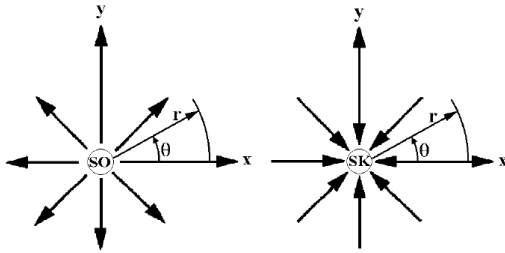


Figure D.6: Potential flow element, source and sink, [Journee and Massie, 2001]

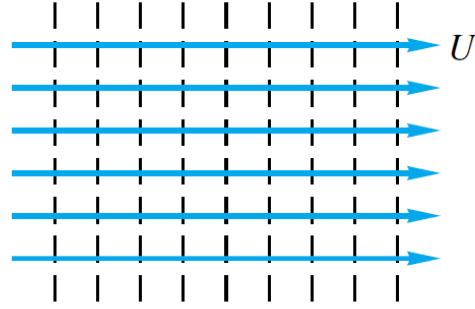


Figure D.7: Potential flow element, uniform flow, [White, 1999]

Sources and sinks both have a potential function and a stream function. Because sources and sinks are describing circles it is easier to display the potential and stream function in polar coordinates:

$$\text{Source :} \quad \phi = \frac{Q}{2\pi} \ln r \quad \psi = \frac{Q}{2\pi} \theta \quad (\text{D.27})$$

$$\text{Sink :} \quad \phi = -\frac{Q}{2\pi} \ln r \quad \psi = -\frac{Q}{2\pi} \theta \quad (\text{D.28})$$

In these equations is Q the source strength, which can be seen as the flow rate with the units m^2/s for two-dimensional flow (plane flow). The potential lines are circles around the source or sink where r is constant. The streamlines are radial spokes with constant θ .

The potential flow elements can be superimposed because the potential flow theory is a linear theory. The result is that the values of the stream functions can be added up. Lines can be drawn connecting equal values of the sum of the individual stream functions. To illustrate this

the following is considered (adapted from White [1999]): a source and a sink of equal strength Q placed on the x-axis with a distance of $2a$ from each other. The coordinates of the source are $(x, y) = (-a, 0)$. The coordinates of the sink are $(x, y) = (+a, 0)$. The resulting stream function in cartesian coordinates becomes:

$$\psi = \psi_{source} + \psi_{sink} = \frac{Q}{2\pi} \arctan\left(\frac{y}{x+a}\right) - \frac{Q}{2\pi} \arctan\left(\frac{y}{x-a}\right) \quad (\text{D.29})$$

The sum of the potential for the source and sink of equal strength Q becomes:

$$\phi = \psi_{source} + \phi_{sink} = \frac{Q}{4\pi} \ln[(x+a)^2 + y^2] - \frac{Q}{4\pi} \ln[(x-a)^2 + y^2] \quad (\text{D.30})$$

In Figure D.8 the blue lines are the streamlines flowing from the source towards the sink. The dashed lines are the the potential lines crossing the stream lines at an angle of 90 degrees. By letting a approaching zero, all the circles will pass the origin. This is called a doublet or a dipole flow, see Figure D.9.

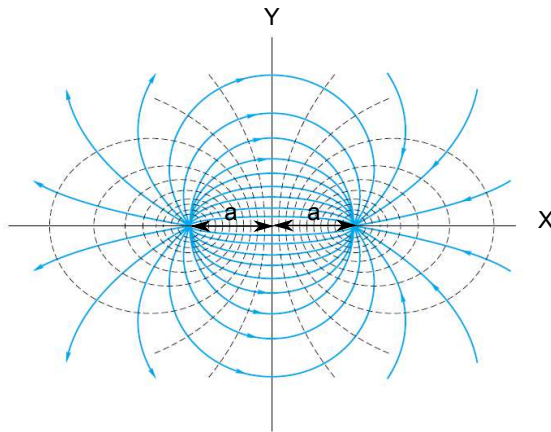


Figure D.8: Potential flow of line source and sink, [White, 1999]

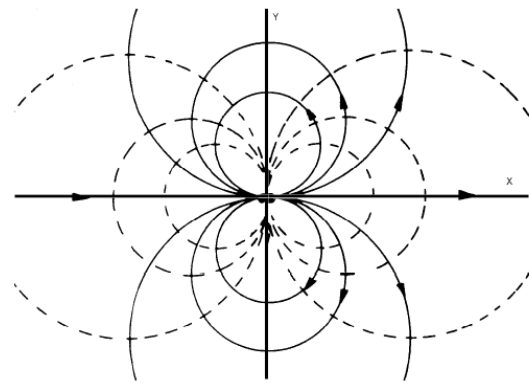


Figure D.9: Doublet or Dipole flow, [Journee and Massie, 2001]

When a source and sink located on the same line are combined with uniform flow the resulting shape is the so called Rankine oval, shown in Figure D.10. The stream lines which are surrounding the source and sink have the shape of an ellipse. The flow from source to sink stays inside this ellipse, while the constant uniform flow passes around these stream lines. A nice practical interpretation of this is that one obtains the same flow field when an impermeable object is placed in uniform flow.

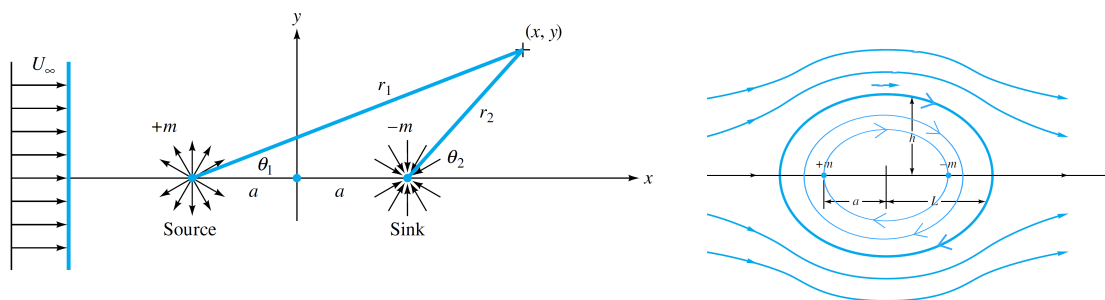


Figure D.10: Rankine oval, [White, 1999]

The name of this ellipse is after the Englishman W.J.M. Rankine. The combination of the potential flow elements discussed above is extended by Rankine around 1870. Rankine was able to generate flatter and thinner surfaces by varying the strength of the source and sink terms. In this way it is possible to model shapes which resembles the shape of a ship [Journee and Massie, 2001].

D.2.3 Hydrodynamic loads

When the velocity potentials are known, forces and moments can be obtained by executing the following steps:

1. Solve the potential function together with the boundary conditions. From this the stream functions and velocity potential functions are obtained.
2. Determine the pressures from the velocity potentials with the linearised Bernoulli equation (Eq.4.8) .
3. Determine the forces and moments by integrating the pressure over the submerged surface (S) of the floating body.

The equations belonging to the three steps above are not discussed into detail, only the result will be discussed. For a more detailed description reference is made to [Journee and Massie, 2001]. The forces and moment are two double integrals of the linearized Bernouilli equation:

$$\vec{F} = \rho \iint_S \left(\frac{\partial \phi_r}{\partial t} + \frac{\partial \phi_w}{\partial t} + \frac{\partial \phi_d}{\partial t} + gz \right) \vec{n} dS = \vec{F}_r + \vec{F}_w + \vec{F}_d + \vec{F}_s \quad (\text{D.31})$$

$$\vec{M} = \rho \iint_S \left(\frac{\partial \phi_r}{\partial t} + \frac{\partial \phi_w}{\partial t} + \frac{\partial \phi_d}{\partial t} + gz \right) (\vec{n} \times \vec{r}) dS = \vec{M}_r + \vec{M}_w + \vec{M}_d + \vec{M}_s \quad (\text{D.32})$$

In Eq.(D.31) and Eq.(D.32) \vec{n} is the outward normal vector on surface dS and \vec{r} is the position vector of surface dS . The result consists of four contributions, namely:

1. Radiated waves generated by the oscillating body in still water, \vec{F}_r, \vec{M}_r
2. Waves which are approaching the fixed body (incident waves), \vec{F}_w, \vec{M}_w
3. Waves which are diffracting around the fixed body, \vec{F}_d, \vec{M}_d
4. Hydrostatic buoyancy in still water, \vec{F}_s, \vec{M}_s

To summarize the above, AQWA solves the potential functions and determines the pressures on the water surface and on the floating body. The pressures at the water surface can be converted to waves. From the pressures at the floating body AQWA calculates the forces and moments by which the equation of motion is derived (Eq.D.33). The fluid force consists of a hydrodynamic force and a hydrostatic force. The hydrostatic force is the buoyancy force in still water. The hydrodynamic force is divided into wave forces and radiation forces. This is graphically shown below in Figure D.11. The equation of motion, which is in fact a damped-spring-mass-system is also shown in this figure.

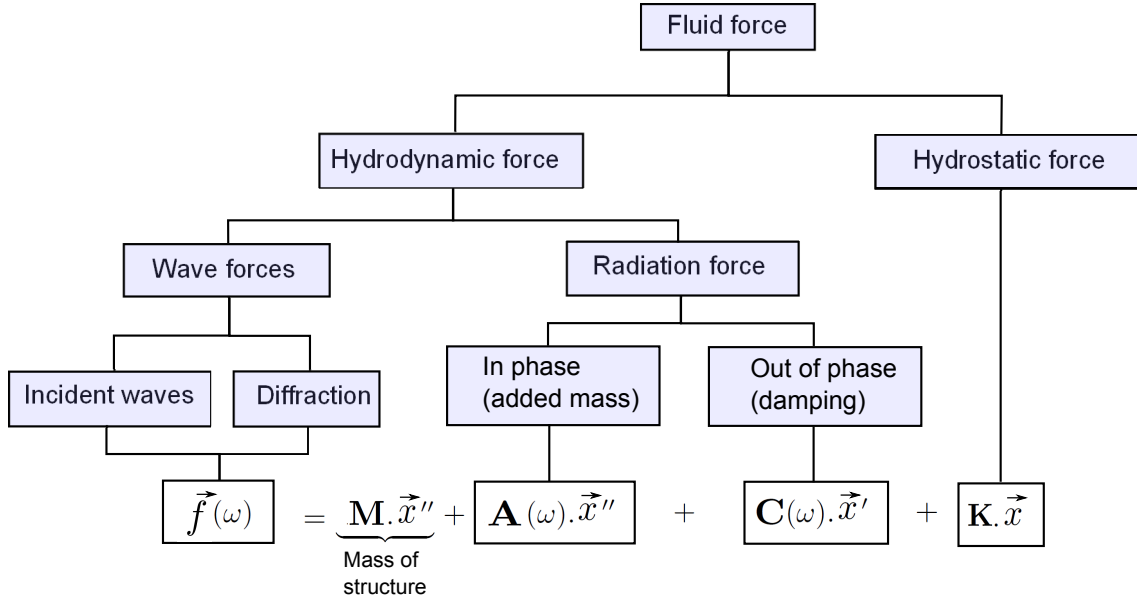


Figure D.11: Summary of fluid forces, [partially adapted from AQWA ANSYS intro lectures presentation]

The equation of motion (see Section 4.3.1) which has to be solved is defined as:

$$(\mathbf{M} + \mathbf{A}(\omega))\ddot{\vec{x}} + \mathbf{C}\dot{\vec{x}} + \mathbf{K}(\omega)\vec{x} = \vec{f}(\omega) \quad (\text{D.33})$$

The solution of the vector \vec{x} is assumed as:

$$\vec{x} = \vec{x} e^{i\omega t} \quad (\text{D.34})$$

After substitution of Eq.(D.34) into Eq.(D.33) and omitting the term $e^{i\omega t}$, the equation of motion becomes:

$$[-\omega^2(\mathbf{A}(\omega) + \mathbf{M}) - i\omega\mathbf{C}(\omega) + \mathbf{K}]\vec{x}(\omega) = \vec{f}(\omega) \quad (\text{D.35})$$

The solution of vector \vec{x} implies the displacement of the floating structure as a function of the radian frequency ω and the angle of displacement of the floating structure as a function of the radian frequency ω . Vector \vec{x} is obtained by taking the inverse of the matrices between brackets at the left hand side of Eq.(D.35). The equation which is solved by AQWA becomes:

$$\vec{x}(\omega) = [-\omega^2(\mathbf{A}(\omega) + \mathbf{M}) - i\omega\mathbf{C}(\omega) + \mathbf{K}]^{-1} \vec{f}(\omega) \quad (\text{D.36})$$

D.3 Validation of AQWA

Below the Root Mean Square Errors (RMSE) are shown of the numerical models which are compared with experimental data. These RMSE are in percentages because the transmission coefficients are represented as percentages.

D.3.1 Fixed breakwaters

| T [s] | f [Hz] | L _{wave} [m] | L _{wg} [m] | Ct _{exp} [-] | Ct _{aqwa} [-] | Ct _{exp} -Ct _{aqwa} [-] |
|-------------|--------|-----------------------|---------------------|-----------------------|------------------------|---|
| 6.97 | 0.14 | 30.12 | 15.06 | 86% | 93% | -7% |
| 5.60 | 0.18 | 23.75 | 11.88 | 83% | 87% | -4% |
| 3.36 | 0.30 | 13.11 | 6.55 | 78% | 80% | -2% |
| 2.78 | 0.36 | 10.20 | 5.10 | 65% | 60% | 5% |
| 2.40 | 0.42 | 8.20 | 4.10 | 41% | 53% | -12% |
| RMSE | | | | | | 7% |

Table D.1: Results AQWA compared with data obtained from Koutandos et al. [2005] for a fixed breakwater, D=0.4m, B=350m, d=2m

| T [s] | f [Hz] | L _{wave} [m] | L _{wg} [m] | Ct _{exp} [-] | Ct _{aqwa} [-] | Ct _{exp} -Ct _{aqwa} [-] |
|-------------|--------|-----------------------|---------------------|-----------------------|------------------------|---|
| 6.97 | 0.14 | 30.12 | 15.06 | 85% | 93% | -7% |
| 5.56 | 0.18 | 23.75 | 11.88 | 81% | 87% | -4% |
| 3.37 | 0.30 | 13.11 | 6.55 | 73% | 73% | 0% |
| 2.79 | 0.36 | 10.20 | 5.10 | 56% | 53% | 5% |
| 2.41 | 0.42 | 8.20 | 4.10 | 38% | 40% | -1% |
| RMSE | | | | | | 4% |

Table D.2: Results AQWA compared with data obtained from Koutandos et al. [2005] for a fixed breakwater, D=0.5m, B=350m, d=2m

| T [s] | f [Hz] | L _{wave} [m] | L _{wg} [m] | Ct _{exp} [-] | Ct _{aqwa} [-] | Ct _{exp} -Ct _{aqwa} [-] |
|-------------|--------|-----------------------|---------------------|-----------------------|------------------------|---|
| 6.94 | 0.14 | 29.90 | 14.95 | 85% | 85% | 0% |
| 5.57 | 0.18 | 23.58 | 11.79 | 81% | 86% | -4% |
| 3.36 | 0.30 | 13.12 | 6.56 | 73% | 72% | 0% |
| 2.78 | 0.36 | 10.17 | 5.08 | 56% | 51% | 5% |
| 2.40 | 0.42 | 8.19 | 4.10 | 38% | 39% | -1% |
| RMSE | | | | | | 3% |

Table D.3: Results AQWA compared with data obtained from Koutandos et al. [2005] for a fixed breakwater, D=0.67m, B=350m, d=2m

D.3.2 Floating breakwaters anchored by piles

| T [s] | f [Hz] | L _{wave} [m] | L _{wg} [m] | C _{t_{exp}} [-] | C _{t_{aqwa}} [-] | C _{t_{exp}} -C _{t_{aqwa}} [-] |
|-------|--------|-----------------------|---------------------|----------------------------------|-----------------------------------|---|
| 6.91 | 0.14 | 28.86 | 14.43 | 86% | 89% | -2% |
| 5.49 | 0.18 | 29.86 | 14.93 | 85% | 89% | -4% |
| 4.27 | 0.23 | 30.86 | 15.43 | 85% | 89% | -5% |
| 3.34 | 0.30 | 31.86 | 15.93 | 82% | 79% | 3% |
| 2.76 | 0.36 | 32.86 | 16.43 | 73% | 69% | 3% |
| 2.39 | 0.42 | 33.86 | 16.93 | 69% | 49% | 20% |
| 2.14 | 0.47 | 34.86 | 17.43 | 47% | 39% | 8% |
| 2.06 | 0.49 | 35.86 | 17.93 | 41% | 40% | 2% |
| | | | | | RMSE | 8% |

Table D.4: Results AQWA compared with data obtained from Koutandos et al. [2005] for a heave floating breakwater, $D=0.4\text{m}$, $L=350\text{m}$, $d=2\text{m}$

D.4 New simulations for areas of interest

D.4.1 Fixed breakwater

In Section 6.2.1 the influence of the draft and the width on the wave transmission coefficient is discussed. Below a number of plots are shown from which the conclusions are derived discussed in section 6.2.1.

Variation of draft

Below three plots are shown where the draft of the breakwater is varied, while the other parameters, e.g. the width and the water depth do not vary.

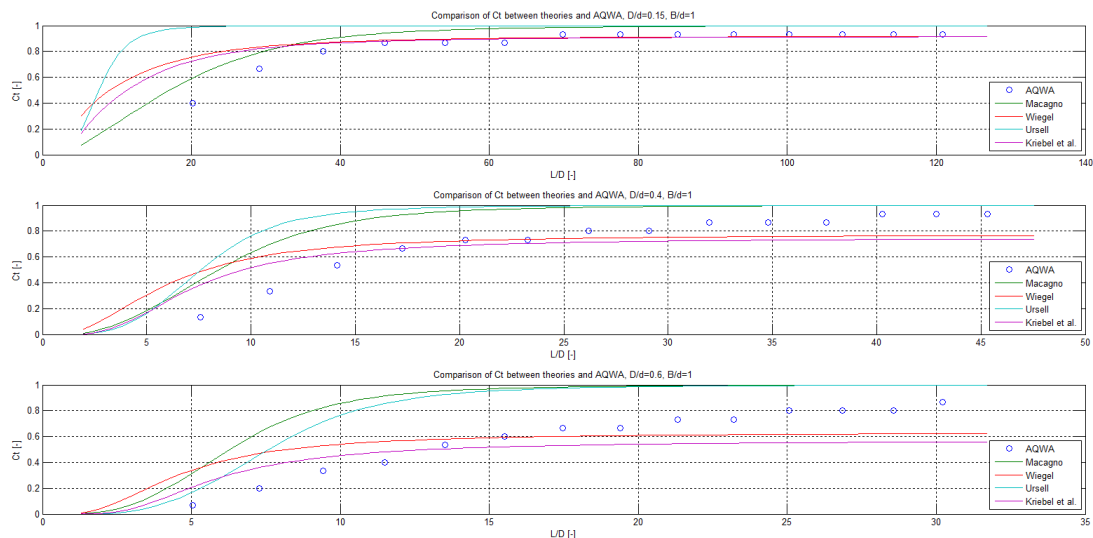


Figure D.12: Effect of draft on C_t modeled with AQWA and compared with wave transmission coefficient theories, regular waves, $d=2\text{m}$, fixed breakwater

From Figure D.12 it becomes clear that for $0.15 < D/d < 0.40$ and for $B/d = 1.0$ the theory of Macagno is applicable when the values of the wave transmission coefficients becomes smaller

than the values of the wave transmission coefficients predicted by Kriebel and Bollmann. When the D/d ratio becomes larger the differences between Wiegel and Kriebel and Bollmann becomes larger as well and the theory of Wiegel is suitable to apply for larger L/D values.

Variation of width

Below three plots are shown where the width of the breakwater is varied, while the other parameters, e.g. the draft and the water depth do not vary.

From Figure D.13 and Figure D.12 it becomes clear that for $0.75 < B/d < 1.0$ and for $0.15 < D/d < 0.40$ the theory of Macagno is applicable as soon as the transmission coefficients predicted by Macagno becomes smaller than the wave transmission coefficients predicted by Kriebel and Bollmann. Furthermore, it can be seen that when the draft and the width are small compared to the water depth, the theory of Macagno is suitable to apply over the full range of wave lengths.

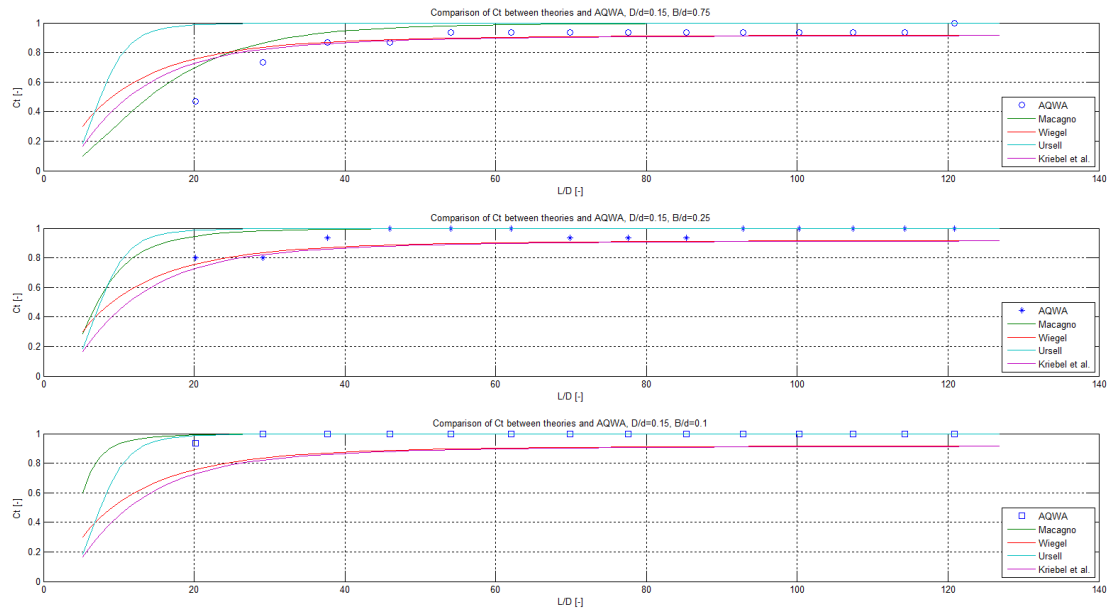


Figure D.13: Effect of width on C_t modelled with AQWA and compared with wave transmission theories, regular waves, $d=2\text{m}$, fixed breakwater

D.4.2 Floating breakwater anchored by piles

In Section 6.2.2 a number of conclusions are drawn based on the comparisons between the data of the model and the experimental data. The figures below show these comparisons.

Variation of draft

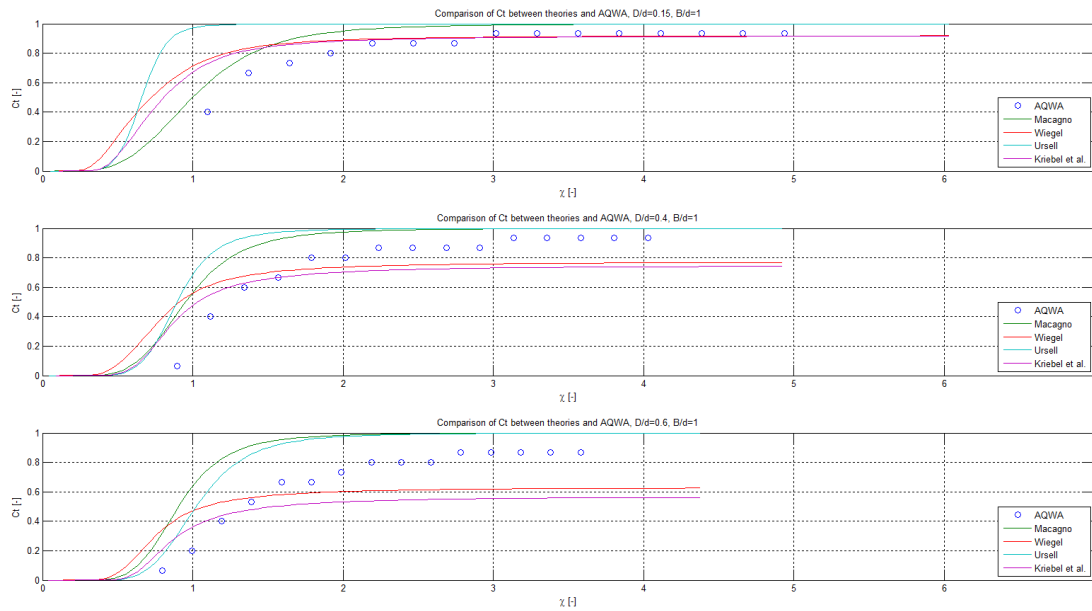


Figure D.14: Effect of draft on C_t modelled with AQWA and compared with wave transmission theories, regular waves, $d=2\text{m}$, floating breakwater with one degree of freedom

From Figure D.14 the first and second panel, it can be seen that for D/d ratios of 0.15 and 0.40 the theory of Macagno approximates the model data over the full range of χ -values quite well. For the middle panel, where $D/d = 0.4$, the theory of Kriebel and Bollmann shows a good agreement for lower χ -values. The lower panel where the relative draft $B/d = 0.6$, there is a large deviation between the model results and the theories for χ -values larger than 2.0.

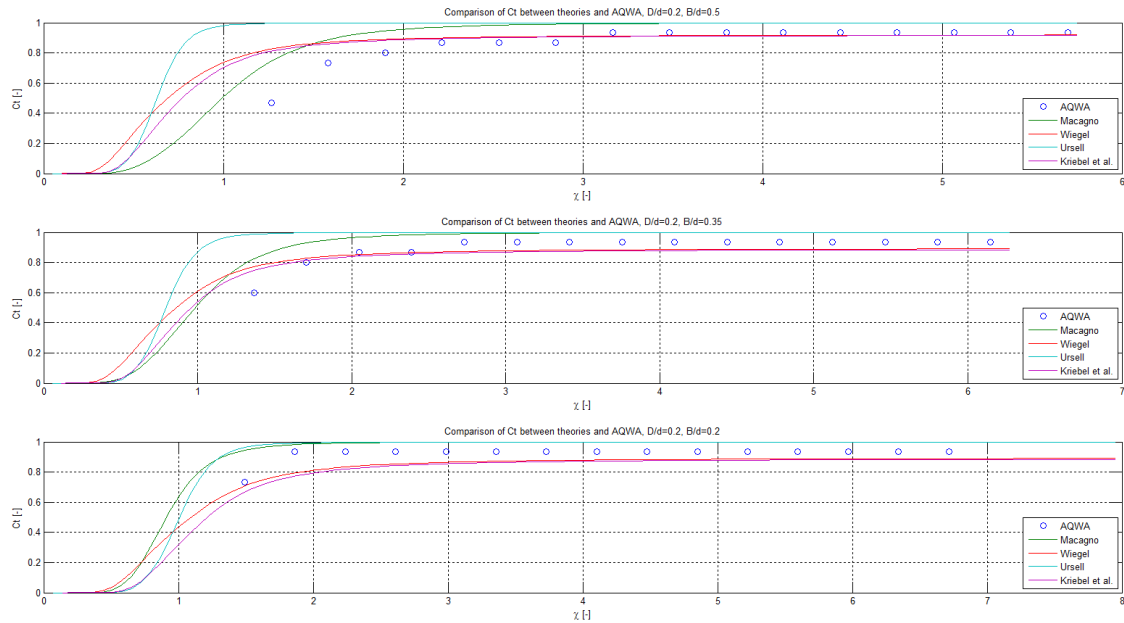


Figure D.15: Effect of width on C_t modelled with AQWA and compared with wave transmission theories, regular waves, $d=2\text{m}$, floating breakwater with one degree of freedom

Variation of the width

Figure D.15 shows the effect of the width of the floating breakwater on the wave transmission. In these calculations the width is changed while the other parameters are constant. From these three plots in this figure it can be seen that the theory of Macagno approximates the model data well. For all the data points the theory of Macagno is overestimating the data.

Bibliography

- A. Ali. Floating transshipment container terminal. M.sc. thesis, Delft University of Technology, 2006.
- P. Bettess, S.C. Liang, and J.A. Bettess. Diffraction of waves by semi-infinite breakwater using finite and infinite elements. *International journal for numerical methods in fluids*, 4(9):813–832, 1984.
- E.C. Bouwmeester and H.M. van der Breggen. Floating breakwaters. Report, Delft University of Technology, 1984.
- A. Brebner and A.O. Ofuya. Floating breakwaters. In *Proceedings of 11th conference on Coastal Engineering*, pages 1055–1094, 1968.
- M. Briggs, W. Ye, Z. Demirbilek, and J. Zhang. Field and numerical comparisons of the ribs floating breakwater. *Journal of Hydraulic Research*, 40(3):289–301, 2002.
- R. Cox, I. Coghlan, and C. Kerry. Floating breakwater performance in irregular waves with particular emphasis on wave transmission and reflection, energy dissipation, motions and restraining forces. *Ocean Engineering*, pages 350–362, 2007.
- R. Drieman. Feasibility study on the use of a floating breakwater to protect a new artificial beach in balchik, bulgaria. Msc thesis, Delft University of Technology, 2011.
- G. Elchahal, R. Younes, and P. Lafon. The effects of reflection coefficient of the harbour sidewall on the performance of floating breakwaters. *Ocean Engineering*, 35(11):1102–1112, 2008.
- M.W. Fousert. Floating breakwaters. M.sc. thesis, Delft University of Technology, 2006.
- M.R. Gesraha. Analysis of shaped floating breakwater in oblique waves: I. impervious rigid wave boards. *Applied Ocean Research*, 28(5):327–338, 2006.
- L.Z. Hales. Floating breakwaters: State-of-the-art literature review. Technical report, DTIC Document, 1981.
- V.W. Harms. Data and procedures for the design of floating tire breakwaters. Technical report, 1979.
- V.W. Harms, J.J. Westerink, R.M. Sorensen, and J.E. AACtamany. Coastal engineering research center. 1982.
- L.H. Holthuijsen. *Waves in oceanic and coastal waters*. Cambridge University Press, 2007.
- J.M.J. Journee and W.W. Massie. Offshore hydromechanics. *Delft University of Technology*, 2001.
- E. Koutandos, P. Prinos, and X. Gironella. Floating breakwaters under regular and irregular wave forcing: reflection and transmission characteristics. *Journal of hydraulic Research*, 43(2): 174–188, 2005.

- D.L. Kriebel and C.A. Bollmann. Wave transmission past vertical wave barriers. In *COASTAL ENGINEERING CONFERENCE*, volume 2, pages 2470–2483. ASCE AMERICAN SOCIETY OF CIVIL ENGINEERS, 1996.
- P.A. Leach, W.G McDougal, and C.K. Sollitt. Hinged floating breakwater. *Journal of Waterway, Port, Coastal, and Ocean Engineering*, 111(5):895–909, 1985.
- E. Macagno. Wave action in a flume containing a submerged culvert. *La Houille Blanche*, 1954.
- L. Martinelli, P. Ruol, and B. Zanuttigh. Wave basin experiments on floating breakwaters with different layouts. *Applied Ocean Research*, 30(3):199–207, 2008.
- E. Peña, J. Ferreras, and F. Sanchez-Tembleque. Experimental study on wave transmission coefficient, mooring lines and module connector forces with different designs of floating breakwaters. *Ocean Engineering*, 38(10):1150–1160, 2011.
- PIANC. *Floating Breakwaters: A Practical Guide for Design and Construction*. PIANC, 1994.
- E.P. Richey and C.K. Sollitt. *Attenuation of Deep Water Waves by a Porous Walled Breakwater*. Charles W. Harris Hydraulics Laboratory, University of Washington, 1969.
- J.F. Ripken. An experimental study of flexible floating breakwaters. Technical report, DTIC Document, 1960.
- G.V.P. de Rooij. A very large floating container terminal. M.sc. thesis, Delft University of Technology, 2006.
- P. Ruol, L. Martinelli, and P. Pezzutto. Formula to predict transmission for π -type floating breakwaters. *Journal of Waterway, Port, Coastal, and Ocean Engineering*, 139(1):1–8, 2013a.
- P. Ruol, L. Martinelli, and P. Pezzutto. Limits of the new transmission formula for pi-type floating breakwaters. *Coastal Engineering Proceedings*, 1(33):structures–47, 2013b.
- F. Ursell. The effect of a fixed vertical barrier on surface waves in deep water. In *Proc. Cambridge Philos. Soc*, volume 43, pages 374–382. Cambridge Univ Press, 1947.
- H.J. Verhagen, K. d’Angremond, and F. van Roode. *Breakwaters and Closure dams*. VSSD, 2009.
- F.M. White. *Fluid mechanics, 4th edn*. McGraw-Hill Singapore, 1999.

